An ocular glymphatic clearance system removes beta-amyloid from the rodent eye

Wang, Xiaowei; Lou, Nanhong; Eberhardt, Allison; Yang, Yujia; Kusk, Peter; Xu, Qiwu; Forstera, Benjamin; Peng, Sisi; Shi, Meng; Ladron-de-Guevara, Antonio; Delle, Christine; Sigurdsson, Bjorn; Xavier, Anna L. R.; Erturk, Ali; Libby, Richard T.; Chen, Lu; Thrane, Alexander S.; Nedergaard, Maiken

Published in:
Science Translational Medicine

DOI:
10.1126/scitranslmed.aaw3210

Publication date:
2020

Document version
Peer reviewed version

Citation for published version (APA):
Wang, X., Lou, N., Eberhardt, A., Yang, Y., Kusk, P., Xu, Q., ... Nedergaard, M. (2020). An ocular glymphatic clearance system removes beta-amyloid from the rodent eye. *Science Translational Medicine*, *12*(536), [eaaw3210]. https://doi.org/10.1126/scitranslmed.aaw3210

Title: The Ocular Glymphatic Clearance System

Authors: Xiaowei Wang[1,2], Nanhong Lou[2], Allison Eberhardt[2], Yujia Yang[3], Peter Kusk[1], Qiwu Xu[2], Benjamin Förstera[4,5], Sisi Peng[2], Meng Shi[3], Antonio Ladrón-de-Guevara[2], Christine Delle[1], Björn Sigurdsson[1], Anna L. R. Xavier[1], Ali Ertürk[4,5], Richard T. Libby[6], Lu Chen[3,*], Alexander S. Thrane[1,7], Maiken Nedergaard[1,2,*]

Affiliations:
[1]Center for Translational Neuromedicine, Faculty of Medical and Health Sciences, University of Copenhagen, Denmark, Blegdamsvej 3B, 2200 Copenhagen N.
[2]Center for Translational Neuromedicine, University of Rochester Medical School, Elmwood Avenue 601, Rochester, NY 14642, USA.
[3]Center for Eye Disease and Development, Vision Science Graduate Program, and School of Optometry, University of California Berkeley, Berkeley, CA 94720, USA.
[4]Institute for Stroke and Dementia Research, Klinikum der Universität München, Ludwig Maximilians University of Munich (LMU), 81377 Munich, Germany.
[5]Institute for Tissue Engineering and Regenerative Medicine (iTERM), Helmholtz Center München, 85764 Munich, Germany.
[6]Department of Ophthalmology, University of Rochester Medical Center, Rochester, NY, 14642, USA.
[7]Department of Ophthalmology, Haukeland University Hospital, Jonas Lies Vei 65, 5021 Bergen, Norway.

*** Correspondence should be addressed to:** Dr. Maiken Nedergaard, Center for Translational Neuromedicine, Faculty of Medical and Health Sciences, University of Copenhagen, Denmark, Blegdamsvej 3B, 2200 Copenhagen N, Denmark. E-mail: nedergaard@sund.ku.dk

Dr. Lu Chen, Center for Eye Disease and Development, Vision Science Graduate Program, and School of Optometry, University of California Berkeley, Berkeley, California, United States. Email: chenlu@berkeley.edu

One Sentence Summary:
Glymphatic pathway clears retinal amyloid-β via optic nerve and fails in glaucoma.

Abstract

Despite high metabolic activity, the retina and optic nerve head lack traditional lymphatic drainage. We here identified an ocular glymphatic clearance route for fluid and wastes via the proximal optic nerve in rodents. Amyloid-β (Aβ) was cleared from the retina and vitreous via a pathway dependent on glial water channel aquaporin-4 (AQP4) and driven by the ocular-cranial pressure difference. After traversing the lamina barrier, intra-axonal Aβ was cleared via the perivenous space and subsequently drained to lymphatic vessels. Light-induced pupil constriction enhanced efflux, whereas atropine or raising intracranial pressure blocked efflux. In two distinct murine models of glaucoma, Aβ leaked from the eye via defects in the lamina barrier instead of directional axonal efflux. The discovery of this pathway for removal of fluid and metabolites from the intraocular space prompts a reevaluation of the core principles governing eye physiology and provides a framework for developing alternative therapeutic approaches to treat common eye diseases, including glaucoma.

Introduction

Like the brain inside the cranial vault, the internal structures of the eye are contained within a confined space, necessitating tight control of fluid homeostasis. Yet, both the eye and the brain are largely devoid of traditional lymphatic vessels, which are critical for the clearance of fluid and solutes from peripheral tissues (*1*, *2*). Recent discoveries have shown the brain possesses a quasi-lymphatic system, termed the glymphatic system (*3*), and traditional lymphatic vessels are also present in the dura mater, one of three layers of fibrous membranes lining the brain's exterior surface (*4*-*6*). Neuroimaging studies have recently documented the existence of a glymphatic/lymphatic system in the human brain with drainage to cervical lymph nodes (*7*-*11*). Glymphatic/lymphatic transport contributes to clearance of amyloid-β (Aβ), a derivative of amyloid precursor protein (APP) that is a main constituent of amyloid plaques in the brain (*12*) and likewise of amyloid deposits in the retina (*13*). Extracellular Aβ and tau are regulated by the sleep-wake cycle (*14*, *15*), possibly reflecting increased production during neural activity (*16*) and/or enhanced clearance during sleep (*17*). Several authors suggested the existence of an ocular glymphatic system based on clinical observations and the identification of missing pieces of how the neuroretina tightly controls volume homeostasis (*18*-*21*). Experimental data supports this concept by demonstrating retrograde cerebrospinal fluid (CSF) transport along the perivascular spaces in the optic nerve (*22*) and more recently an impairment of retrograde transport in glaucoma (*23*). However, the primary function of glymphatic transport is clearance of metabolic waste. In the eye, it is the highly active retinal neurons that are producing waste products and therefore in need of a clearance system. We here asked whether the optic nerve might serve as a pathway for efflux of ocular fluid and thereby supporting clearance of waste products from the retina.

Results

Tracer imaging supports the existence of an ocular glymphatic clearance system

Since the electrically active neural tissues of the retina produce Aβ (*3*, *24*) and other potentially neurotoxic protein cleavage products like tau (*25*), we explicitly sought evidence of an intraocular anterograde glymphatic/lymphatic clearance system in mice. First, we injected HiLyte-594-tagged human amyloid-β (hAβ) into the vitreous body of mice and visualized tracer distribution one hour later. Then we used ultimate 3D imaging of Solvent-Cleared Organs (uDISCO) whole-body clearing (*26*) to analyze the eye and tracer in transparent mouse heads. Three-dimensional reconstruction of light-sheet microscopy data suggested that in addition to anterior routes, hAβ tracer exited the eye along the optic nerve (**Fig. 1A, fig. S1A**). Transport along the optic nerve also occurred following non-invasive intravascular delivery of either the radiolabeled K^+-analogue ($^{86}Rb^+$) or FITC-cadaverine, a tracer that permeates the blood-retinal barrier but not the blood-brain barrier (*27*) (**fig. S1B-D).** Whole-mount preparation of the optic nerve confirmed hAβ tracer is transported anterograde along the nerve (**Fig. 1B**). Moreover, use of reporter mice in which arteries and arterioles are identified by DsRed expression in mural cells (*28*) revealed that hAβ tracer preferentially accumulated in the perivascular space along the optic nerve veins rather than along arterioles (**Fig. 1C**). In contrast to hAβ tracer, Alexa Fluor (AF)-dextran (3, 10, and 500 kDa) did not enter the nerve after intravitreal administration (**Fig. 1D, fig. S1E, table S1)** Following suprachoroidal delivery, tracer was also transported along the optic nerve (**fig. S1F**). The injection of trace amounts of hAβ tracer was not associated with retinal cytokine release, glial activation, apoptosis, or alteration in blood-retinal barrier (BRB) permeability (**fig. S2A-G, table S2**). Sectioning and high-resolution imaging of the eye showed that, in addition to perivenous accumulation, hAβ tracer was taken up by retinal ganglion cells (RGCs, $RBPMS^+$) as well as amacrine cells (AP-2α^+) (**fig. S3A-E**), and transported along neuron-specific class III β-tubulin (TUJ1)-positive axons, consistent with rapid neuronal uptake of hAβ (*29*) (**Fig. 1E-F**). In the optic nerve, glial cells of the oligodendrocytic (OLIG2$^+$) and astrocytic (GLT-1$^+$) lineages also exhibited sparse hAβ tracer uptake (**fig. S3F-I**). The hAβ tracer accumulation peaked 274 ± 20 μm from the optic nerve head (ONH) and tapered off gradually in the distal nerve (**table S1**), suggesting hAβ tracer exits the nerve anterior to the optic chiasm. This notion was supported by the observation that the dural sheath surrounding the proximal segment of the optic nerve densely accumulated tracer (**Fig. 1E, fig. S3J**). Additional analysis revealed traditional lymphatic vessels embedded in the dural sheath and surrounding loose tissue (*30*-*32*) (**fig. S3K-M**). These vessels did not contain red blood cells or stain with intravascularly-delivered lectin, but they labeled positive for the conventional lymphatic markers, lymphatic vessel endothelial hyaluronan receptor 1 (LYVE1), vascular endothelial growth factor receptor 3 (VEGFR3), Prospero homeobox protein 1(*Prox1*) and podoplanin (PDPN) (*2, 5*). In support of this, hAβ had accumulated in the ipsilateral cervical lymph nodes in animals examined three hours after intravitreal injection (*33*) (**Fig. 1G**). Imaging after dual injections of hAβ tracer in the vitreous body in conjunction with a tracer in the cisterna magna (CM) highlighted tracer transport within the optic nerve in both anterograde and retrograde directions with limited spatial overlap (**Fig. 1H-I**). As reported previously, tracers injected in the CM were transported along perivascular spaces in the optic nerve (*22*). Use of NG2-DsRed-expressing reporter mice revealed CM-injected tracers were predominantly transported along the peri-arterial and peri-capillary spaces (**Fig. 1J-K, fig. S3N**), in contrast to the intravitreal tracers, which accumulated along the veins (**Fig. 1C**). Collectively, these observations show hAβ is transported by axons and along the perivenous space in the optic nerve after intravitreal delivery. From there, hAβ exits the nerve via dural lymph vessels located in the outer (dural) layer of meninges lining the optic nerve and orbital lymphatics (**fig. S3J-L**), consistent with recent reports lymphatic CSF drainage (*4*, *34*). Anterior lymphatic drainage pathways may also have contributed to the tracer accumulation described in our study (*2*, *35*).

Ocular amyloid-β clearance is affected by glial water channel aquaporin-4 (AQP4)

Astroglial expression of water channel AQP4 on endfeet plastering nearly the entire brain vasculature has been shown to facilitate cerebral clearance of amyloid-β (*3, 17, 36, 37*). Since retinal Müller glia express abundant AQP4, we next asked if glial AQP4 facilitates Aβ clearance from the retina and along the optic nerve. We performed intravitreal injection of fluorescently tagged hAβ as described above and compared tracer movement in $Aqp4^{-/-}$ and $Aqp4^{+/+}$ mice. Baseline intraocular pressure (IOP) was comparable for $Aqp4^{-/-}$ and wild-type mice (**Fig. 2A**). *Aqp4* deletion was associated with a significantly reduced retinal hAβ penetration ($p < 0.05$, **Fig. 2B-C**). Similarly, *Aqp4* deletion caused a significant reduction in the clearance of hAβ tracer into the optic nerve ($p < 0.05$, **Fig. 2D-G**). These data demonstrate that ocular clearance is facilitated by AQP4 expression in retinal Müller glia and pre-laminar astrocytes.

Translaminar pressure difference (TPD) drives ocular clearance

Pressure difference is a principal driving force of directional fluid transport. Since IOP under physiological conditions exceeds intracranial pressure (ICP), it is possible that the pressure difference across the lamina cribrosa contributes to fluid flow along the optic nerve (*38*). To define the role of the TPD in transport of hAβ tracer, we manipulated ICP by either withdrawal or infusion of artificial CSF in the CM while monitoring ICP. ICP manipulation with these methods was not associated with IOP alteration (*39*) (**Fig. 3A**). Decreasing ICP from baseline (3.6 ± 0.4 mmHg) to

0.5 ± 0.2 mmHg was associated a sharp increase in the total hAβ tracer signal and peak intensity of hAβ tracer transport in the proximal optic nerve 30 min after intravitreal injection (**Fig. 3B-E**). Conversely, increasing ICP to 16.7 ± 0.6 mmHg significantly decreased hAβ tracer clearance into the nerve ($p < 0.001$, **Fig. 3B-E**). Combined, these data show hAβ tracer transport along the nerve is reduced when TPD is decreased and is increased when TPD is elevated.

Light-induced pupil constriction increases ocular glymphatic clearance

Prior observations have shown repeated constriction of the pupil and ciliary body during accommodation enhances aqueous outflow in healthy human subjects, hypothesized to be via trabecular and uveoscleral routes (*40, 41*). We next asked whether transport of hAβ along the optic nerve is influenced by physiological pupil constriction *in vivo.* To address this question, we compared transport of hAβ tracer in mice stimulated with light at 1 Hz to control mice kept in darkness. A subset of mice exposed to stimulation received atropine (1%, eye drops) to block the light-induced pupillary constriction reflex, and another subset of mice received pilocarpine (2%, eye drops) to achieve static constriction without light stimulation (**Fig. 4A**). The analysis showed light stimulation increased hAβ transport in the optic nerve. The total hAβ tracer signal, peak intensity, and distance of transport were all sharply increased by light stimulation at 30 min after hAβ administration (**Fig. 4B-D**; the findings were reproduced in rats: **fig. S4A-E**, and not influenced by varying the injection rate or volume: **fig. S4F**). Tracer accumulation in mice kept in darkness increased slowly and reached the same amplitude as that in the light-stimulated ones at two hours after intravitreal injection of hAβ tracer (**fig. S5A-I**). Infrared pupillometry confirmed that light stimulation induced alternating constriction and dilation of the pupil, detected as high variance in pupil size. In contrast, animals kept in darkness, as well as light-stimulated animals pretreated with atropine, exhibited essentially no pupil movement (**Fig. 4E-G**). Atropine completely blocked light-induced pupil constriction, as well as the light-related acceleration of hAβ tracer transport (**Fig. 4B-G**), whereas pilocarpine-induced tonic pupillary constriction did not appear to affect transport (**Fig. 4B-D**). Rebound and intracameral tonometry failed to demonstrate a consistent effect of repeated light stimulation and pupillary constriction on IOP in the short timescale of our experiment (**fig. S5J-L**), although vitreous pressure transients have been demonstrated previously in larger animals (primates) during ciliary body contraction (*41*). Intravitreal hAβ tracer was not transported postmortem (**Fig. 4B**, **fig. S5B, F, table S1**), indicating that passive diffusion did not contribute to hAβ tracer dispersion along the optic nerve. These data suggest repeated pupil and potentially ciliary body constriction propels intraocular fluid dispersion along the optic nerve, resulting in enhanced hAβ tracer transport. Combining light stimulation with manipulations of ICP did not change net hAβ tracer transport compared with either low or high ICP alone (**fig. S6A-E**). Thus, sufficiently large pressure changes can override the effect of natural light stimulation. Conversely, dextran transport was not affected by transiently increasing TPD (**fig. S6F**).

Lamina barrier defects lead to excessive and pathological glymphatic outflow in glaucoma

Glaucoma is a group of diseases characterized by progressive and irreversible injury to the ONH and RGC degeneration, leading to blindness (*42*). Increased IOP is a leading risk factor for glaucoma. Our present observations raised the question of whether glaucoma is linked to pathological changes in ocular glymphatic solute transport. To test this, we undertook tracer studies in two distinct murine models of glaucoma and chronic ocular hypertension based on two separate mouse strains (**Fig. 5A-K, fig. S7A-G, fig. S8A-L**). DBA/2J mice develop a depigmenting iris disease that leads to age-related ocular hypertension (*43*) (**Fig. 5A**). Chronic IOP elevation results in significant RGC loss and glaucomatous optic nerve degeneration in the majority of aged eyes from DBA/2J mice (*44*) ($p < 0.01$, **fig. S7D**). Rectifying their IOP with pharmacological, genetic, or surgical interventions has been shown to ameliorate RGC death (*45*). The chronic circumlimbal suture (CLS) model employs oculopression to reduce aqueous drainage and thus increase IOP to 28 ± 1.6mmHg (vs. 15 ± 0.4mmHg in controls) in non-pigmented CD-1 mice. This model has also been shown to cause RGC loss (*46*). Our analysis of young DBA/2J mice showed neither IOP nor hAβ tracer transport along the optic nerve differed from that in the DBA/2J-*Gpnmb*$^{+}$/SjJ (D2-control) mice, a genetically-matched control strain that does not develop ocular hypertension (**Fig. 5A-D, table S3**). About 50% of DBA/2J mice are severely affected by glaucoma at 11 months, but IOP is usually normalized or only mildly elevated at this stage of the disease and thus less likely to directly influence tracer outflow (*44*). Using whole-mounts of optic nerve, we found hAβ tracer transport was sharply increased in an equivalent subset of 11-month-old DBA/2J mice (**Fig. 5A-D, fig. S8D**), with total hAβ tracer signal significantly increased in 11-month-old DBA/2J mice compared with age-matched D2-control mice ($p < 0.05$, **Fig. 5B-D, fig. S8C-D**). Similarly, we found CD-1 CLS, but not sham control mice, exhibited significantly increased hAβ tracer transport one month after surgery, when IOP had normalized (*46*) (p < 0.05, **Fig. 5B-D, fig. S8D**). High-resolution confocal imaging of 11-month-old DBA/2J optic nerves revealed hAβ tracer was located primarily in the perivascular space, or outside the RGC axons, as opposed to the intra-axonal distribution noted in young DBA/2J mice and age-matched controls (**fig. S7A**). This prompted us to ask whether the glial lamina normally acts as a high-resistance barrier that hinders transport of macromolecules. If so, then a corollary of this proposition would be that a failure of the lamina barrier might be a hallmark of glaucoma in these mouse models (*47*, *48*). To test this dual hypothesis, we assessed the passage of increasing molecular sizes of AF-dextran across the lamina following intravitreal injection in D2-control and DBA/2J mice (3, 10, 500 kDa), as well as CLS and sham control CD-1 mice (500 kDa) (**fig. S8F-L**). We found dextrans as small as hAβ (3kDa vs. 4.3kDa) failed to pass the glial lamina in the mice without glaucoma, despite a transient increase in TPD (**Fig. 5E-H, fig. S8, fig. S6F**). In contrast, we saw i dispersion of dextrans in 11-month-old DBA/2J and CLS mice, with tracer detectable several mm distal to the lamina (**Fig. 5E-H, fig. S8B-L**). Confocal imaging confirmed the dextrans were present in the perivascular space or outside the few remaining axons in 11-month-old DBA/2J mice (**fig. S7B-C, fig. S8B**). These observations suggest the lamina barrier in the healthy eye diverts extracellular fluid into the axonal compartment at the ONH and thus facilitates directional axonal fluid transport. Although our data do not aim to address the proximal cause of lamina barrier failure, they show that openings in the barrier divert flow of the ocular fluid in the optic nerve from the axonal to the extracellular compartment. Ultrastructural analysis revealed large defects in the glial barrier in old DBA/2J mice, as previously reported (*47, 49, 50*) (**Fig. 5I, fig. S7E**). We also tested the alternative hypothesis of axonal loss in old DBA/2J mice causing a general expansion of the extracellular space volume fraction. Such an increase in extracellular space of the optic nerve would be expected to facilitate pressure-driven hAβ transport. However, real-time TMA^+ iontophoresis analysis failed to confirm this hypothesis; the mean volume fraction (α) was ~10% of the total volume and did not differ between D2-control mice and DBA/2J mice. The tortuosity factor (λ) was not affected in old DBA/2J (**Fig. 5J-K**).

Discussion

Traditionally, the trabecular and uveoscleral outflow routes are considered the two main pathways for efflux of ocular fluid (*51*). We here suggest the existence of an additional clearance route, present in the eyes of both mice and rats. Efflux via this pathway is facilitated by glial water channel AQP4 and driven by the TPD and light-induced pupil constriction, two important physiological factors associated with normal eye function. Using two distinct murine models, we show an excessive and pathological alteration of glymphatic outflow in glaucomatous eyes. The discovery of this fluid efflux route prompts a re-examination of ocular fluid dynamics and may open up new avenues for treatment of sight-threatening conditions, most notably glaucoma (*52*).

The existence of the efflux system described here raises several important questions that need to be addressed in future works. For example, is the ocular glymphatic system the principal clearance route for protein metabolites such as Aβ produced by RGCs and other retinal cells? Are any subtypes of RGCs more important for the transport than others? We observed that light stimulation accelerated ocular glymphatic clearance by nearly two-fold. This increase was eliminated when the pupillary light reflex was pharmacologically blocked with atropine or pupil constriction was pharmacologically induced with pilocarpine, in contrast to the well-known effect of these drugs on the conventional outflow (*53*). We hypothesize that light-induced pupil movement propels the clearance of retinal metabolic wastes, which raises further questions such as: does solute elimination by this pathway occur preferentially during daytime visual activity, driven by pupil constriction and accommodation, and would this explain why ageing and diseases affecting the iris/pupil/ciliary body are so closely linked to glaucoma (*54*, *55*)?

Most descriptions of ocular fluid homeostasis to date focus on the anterior eye, away from the highly metabolically active retina. However, it is perhaps not surprising that a system for waste export from the posterior eye might exist, and the ocular glymphatic system has indeed been predicted by several experienced investigators: In 2015, the Denniston and Wostyn labs independently published hypothesis-driven reports (*18*, *21*), providing key arguments for the necessity of a glymphatic system in the eye. As visualized by ultrahigh-resolution adaptive optics, the human retinal vasculature is surrounded by perivascular spaces (*18*). Postmortem administration of India ink into the subarachnoid space resulted in its accumulation in perivascular spaces of the optic nerve and in collagen fiber bundles that are continuous with the perivascular spaces and radiate out to separate the white matter bundles (*56*, *57*). It was also speculated that Aβ could be cleared from the retina by perivascular transport, and pathological changes in IOP might interfere with glymphatic flow and trigger neurotoxicity by Aβ accumulation (*21*). Similarly, glymphatic dysregulation due to microgravity could contribute to optic disc edema in astronauts (*58*, *59*). The Yucel lab recently provided experimental evidence of a perivascular transport system in the optic nerve following intracisternal tracer administration in live mice (*22*, *23*). We here confirmed and extended these reports by showing CSF tracer influx occurs along the peri-arterial and peri-capillary spaces in the optic nerve. The focus of our report is, however, transport of tracers in the other direction, from the retina to the CSF. We speculated that fluid transport in this direction would facilitate export of waste products from the metabolically active retina. Our analysis confirmed the hypothesis-driven reports discussed above, but it also demonstrates that the ocular clearance path described here differs in important ways from the initial predictions of ocular glymphatic system. We would argue that the best way of addressing the unique features of the ocular glymphatic system might be to compare them to the brain glymphatic system: The ocular and brain glymphatic fluid transport systems share a highly-polarized route of CSF influx along the peri-arterial space, an efflux path along the perivenous space, and a final fluid collection site by the dural and cervical lymphatic vessels. In fact, the two efflux pathways merge; tracers injected in either the eye or the brain are eventually trapped in cervical lymph nodes, and exchange or watershed zones between CSF and intraocular fluid in the retrobulbar optic nerve may explain some of the proclivities for disease to affect this region (*19*).

The similarities between the brain and ocular glymphatic systems also extend to the molecular mechanisms facilitating fluid transport. In the brain, AQP4 is highly polarized toward the vascular endfeet of astrocytes, and orthogonal arrays of AQP4 constitute as much as 50% of the surface of their plasma membrane facing the vessel wall (*36*, *60*). Not surprisingly, AQP4 has been shown to facilitate both glymphatic CSF influx and clearance (*3*, *36*, *37*). In the eye, radial Müller cells spanning the neuroretina express similarly abundant AQP4 on perivascular endfoot membranes, as well as in their processes facing the vitreous (*61*). Fibrous astrocytes along the optic nerve also express AQP4, and we show here that efflux of hAβ, similar to the brain, was facilitated by AQP4 in both the retina and the optic nerve. However, the ocular fluid transport system is distinctly different from the brain at the lamina cribrosa. The hydraulic barrier provided by the lamina cribrosa permits higher pressure in the intraocular compartment than the intracranial one. The human lamina cribrosa is composed mainly of a meshwork of collagen and elastin fibers and penetrated by RGC axons and retinal vessels. In rodents, the lamina is comprised primarily of astrocytes, whose processes wrap tightly around the RGC axons, forming a barrier that excludes the passage of even low molecular weight dextrans. Astrocytes in the lamina cribrosa are notably devoid of AQP4 and other aquaporins except for the metabolite permeable aquaglyceroporin AQP9 (*61*, *62*). The unique lack of AQP4 in astrocytes of the lamina cribrosa may be a manifestation of the need to restrict fluid transfer between the perivascular space and the optic nerve at this junction, which is critical for maintaining a pressure difference (*61*). In fact, the lack of astrocytic AQP4 at the lamina could guide axonal fluid transport by restricting water permeability along alternative routes surrounding or within the astrocytes. Thus, although the brain and ocular glymphatic systems share key features, including polarization of fluid transport and a dependence on AQP4, it is clear the ocular glymphatic system is specialized around the lamina cribrosa barrier. We document that the lamina cribrosa effectively prevents efflux of extracellular tracers delivered to the vitreous compartment. Only tracers taken up by RGCs (hAβ, cadaverine, K^+-analogue $^{86}Rb^+$) and transported along their axons could pass the lamina barrier. Extracellular tracers, such as dextrans, were only able to enter the nerve in glaucomatous eyes with lamina defects (*63*). It cannot be excluded that the increased hAβ tracer signal in the optic nerve of 11-month-old DBA mice reflected a decreased influx of CSF in the optic nerve as reported by Mathieu et al. (*23*). However, the finding that glaucoma is associated with openings in the lamina cribrosa that allow passage of extracellular tracers does not support the idea that CSF washout plays a role in efflux of tracers delivered intravitreally to the optic nerve. As shown by the Yucel lab (*22*) and confirmed here, the lamina cribrosa also effectively inhibits peri-arterial influx of CSF tracers into the retina. In the brain, no such barrier has been described, and CSF tracers distribute brain-wide, albeit with regional differences in influx kinetics (*3*).

Our most surprising observation is that accumulation of APP and Aβ in experimental glaucoma is not the consequence of reduced outflow. An unexpected, excessive tracer efflux along the optic nerve was observed in two distinct models of glaucoma. Such excessive flow, due to the destruction of the glial barrier at the level of the lamina, leads to unspecific tracer efflux via the extracellular space, which we propose results in stagnation of the intra-axonal transport of APP and its cleavage product, Aβ. Considering the net decrease of outflow facility known to occur in glaucoma, the posterior efflux route described here makes a smaller contribution to the overall ocular outflow than anterior routes (*64*). However, the functional importance of this smaller volume should not be underestimated, as it may be critical for fluid/waste elimination from the retina and optic nerve (*19*).

The discovery of an ocular glymphatic system as a fluid efflux path may shed new light upon several pathologies in the eye. Up to 2.4% of the general population has a sub-clinical build-up of amyloid and other wastes in the ONH (ONH drusen), which is seen more frequently in patients with narrow scleral canals (*65*). Age-related macular degeneration (AMD), a major cause of visual loss, is also characterized by subretinal build-up of waste products, including amyloid in drusenoid deposits (*66*). Another major cause of blindness, glaucoma, was directly examined in this study. We speculate that abnormal transport of APP/Aβ or other metabolites driven by the increase in translaminar pressure contributes to the degeneration of RGC axons in early stages of glaucoma or following optic nerve injury (*67*, *68*). Additionally, the pathological increase in extracellular ocular fluid fluxes along the nerve in later-stage glaucoma might trigger additional stress in the form of both heightened metabolic demands and loss of essential cytosolic components, such as vitamin B_3 (*69*). Another important yet currently unresolved aspect of glaucoma is the large proportion (30-40%) of patients with demonstrable glaucomatous optic nerve damage who lack elevated IOP (*70*). We here propose the hypothesis that structural weakness or defects in the lamina cribrosa can lead to glaucoma in the absence of increased IOP, since the long-term redirection of glymphatic outflow from the intra-axonal to extracellular space may lead to the degeneration of RGCs (*19*, *63*).

It is important to consider the limitations of this report. Our analysis demonstrates the existence of an ocular glymphatic clearance path in several strains of mice and rats. Due to the close anatomical and physiological resemblance to human ocular drainage (*71, 72*), rodent models have been extensively used in the study of glaucoma pathophysiology and have proven valuable for drug screening (*43, 45, 46, 69, 73*). Nevertheless, examination using a primate model of glaucoma would be important in future studies. Another potential caveat is that most of the data was collected postmortem after harvesting the eye and optic nerve. Microscopic resolution is needed to map the cellular details of the flow, yet it is not possible to image tracer transport along the distal optic nerve *in vivo* since the nerve is solidly embedded in the skull. We did, however, collect a set of *in vivo* observations supporting the model proposed in **fig. S9**. Using a funduscope, we imaged real-time dispersion of cadaverine after administration in the suprachoroidal space. The analysis showed that cadaverine was transported along the optic nerve similarly to the *ex vivo* observations. Alternative approaches, such as magnetic resonance or positron emission tomography, may allow for real-time *in vivo* imaging of ocular transport. However, such studies will require identification of contrast agents or PET tracers taken up by RGCs. Alternatively, improvement of the resolution of proton (water) diffusion by magnetic resonance imaging (MRI) is of particular interest since the movement of fluid is key to understanding the ocular glymphatic system. Imaging of protons will also avoid the use of invasive vitreous injections. In fact, a limitation of this and other reports is the use of tracers to indirectly map fluid transport. The main observation reported is that tracers that exhibit cellular uptake (hAβ, cadaverine, and $^{86}Rb^{+}$) can pass the lamina cribrosa, which acts as a barrier for extracellular tracers, such as dextran and ovalbumin. We observed that hAβ transport was restricted to axons, consistent with the avid neuronal uptake of hAβ (*29*). However, it is possible that tracers taken up by astrocytes, such as cadaverine and $^{86}Rb^{+}$, are also transported across the lamina cribrosa via the astrocytic cytosol. We were concerned that vitreous injections could artificially contribute to tracer transport, but we conclude based on the arguments listed below that our methodology did not in fact lead to artefactual tracer dispersion. We show that the distribution of hAβ is independent of (1) total volume injected and (2) rate of infusion. Moreover, (3) our infusion protocol does not increase IOP, and (4) rats with much larger eyes exhibit the same pattern of hAβ transport as mice, including acceleration of transport in response to light stimulation. Finally, the presence of intravitreal-injected tracers in the cervical lymph nodes does not prove the tracers reached the cervical lymphatic system only by transport along the optic nerve. Efflux of ocular fluid from trabecular and uveoscleral pathways also accumulates in cervical lymph nodes (*2, 35*). The analysis of cervical lymph nodes was included here to outline the entire ocular export pathway.

Toxicity of amyloid-β was not a limitation of the study. An in-depth analysis of two eyes from the same mouse injected with either vehicle or hAβ tracer found no evidence of either reactive astro- or microgliosis or caspase-3 activation. We also found no sign of BRB opening in response to vitreous administration of hAβ. In fact, a screen for 32 cytokines/chemokines showed that our protocol for hAβ intravitreal tracer injection did not evoke an immune response within the experimental timeframe. Earlier reports have noted that subretinal injection and prolonged exposure to elevated amounts of hAβ (days to weeks) can induce toxicity (*74, 75*), but such effects were not noted in our study, which was limited to at most two hours exposure to hAβ. Thus, we are confident that the current study design likely avoided activation of hAβ-induced pathological processes.

Taken together, our analysis provides evidence for the existence of a highly-polarized ocular clearance system that might have implications for our understanding of eye health and disease.

Materials and Methods

Study design

The goal of this study was to understand how the metabolically-active retina and optic nerve, being both devoid of lymphatics and distant from traditional ocular fluid efflux mechanisms, handle waste/fluid. By injecting multiple biologically-relevant or inert tracers into the vitreous, with which the retina directly and freely exchanges fluid, we anatomically characterized an eye-to-CSF clearance pathway that resembles the brain's glymphatic. We then sought to evaluate how physiological conditions of the ocular system interact with this clearance system by applying visual stimulation or manipulating the TPD. Finally, using two distinct murine models of glaucoma, we examined how waste/fluid handling changed in pathological conditions.

Animal sample sizes were calculated on the basis of a pilot study. Outlier detection based on the ROUT method (*76*) was performed before statistical analysis with confidence threshold Q = 0.1%. Mice with initial IOP > 55 mmHg following CLS were excluded, as this elevation of IOP can impair retinal perfusion (*46*). Animals were randomly assigned and blinding was done for investigators carrying out analysis. Group and sample sizes for each experiment are indicated in the figure legends.

Statistical analysis

Statistical analysis was performed with the aid of GraphPad Prism 6.0c (GraphPad Software). Normality of the data was tested by Kolmogorov Smirnov test. For variables that passed the normality test (at significance level of $\alpha = 0.05$), parametric statistical methods, such as the two-sample Welch *t*-test (for comparing the mean equality of two samples) or one-way ANOVA *F*-test (for testing mean equality among more than two groups), were employed. Following one-way ANOVA analyses, Tukey's or Dunnett's *post hoc* analyses were performed to identify significant pairwise group mean differences. For those variables that did not pass the normality test, nonparametric methods, such as the Mann-Whitney *U* test (for independent two-group comparisons), Wilcoxon signed-rank test (for comparing matched samples), or Kruskal-Wallis test (for comparing multiple groups), were used instead. Following Kruskal-Wallis one-way ANOVA, Dunn's *post hoc* analyses were performed to detect significant pairwise group median differences. Two-way ANOVA followed by Sidak's multiple comparisons was performed when two different categorical independent variables were assessed. A significance level of $\alpha = 0.05$ was used in all statistical tests performed in this study. Values are expressed as the mean ± SEM if not otherwise stated.

Supplementary Materials

Supplementary materials and methods

Fig. S1 Characterization of additional tracers and tracer delivery routes.

Fig. S2 Brief retinal exposure to trace amounts of hAβ using our intravitreal infusion paradigm does not induce gliosis, microglial activation, apoptosis or blood-retinal barrier disruption.

Fig. S3 Detailed analysis of ocular glymphatic clearance route.

Fig. S4 Validation of tracer delivery model in another species and with different infusion parameters.

Fig. S5 Light stimulation accelerates hAβ tracer movement along the optic nerve.

Fig. S6 Influence of the translaminar pressure difference on stimulated and unstimulated tracer movement.

Fig. S7 Tracer efflux pattern in murine glaucoma model indicates leaky lamina that may allow bypass of intra-axonal transport via extracellular route.

Fig. S8 Murine glaucoma models reveal defects in the lamina barrier allowing escape of large intraocular tracers.

Fig. S9 Schematic model of the ocular glymphatic clearance system and its dysfunction in a murine model of glaucoma.

Table S1. Tabular summary of all the data.

Table S2 Retinal cytokine assay comparing intravitreal hAβ injection to vehicle

Table S3 Comparing the controls for the DBA/2J strain.

Table S4 Tracers used and their route of administration.

Captions for Movie S1

Movie S1 Animation of the proposed mechanism for ocular glymphatic clearance in the healthy optic nerve and glaucoma.

References and Notes

1. K. Aukland, R. K. Reed, Interstitial-lymphatic mechanisms in the control of extracellular fluid volume. *Physiological reviews* **73**, 1-78 (1993).
2. Y. H. Yucel, M. G. Johnston, T. Ly, M. Patel, B. Drake, E. Gumus, S. A. Fraenkl, S. Moore, D. Tobbia, D. Armstrong, E. Horvath, N. Gupta, Identification of lymphatics in the ciliary body of the human eye: a novel "uveolymphatic" outflow pathway. *Experimental eye research* **89**, 810-819 (2009).
3. J. J. Iliff, M. Wang, Y. Liao, B. A. Plogg, W. Peng, G. A. Gundersen, H. Benveniste, G. E. Vates, R. Deane, S. A. Goldman, E. A. Nagelhus, M. Nedergaard, A paravascular pathway facilitates CSF flow through the brain parenchyma and the clearance of interstitial solutes, including amyloid beta. *Science translational medicine* **4**, 147ra111 (2012).
4. A. Louveau, I. Smirnov, T. J. Keyes, J. D. Eccles, S. J. Rouhani, J. D. Peske, N. C. Derecki, D. Castle, J. W. Mandell, K. S. Lee, T. H. Harris, J. Kipnis, Structural and functional features of central nervous system lymphatic vessels. *Nature* **523**, 337-341 (2015).
5. A. Aspelund, S. Antila, S. T. Proulx, T. V. Karlsen, S. Karaman, M. Detmar, H. Wiig, K. Alitalo, A dural lymphatic vascular system that drains brain interstitial fluid and macromolecules. *The Journal of experimental medicine* **212**, 991-999 (2015).
6. J. H. Ahn, H. Cho, J. H. Kim, S. H. Kim, J. S. Ham, I. Park, S. H. Suh, S. P. Hong, J. H. Song, Y. K. Hong, Y. Jeong, S. H. Park, G. Y. Koh, Meningeal lymphatic vessels at the skull base drain cerebrospinal fluid. *Nature* **572**, 62-66 (2019).

7. P. K. Eide, S. A. S. Vatnehol, K. E. Emblem, G. Ringstad, Magnetic resonance imaging provides evidence of glymphatic drainage from human brain to cervical lymph nodes. *Scientific reports* **8**, 7194 (2018).

8. M. Absinta, S. K. Ha, G. Nair, P. Sati, N. J. Luciano, M. Palisoc, A. Louveau, K. A. Zaghloul, S. Pittaluga, J. Kipnis, D. S. Reich, Human and nonhuman primate meninges harbor lymphatic vessels that can be visualized noninvasively by MRI. *eLife* **6**, (2017).

9. T. Myllyla, M. Harju, V. Korhonen, A. Bykov, V. Kiviniemi, I. Meglinski, Assessment of the dynamics of human glymphatic system by near-infrared spectroscopy. *Journal of biophotonics* **11**, e201700123 (2018).

10. G. Ringstad, S. A. S. Vatnehol, P. K. Eide, Glymphatic MRI in idiopathic normal pressure hydrocephalus. *Brain : a journal of neurology* **140**, 2691-2705 (2017).

11. V. Kiviniemi, X. Wang, V. Korhonen, T. Keinanen, T. Tuovinen, J. Autio, P. LeVan, S. Keilholz, Y. F. Zang, J. Hennig, M. Nedergaard, Ultra-fast magnetic resonance encephalography of physiological brain activity - Glymphatic pulsation mechanisms? *Journal of cerebral blood flow and metabolism : official journal of the International Society of Cerebral Blood Flow and Metabolism* **36**, 1033-1045 (2016).

12. M. Nedergaard, Neuroscience. Garbage truck of the brain. *Science (New York, N.Y.)* **340**, 1529-1530 (2013).

13. Y. Koronyo, D. Biggs, E. Barron, D. S. Boyer, J. A. Pearlman, W. J. Au, S. J. Kile, A. Blanco, D. T. Fuchs, A. Ashfaq, S. Frautschy, G. M. Cole, C. A. Miller, D. R. Hinton, S. R. Verdooner, K. L. Black, M. Koronyo-Hamaoui, Retinal amyloid pathology and proof-of-concept imaging trial in Alzheimer's disease. *JCI insight* **2**, (2017).

14. J. E. Kang, M. M. Lim, R. J. Bateman, J. J. Lee, L. P. Smyth, J. R. Cirrito, N. Fujiki, S. Nishino, D. M. Holtzman, Amyloid-beta dynamics are regulated by orexin and the sleep-wake cycle. *Science (New York, N.Y.)* **326**, 1005-1007 (2009).
15. J. K. Holth, S. K. Fritschi, C. Wang, N. P. Pedersen, J. R. Cirrito, T. E. Mahan, M. B. Finn, M. Manis, J. C. Geerling, P. M. Fuller, B. P. Lucey, D. M. Holtzman, The sleep-wake cycle regulates brain interstitial fluid tau in mice and CSF tau in humans. *Science (New York, N.Y.)* **363**, 880-884 (2019).
16. K. Yamamoto, Z. I. Tanei, T. Hashimoto, T. Wakabayashi, H. Okuno, Y. Naka, O. Yizhar, L. E. Fenno, M. Fukayama, H. Bito, J. R. Cirrito, D. M. Holtzman, K. Deisseroth, T. Iwatsubo, Chronic optogenetic activation augments abeta pathology in a mouse model of Alzheimer disease. *Cell Rep* **11**, 859-865 (2015).
17. L. Xie, H. Kang, Q. Xu, M. J. Chen, Y. Liao, M. Thiyagarajan, J. O'Donnell, D. J. Christensen, C. Nicholson, J. J. Iliff, T. Takano, R. Deane, M. Nedergaard, Sleep drives metabolite clearance from the adult brain. *Science (New York, N.Y.)* **342**, 373-377 (2013).
18. A. K. Denniston, P. A. Keane, Paravascular Pathways in the Eye: Is There an 'Ocular Glymphatic System'? *Investigative ophthalmology & visual science* **56**, 3955-3956 (2015).
19. P. Wostyn, V. De Groot, D. Van Dam, K. Audenaert, H. E. Killer, P. P. De Deyn, The Glymphatic Hypothesis of Glaucoma: A Unifying Concept Incorporating Vascular, Biomechanical, and Biochemical Aspects of the Disease. *BioMed research international* **2017**, 5123148 (2017).
20. A. Petzold, Retinal glymphatic system: an explanation for transient retinal layer volume changes? *Brain : a journal of neurology* **139**, 2816-2819 (2016).

21. P. Wostyn, D. Van Dam, K. Audenaert, H. E. Killer, P. P. De Deyn, V. De Groot, A new glaucoma hypothesis: a role of glymphatic system dysfunction. *Fluids Barriers CNS* **12**, 16 (2015).

22. E. Mathieu, N. Gupta, A. Ahari, X. Zhou, J. Hanna, Y. H. Yucel, Evidence for Cerebrospinal Fluid Entry Into the Optic Nerve via a Glymphatic Pathway. *Investigative ophthalmology & visual science* **58**, 4784-4791 (2017).

23. E. Mathieu, N. Gupta, L. A. Paczka-Giorgi, X. Zhou, A. Ahari, R. Lani, J. Hanna, Y. H. Yucel, Reduced Cerebrospinal Fluid Inflow to the Optic Nerve in Glaucoma. *Investigative ophthalmology & visual science* **59**, 5876-5884 (2018).

24. Y. Ito, M. Shimazawa, K. Tsuruma, C. Mayama, K. Ishii, H. Onoe, M. Aihara, M. Araie, H. Hara, Induction of amyloid-beta(1-42) in the retina and optic nerve head of chronic ocular hypertensive monkeys. *Molecular vision* **18**, 2647-2657 (2012).

25. K. U. Loffler, D. P. Edward, M. O. Tso, Immunoreactivity against tau, amyloid precursor protein, and beta-amyloid in the human retina. *Investigative ophthalmology & visual science* **36**, 24-31 (1995).

26. C. Pan, R. Cai, F. P. Quacquarelli, A. Ghasemigharagoz, A. Lourbopoulos, P. Matryba, N. Plesnila, M. Dichgans, F. Hellal, A. Erturk, Shrinkage-mediated imaging of entire organs and organisms using uDISCO. *Nature methods* **13**, 859-867 (2016).

27. A. Armulik, G. Genove, M. Mae, M. H. Nisancioglu, E. Wallgard, C. Niaudet, L. He, J. Norlin, P. Lindblom, K. Strittmatter, B. R. Johansson, C. Betsholtz, Pericytes regulate the blood-brain barrier. *Nature* **468**, 557-561 (2010).

28. W. L. Murfee, T. C. Skalak, S. M. Peirce, Differential arterial/venous expression of NG2 proteoglycan in perivascular cells along microvessels: Identifying a venule-specific phenotype. *Microcirculation* **12**, 151-160 (2005).

29. T. Kanekiyo, J. R. Cirrito, C. C. Liu, M. Shinohara, J. Li, D. R. Schuler, M. Shinohara, D. M. Holtzman, G. Bu, Neuronal clearance of amyloid-beta by endocytic receptor LRP1. *The Journal of neuroscience : the official journal of the Society for Neuroscience* **33**, 19276-19283 (2013).

30. R. E. Gausas, R. S. Gonnering, B. N. Lemke, R. K. Dortzbach, D. D. Sherman, Identification of human orbital lymphatics. *Ophthalmic Plast Reconstr Surg* **15**, 252-259 (1999).

31. H. E. Killer, H. R. Laeng, P. Groscurth, Lymphatic capillaries in the meninges of the human optic nerve. *J Neuroophthalmol* **19**, 222-228 (1999).

32. L. Chen, Ocular lymphatics: state-of-the-art review. *Lymphology* **42**, 66-76 (2009).

33. E. Mathieu, N. Gupta, R. L. Macdonald, J. Ai, Y. H. Yucel, In vivo imaging of lymphatic drainage of cerebrospinal fluid in mouse. *Fluids Barriers CNS* **10**, 35 (2013).

34. Q. Ma, B. V. Ineichen, M. Detmar, S. T. Proulx, Outflow of cerebrospinal fluid is predominantly through lymphatic vessels and is reduced in aged mice. *Nature communications* **8**, 1434 (2017).

35. Y. H. Yucel, K. Cardinell, S. Khattak, X. Zhou, M. Lapinski, F. Cheng, N. Gupta, Active Lymphatic Drainage From the Eye Measured by Noninvasive Photoacoustic Imaging of Near-Infrared Nanoparticles. *Investigative ophthalmology & visual science* **59**, 2699-2707 (2018).

36. T. M. Mathiisen, K. P. Lehre, N. C. Danbolt, O. P. Ottersen, The perivascular astroglial sheath provides a complete covering of the brain microvessels: an electron microscopic 3D reconstruction. *Glia* **58**, 1094-1103 (2010).

37. H. Mestre, L. M. Hablitz, A. L. Xavier, W. Feng, W. Zou, T. Pu, H. Monai, G. Murlidharan, R. M. Castellanos Rivera, M. J. Simon, M. M. Pike, V. Pla, T. Du, B. T. Kress, X. Wang, B. A. Plog, A. S. Thrane, I. Lundgaard, Y. Abe, M. Yasui, J. H. Thomas, M. Xiao, H. Hirase, A. Asokan, J. J. Iliff, M. Nedergaard, Aquaporin-4-dependent glymphatic solute transport in the rodent brain. *eLife* **7**, (2018).

38. J. E. Morgan, Circulation and axonal transport in the optic nerve. *Eye* **18**, 1089-1095 (2004).

39. D. M. Nusbaum, S. M. Wu, B. J. Frankfort, Elevated intracranial pressure causes optic nerve and retinal ganglion cell degeneration in mice. *Experimental eye research* **136**, 38-44 (2015).

40. S. A. Read, M. J. Collins, H. Becker, J. Cutting, D. Ross, A. K. Savill, B. Trevor, Changes in intraocular pressure and ocular pulse amplitude with accommodation. *The British journal of ophthalmology* **94**, 332-335 (2010).

41. D. J. Coleman, On the hydraulic suspension theory of accommodation. *Trans Am Ophthalmol Soc* **84**, 846-868 (1986).

42. R. N. Weinreb, T. Aung, F. A. Medeiros, The pathophysiology and treatment of glaucoma: a review. *Jama* **311**, 1901-1911 (2014).

43. M. G. Anderson, R. S. Smith, N. L. Hawes, A. Zabaleta, B. Chang, J. L. Wiggs, S. W. John, Mutations in genes encoding melanosomal proteins cause pigmentary glaucoma in DBA/2J mice. *Nature genetics* **30**, 81-85 (2002).

44. R. T. Libby, M. G. Anderson, I. H. Pang, Z. H. Robinson, O. V. Savinova, I. M. Cosma, A. Snow, L. A. Wilson, R. S. Smith, A. F. Clark, S. W. John, Inherited glaucoma in DBA/2J mice: pertinent disease features for studying the neurodegeneration. *Visual neuroscience* **22**, 637-648 (2005).
45. K. A. Fernandes, J. M. Harder, P. A. Williams, R. L. Rausch, A. E. Kiernan, K. S. Nair, M. G. Anderson, S. W. John, G. R. Howell, R. T. Libby, Using genetic mouse models to gain insight into glaucoma: Past results and future possibilities. *Experimental eye research* **141**, 42-56 (2015).
46. H. H. Liu, L. Zhang, M. Shi, L. Chen, J. G. Flanagan, Comparison of laser and circumlimbal suture induced elevation of intraocular pressure in albino CD-1 mice. *PloS one* **12**, e0189094 (2017).
47. M. D. Roberts, V. Grau, J. Grimm, J. Reynaud, A. J. Bellezza, C. F. Burgoyne, J. C. Downs, Remodeling of the connective tissue microarchitecture of the lamina cribrosa in early experimental glaucoma. *Investigative ophthalmology & visual science* **50**, 681-690 (2009).
48. S. Tehrani, E. C. Johnson, W. O. Cepurna, J. C. Morrison, Astrocyte processes label for filamentous actin and reorient early within the optic nerve head in a rat glaucoma model. *Investigative ophthalmology & visual science* **55**, 6945-6952 (2014).
49. W. K. Ju, K. Y. Kim, J. D. Lindsey, M. Angert, K. X. Duong-Polk, R. T. Scott, J. J. Kim, I. Kukhmazov, M. H. Ellisman, G. A. Perkins, R. N. Weinreb, Intraocular pressure elevation induces mitochondrial fission and triggers OPA1 release in glaucomatous optic nerve. *Investigative ophthalmology & visual science* **49**, 4903-4911 (2008).

50. R. Wang, P. Seifert, T. C. Jakobs, Astrocytes in the Optic Nerve Head of Glaucomatous Mice Display a Characteristic Reactive Phenotype. *Investigative ophthalmology & visual science* **58**, 924-932 (2017).

51. M. Goel, R. G. Picciani, R. K. Lee, S. K. Bhattacharya, Aqueous humor dynamics: a review. *Open Ophthalmol J* **4**, 52-59 (2010).

52. P. Wostyn, D. Van Dam, P. P. De Deyn, Intracranial pressure and glaucoma: Is there a new therapeutic perspective on the horizon? *Med Hypotheses* **118**, 98-102 (2018).

53. A. K. Palkama, D. Velasquez, J. Reynaud, H. W. Thompson, R. W. Beuerman, Regulatory effect of pilocarpine and/or atropine on the facility of outflow in perfused bovine anterior eye segments and intact trabecular meshwork and ciliary. *Investigative ophthalmology & visual science* **43**, U900-U900 (2002).

54. M. A. Croft, E. Lutjen-Drecoll, P. L. Kaufman, Age-related posterior ciliary muscle restriction - A link between trabecular meshwork and optic nerve head pathophysiology. *Experimental eye research* **158**, 187-189 (2017).

55. R. Christen, M. Pache, B. Teuchner, P. Meyer, C. Prunte, J. Flammer, Iris transillumination defects in patients with primary open angle glaucoma. *European journal of ophthalmology* **13**, 365-369 (2003).

56. P. Wostyn, V. De Groot, D. Van Dam, K. Audenaert, P. P. De Deyn, H. E. Killer, The Glymphatic System: A New Player in Ocular Diseases? *Investigative ophthalmology & visual science* **57**, 5426-5427 (2016).

57. P. Wostyn, H. E. Killer, P. P. De Deyn, Glymphatic stasis at the site of the lamina cribrosa as a potential mechanism underlying open-angle glaucoma. *Clinical & experimental ophthalmology* **45**, 539-547 (2017).

58. P. Wostyn, P. P. De Deyn, The "Ocular Glymphatic System": An Important Missing Piece in the Puzzle of Optic Disc Edema in Astronauts? *Investigative ophthalmology & visual science* **59**, 2090-2091 (2018).

59. P. Wostyn, F. De Winne, C. Stern, P. P. De Deyn, Dilated Prelaminar Paravascular Spaces as a Possible Mechanism for Optic Disc Edema in Astronauts. *Aerosp Med Hum Perform* **89**, 1089-1091 (2018).

60. J. E. Rash, T. Yasumura, Direct immunogold labeling of connexins and aquaporin-4 in freeze-fracture replicas of liver, brain, and spinal cord: factors limiting quantitative analysis. *Cell Tissue Res* **296**, 307-321 (1999).

61. E. A. Nagelhus, M. L. Veruki, R. Torp, F. M. Haug, J. H. Laake, S. Nielsen, P. Agre, O. P. Ottersen, Aquaporin-4 water channel protein in the rat retina and optic nerve: polarized expression in Muller cells and fibrous astrocytes. *The Journal of neuroscience : the official journal of the Society for Neuroscience* **18**, 2506-2519 (1998).

62. M. Naka, A. Kanamori, A. Negi, M. Nakamura, Reduced expression of aquaporin-9 in rat optic nerve head and retina following elevated intraocular pressure. *Investigative ophthalmology & visual science* **51**, 4618-4626 (2010).

63. C. F. Burgoyne, J. C. Downs, A. J. Bellezza, J. K. Suh, R. T. Hart, The optic nerve head as a biomechanical structure: a new paradigm for understanding the role of IOP-related stress and strain in the pathophysiology of glaucomatous optic nerve head damage. *Prog Retin Eye Res* **24**, 39-73 (2005).

64. S. C. Sacca, S. Gandolfi, A. Bagnis, G. Manni, G. Damonte, C. E. Traverso, A. Izzotti, The Outflow Pathway: A Tissue With Morphological and Functional Unity. *J Cell Physiol* **231**, 1876-1893 (2016).

65. L. Malmqvist, X. Q. Li, C. L. Eckmann, A. M. Skovgaard, E. M. Olsen, M. Larsen, I. C. Munch, S. Hamann, Optic Disc Drusen in Children: The Copenhagen Child Cohort 2000 Eye Study. *J Neuroophthalmol* **38**, 140-146 (2018).
66. D. H. Anderson, K. C. Talaga, A. J. Rivest, E. Barron, G. S. Hageman, L. V. Johnson, Characterization of beta amyloid assemblies in drusen: the deposits associated with aging and age-related macular degeneration. *Experimental eye research* **78**, 243-256 (2004).
67. B. P. Buckingham, D. M. Inman, W. Lambert, E. Oglesby, D. J. Calkins, M. R. Steele, M. L. Vetter, N. Marsh-Armstrong, P. J. Horner, Progressive ganglion cell degeneration precedes neuronal loss in a mouse model of glaucoma. *The Journal of neuroscience : the official journal of the Society for Neuroscience* **28**, 2735-2744 (2008).
68. C. Liu, C. W. Zhang, Y. Zhou, W. Q. Wong, L. C. Lee, W. Y. Ong, S. O. Yoon, W. Hong, X. Y. Fu, T. W. Soong, E. H. Koo, L. W. Stanton, K. L. Lim, Z. C. Xiao, G. S. Dawe, APP upregulation contributes to retinal ganglion cell degeneration via JNK3. *Cell death and differentiation* **25**, 661-676 (2018).
69. P. A. Williams, J. M. Harder, N. E. Foxworth, K. E. Cochran, V. M. Philip, V. Porciatti, O. Smithies, S. W. John, Vitamin B3 modulates mitochondrial vulnerability and prevents glaucoma in aged mice. *Science (New York, N.Y.)* **355**, 756-760 (2017).
70. A. Sommer, J. M. Tielsch, J. Katz, H. A. Quigley, J. D. Gottsch, J. Javitt, K. Singh, Relationship between Intraocular-Pressure and Primary Open Angle Glaucoma among White and Black-Americans - the Baltimore Eye Survey. *Arch Ophthalmol-Chic* **109**, 1090-1095 (1991).

71. R. S. Smith, A. Zabaleta, O. V. Savinova, S. W. John, The mouse anterior chamber angle and trabecular meshwork develop without cell death. *BMC developmental biology* **1**, 3-3 (2001).

72. M. Johnson, J. W. McLaren, D. R. Overby, Unconventional aqueous humor outflow: A review. *Experimental eye research* **158**, 94-111 (2017).

73. W. M. Dismuke, D. R. Overby, M. M. Civan, W. D. Stamer, The Value of Mouse Models for Glaucoma Drug Discovery. *J Ocul Pharmacol Ther* **32**, 486-487 (2016).

74. V. Dinet, J. Bruban, N. Chalour, A. Maoui, N. An, L. Jonet, A. Buret, F. Behar-Cohen, C. Klein, J. Treton, F. Mascarelli, Distinct effects of inflammation on gliosis, osmohomeostasis, and vascular integrity during amyloid beta-induced retinal degeneration. *Aging Cell* **11**, 683-693 (2012).

75. M. A. Mohd Lazaldin, I. Iezhitsa, R. Agarwal, N. S. Bakar, P. Agarwal, N. Mohd Ismail, Time- and dose-related effects of amyloid beta1-40 on retina and optic nerve morphology in rats. *Int J Neurosci* **128**, 952-965 (2018).

76. H. J. Motulsky, R. E. Brown, Detecting outliers when fitting data with nonlinear regression - a new method based on robust nonlinear regression and the false discovery rate. *BMC Bioinformatics* **7**, 123 (2006).

77. A. S. Thrane, P. M. Rappold, T. Fujita, A. Torres, L. K. Bekar, T. Takano, W. Peng, F. Wang, V. Rangroo Thrane, R. Enger, N. N. Haj-Yasein, O. Skare, T. Holen, A. Klungland, O. P. Ottersen, M. Nedergaard, E. A. Nagelhus, Critical role of aquaporin-4 (AQP4) in astrocytic Ca2+ signaling events elicited by cerebral edema. *Proceedings of the National Academy of Sciences of the United States of America* **108**, 846-851 (2011).

78. G. J. Kang, T. Ecoiffier, T. Truong, D. Yuen, G. Li, N. Lee, L. Zhang, L. Chen, Intravital Imaging Reveals Dynamics of Lymphangiogenesis and Valvulogenesis. *Scientific reports* **6**, 19459 (2016).

79. H. H. Liu, B. V. Bui, C. T. Nguyen, J. M. Kezic, A. J. Vingrys, Z. He, Chronic ocular hypertension induced by circumlimbal suture in rats. *Investigative ophthalmology & visual science* **56**, 2811-2820 (2015).

80. B. Gu, J. K. Liu, X. L. Li, Q. K. Ma, M. X. Shen, L. Y. Cheng, Real-Time Monitoring of Suprachoroidal Space (SCS) Following SCS Injection Using Ultra-High Resolution Optical Coherence Tomography in Guinea Pig Eyes. *Investigative ophthalmology & visual science* **56**, 3623-3634 (2015).

81. W. Peng, T. M. Achariyar, B. Li, Y. Liao, H. Mestre, E. Hitomi, S. Regan, T. Kasper, S. Peng, F. Ding, H. Benveniste, M. Nedergaard, R. Deane, Suppression of glymphatic fluid transport in a mouse model of Alzheimer's disease. *Neurobiol Dis* **93**, 215-225 (2016).

82. C. Zhang, J. Lin, F. Wei, J. Song, W. Chen, L. Shan, R. Xue, G. Wang, J. Tao, G. Zhang, G. Y. Xu, L. Wang, Characterizing the glymphatic influx by utilizing intracisternal infusion of fluorescently conjugated cadaverine. *Life sciences* **201**, 150-160 (2018).

83. F. Wei, C. Zhang, R. Xue, L. D. Shan, S. Gong, G. Q. Wang, J. Tao, G. Y. Xu, G. X. Zhang, L. H. Wang, The pathway of subarachnoid CSF moving into the spinal parenchyma and the role of astrocytic aquaporin-4 in this process. *Life sciences* **182**, 29-40 (2017).

84. A. Santillan, D. G. Rubin, C. P. Foley, D. Sondhi, R. G. Crystal, Y. P. Gobin, D. J. Ballon, Cannulation of the internal carotid artery in mice: a novel technique for intra-arterial delivery of therapeutics. *J Neurosci Methods* **222**, 106-110 (2014).

85. I. Adini, K. Ghosh, Mouse Retinal Whole Mounts and Quantification of Vasculature Protocol. *Bio Protoc* **5**, (2015).

86. A. R. Rodriguez, L. P. D. Muller, N. C. Brecha, The RNA binding protein RBPMS is a selective marker of ganglion cells in the mammalian retina. *J Comp Neurol* **522**, 1411-1443 (2014).

87. S. W. John, J. R. Hagaman, T. E. MacTaggart, L. Peng, O. Smithes, Intraocular pressure in inbred mouse strains. *Investigative ophthalmology & visual science* **38**, 249-253 (1997).

88. C. Nicholson, Ion-selective microelectrodes and diffusion measurements as tools to explore the brain cell microenvironment. *J Neurosci Methods* **48**, 199-213 (1993).

89. Q. Xu, T. Qaum, A. P. Adamis, Sensitive blood-retinal barrier breakdown quantitation using Evans blue. *Investigative ophthalmology & visual science* **42**, 789-794 (2001).

Acknowledgements

We thank Karen L. Bentley and Gayle Schneider from the URMC Electron Microscope Research Core Facility, Wei Song, Shinya Sakurai and Jinwook Jung for technical support; Charles Nicholson for discussions, Vinita Rangroo Thrane and Paul Cumming for comments on the manuscript, and Dan Xue for graphic illustrations and animations. We thank Xing Qiu and Jiatong Sui for their statistical expertise. **Funding:** This project has received funding from the European Research Council (ERC) under the European Union's Horizon 2020 research and innovation program (grant agreement no. 742112), the Novo Nordisk and the Lundbeck Foundations, the Dr. Miriam and Sheldon G. Adelson Medical Research Foundation, the NIH/NINDS/NIA/NEI (R01NS100366, RF1AG057575, R01EY028995), the Research to Prevent Blindness Foundation (Dr. Nedergaard is a recipient of a Research to Prevent Blindness Stein Innovation Award) and the Cure Alzheimer's Fund. Western Norway Regional Health Authority (Helse Vest grants nos. 912179 and 912230), Norwegian Glaucoma Research Foundation. The content is solely the responsibility of the authors and does not necessarily represent the official views of the sponsors. **Author contributions:** M.N. and L.C. supervised research. X.W., N.L., A.S.T. and M.N. designed the experiments, performed the data analysis, prepared the figures and wrote the manuscript. B.F. and X.W. performed uDISCO experiments. Q.X. performed TMA^+ recordings. X.W. and P.K.J. performed pupillometry. X.W., A.E., Y.Y., N.L. performed IOP recordings. X.W., N.L., A.E., Y.Y., A.L., Q.X., S.P., A.L.R.X., C.D., B.S. performed the remainder of imaging, data collection and analysis. X.W., L.C., Y.Y., M.S., N.L., and R.T.L. generated murine models. Data needed to evaluate the conclusion is presented in this manuscript or supplementary material. **Competing interests:** The authors declare no competing interests. **Data and materials availability:** All data associated with this study are present in the paper or the Supplementary Materials.

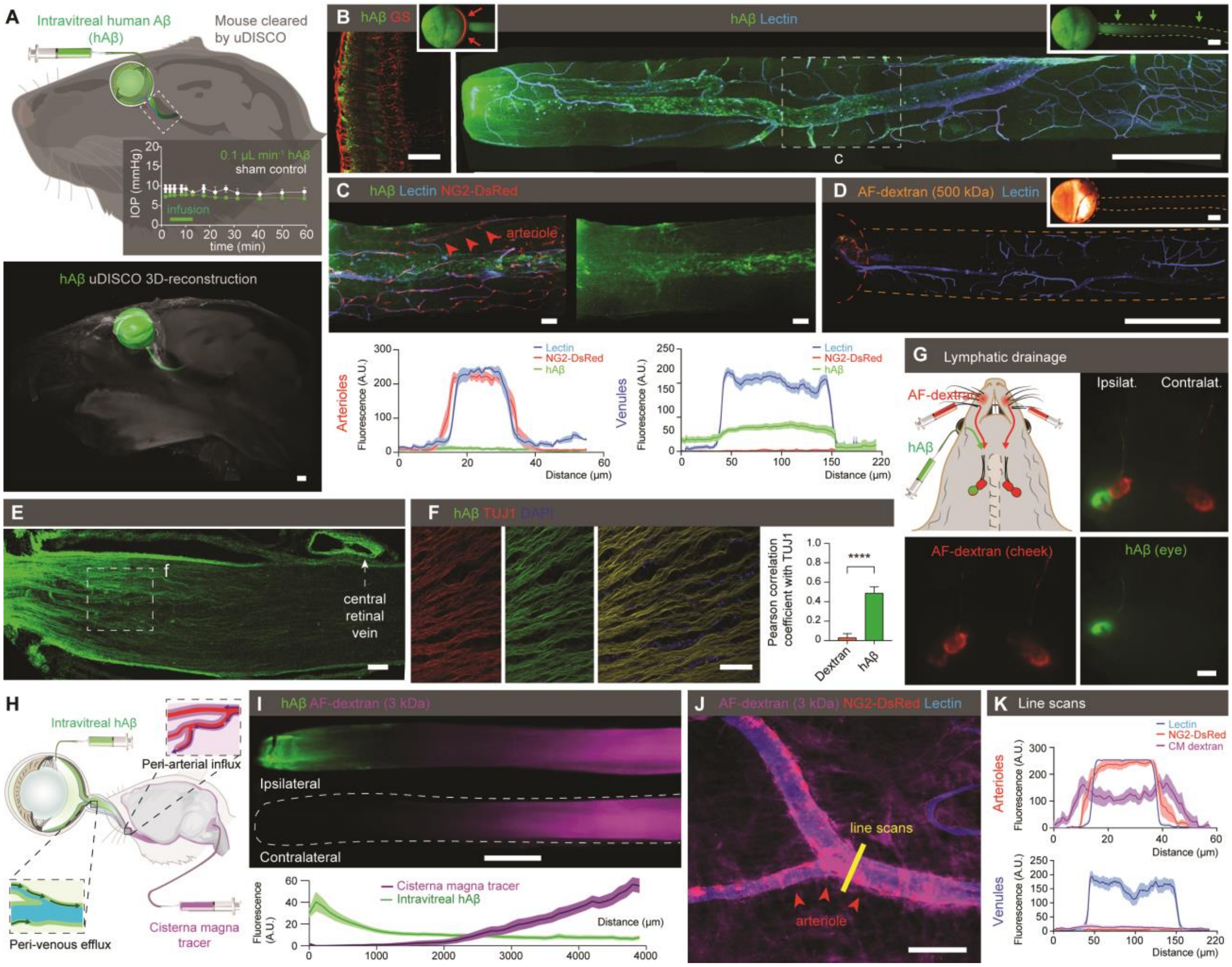

Figure 1. Existence of an ocular glymphatic clearance system. (**A**) Top: Schematic of intravitreal injection of hAβ. Insert: IOP during injection (n = 5, p = 0.0516-0.543, unpaired two-tailed t-test). Rectangle indicates proximal optic nerve displayed in panels **B-J.** Bottom: uDISCO-cleared transparent mouse heads one hour after hAβ injection. (**B**) Confocal images of ipsilateral retina (left) and optic nerve (right) following hAβ intravitreal injection. **B** and **D** inserts display macroscopic images of the eye and optic nerve injected with respective tracers without background subtraction. (**C**) Confocal imaging and quantification of optic nerve from reporter mouse with DsRed-tagged mural cells (vascular smooth muscle cells and pericytes) 30min following intravitreal hAβ injection (mean ± SEM, n = 12-19). (**D**) Confocal image of mouse optic nerve 30min following intravitreal AF-dextran injection. (**E-F**) Confocal imaging and quantification of optic nerve co-labeling with TUJ1 following tracer administration (n = 9-11 ****p <

0.0001 unpaired, two-tailed *t*-test). (**G**) Cervical lymph nodes exhibiting intense hAβ labeling three hours after injection. (**H**) Schematic of the double injections. (**I**) Representative image and quantification of double injections of hAβ intravitreally and fluorescent tracer intercisternally (mean ± SEM, $n = 12$). (**J**) Confocal imaging of optic nerve from reporter mouse with DsRed-tagged mural cells (vascular smooth muscle cells and pericytes) following intracisternal dextran injection with line scan quantified in (K) (mean ± SEM, $n = 8$-9). (Scales: **A**, **B** right, **D**, **G, I**: 500 µm; **B** left, **C**, **E**, **F**, **J**: 50 µm).

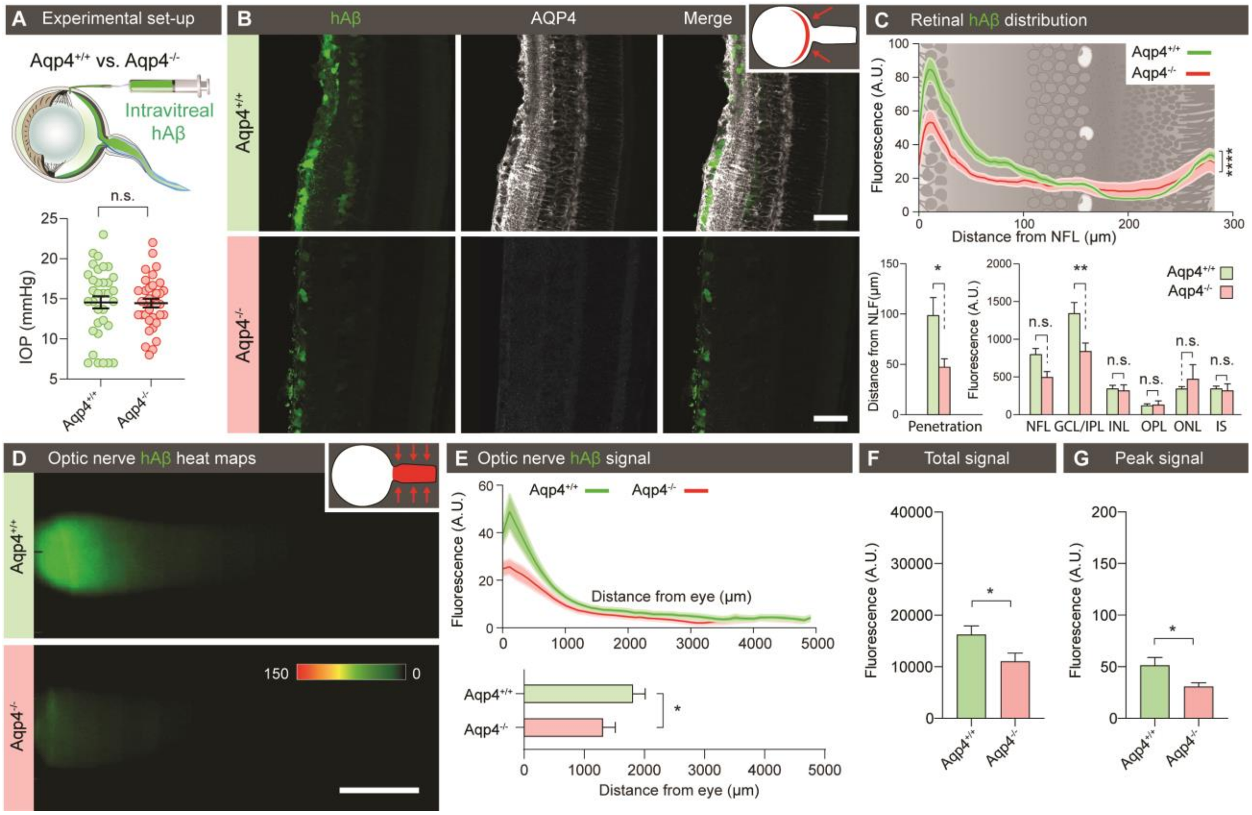

Figure 2. Ocular glymphatic clearance is AQP4-dependent. (**A**) Top: Experimental set-up comparing tracer clearance from the retina and optic nerve following intravitreal injection in *Aqp4*$^{+/+}$ and *Aqp4*$^{-/-}$ mice. Bottom: scatter plot with mean ± SEM overlaid, comparing intraocular pressure (IOP) in *Aqp4*$^{+/+}$ and *Aqp4*$^{-/-}$ mice prior to the injection. (**B**) Representative transverse sections of retina collected 30 min after intravitreal hAβ injection and counter-stained for AQP4. (**C**) Line graph overlaid on retinal illustration (left panel) and bar graphs (right panel) comparing hAβ tracer penetration (n = 7-9, *$p < 0.05$, Man-Whitney test) into the various retinal layers (n = 7-9, ** $p < 0.01$, ****$p < 0.0001$, two-way ANOVA followed by Sidak's multiple comparisons test). (**D**) Representative background-subtracted heat-maps of hAβ signal in the optic nerves of *Aqp4*$^{+/+}$ and *Aqp4*$^{-/-}$ mice 30 min after intravitreal injection. (**E**) Upper-panel: Averaged fluorescent intensity profiles of hAβ in the optic nerves from the two groups. Lower-panel: The distance of tracer transport (n = 24-25 *$p < 0.05$ Mann-Whitney test). (**F-G**) Total hAβ signal and peak intensity in the optic nerve 30 min after intravitreal injection (n = 24-25 *$p < 0.05$, unpaired two-tailed t-test for total signal Mann-Whitney test for peak). (Scales: **B**: 50 μm, **D**: 100 μm).

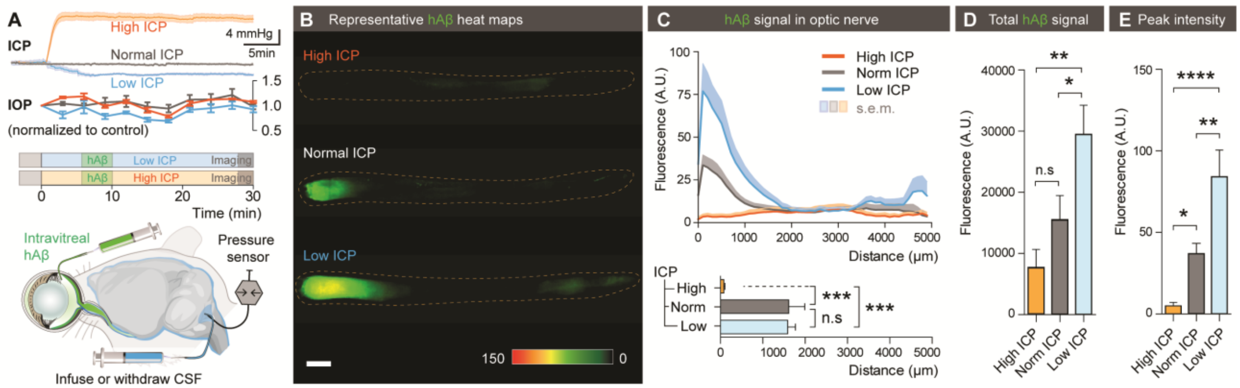

Figure 3. The translaminar pressure difference drives ocular glymphatic outflow. (**A**) Schematic of the setup used for analyzing hAβ transport following intravitreal injection while manipulating ICP. Upper-panel: Mean ICP and IOP normalized to control (± SEM) plotted as a function of time in the high, normal, and low ICP groups (*n* = 10-12 for ICP and *n* = 3-4 for IOP measurements). (**B**) Representative background-subtracted heat-maps of hAβ in the optic nerve from high, normal, and low ICP groups. (**C**) Top: Averaged fluorescent intensity profiles of hAβ in the optic nerves from the three groups. Bottom: The distance of tracer transport (*n* = 6-8, ***$p < 0.001$, n.s. $p = 0.9976$ one-way ANOVA followed by Tukey's *post hoc* test). (**D-E**) Total hAβ signal and peak intensities in the optic nerve 30 min after intravitreal injection (*n* = 6-8 for each group, *$p < 0.05$, **$p < 0.01$, ****$p < 0.0001$, n.s. = 0.2996 one-way ANOVA followed by Tukey's *post hoc* test). (Scale: **B**: 500µm).

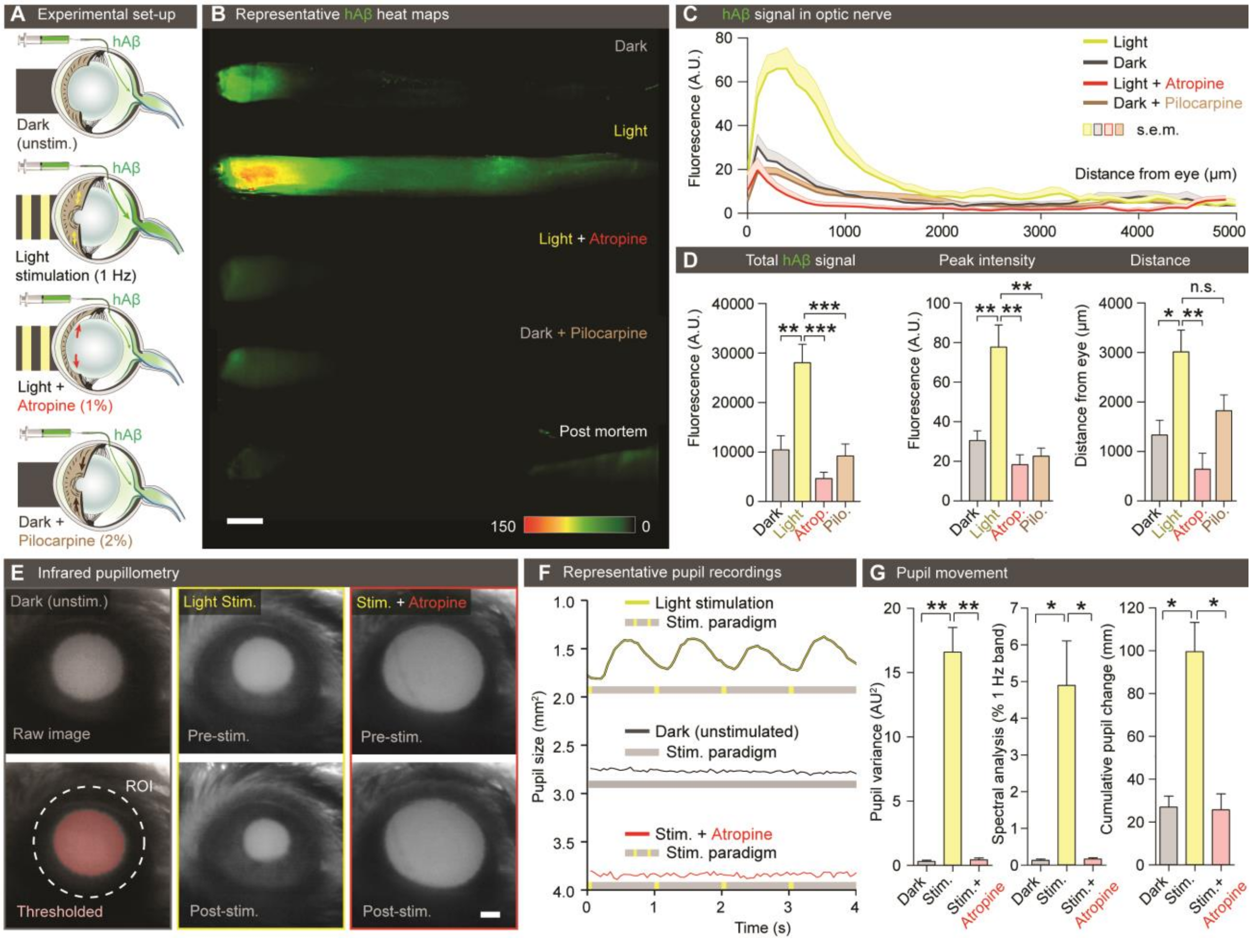

Figure 4. Light stimulation enhances hAβ along the optic nerve. (**A**) Schematic of the experimental groups. The first group was kept in darkness. The second group was exposed to 1 Hz light-stimulation (100 ms duration, 5 lumens). The third group was pretreated with atropine (1%) before exposure to 1 Hz light-stimulation. The fourth group was pretreated with pilocarpine (2%) and kept in darkness. (**B**) Representative background-subtracted heat-maps of optic nerves from the four groups 30 min after injection of hAβ and a postmortem group 120 min after injection of hAβ. (**C**) Averaged fluorescent intensity profiles of optic nerves from the four groups (n = 6-19). (**D**) hAβ signal mapped as total signal, peak intensity, and distance of the hAβ transport (n = 6-19, *p < 0.05, **p < 0.01, ***p < 0.001, n.s. p = 0.0756, one-way ANOVA followed by Dunnett's *post hoc* test). (**E**) Infrared pupillometry tracking of the pupil size and light-induced constriction with and without atropine pre-treatment. The pupil area (mm^2) was determined by auto-thresholding. (**F**) Representative pupillometry recordings in dark-exposed and light-stimulated mice with

and without atropine administration. (**G**) Left: Comparison of the variance of pupil area in these groups ($n = 3$, **$p < 0.01$, one-way ANOVA followed by Dunnett's multiple test); Middle: Spectral analysis of pupil response in these groups calculated as % of 1Hz band ($n = 3$-6, *$p < 0.05$, One-way ANOVA followed by Dunnett's multiple comparison); Right: Cumulative pupil diameter change over the time of experiment in these groups ($n = 3$-6, *$p < 0.05$, Kruskal-Wallis test followed by Dunnett's multiple comparison . (Scale: **B**, **E**: 500µm).

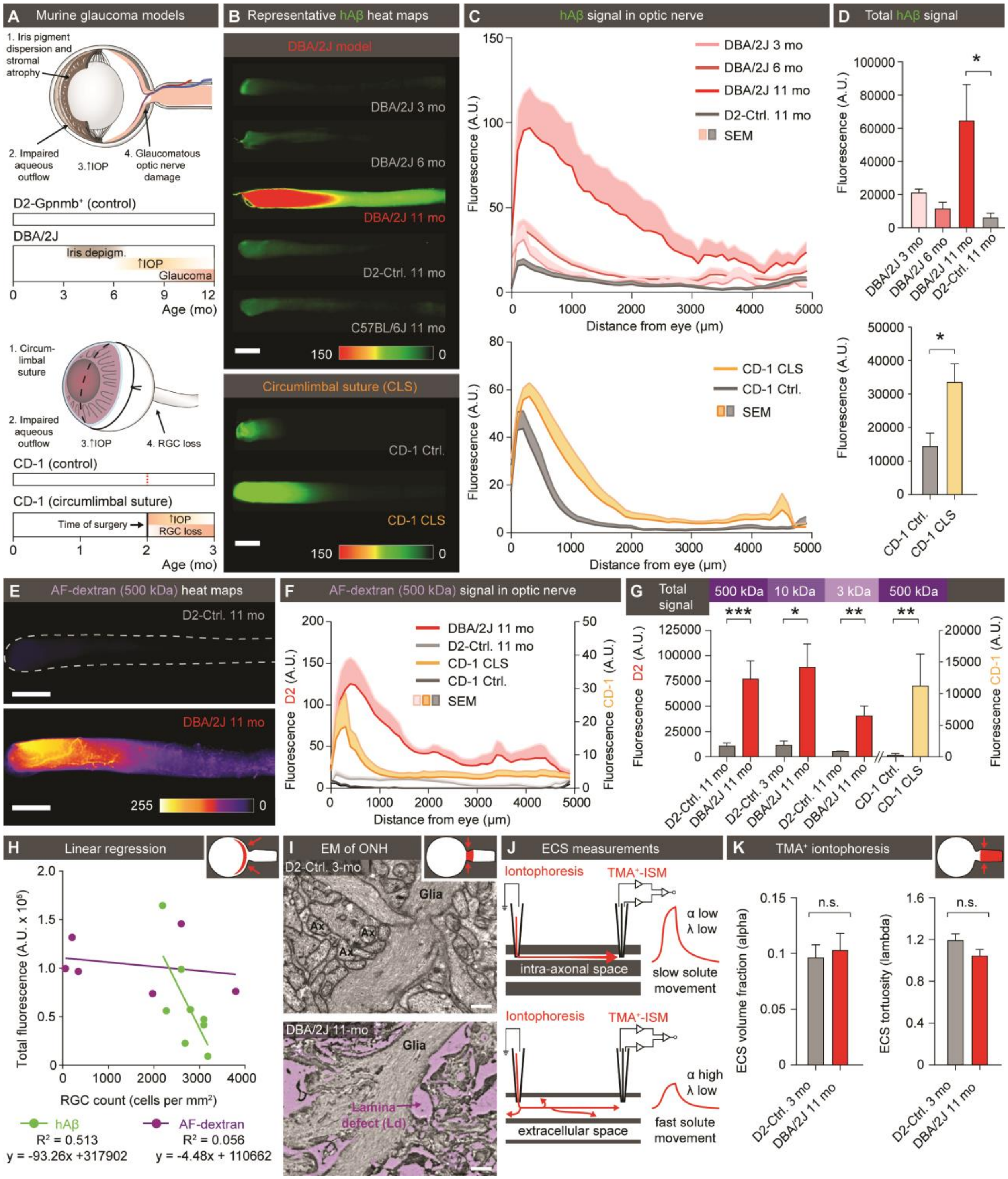

Figure 5. Disruption of the lamina barrier in two distinct murine models of glaucoma reveals a redirection and pathological enhancement of ocular glymphatic outflow. (**A**) Schematic of disease progression in the DBA/2J strain and chronic CLS model (CD-1) (*44*, *46*). (**B**) Representative background-

subtracted heat-maps of optic nerves 30 min after hAβ injection in young, middle-aged, and old DBA/2J mice and old D2-control mice, as well as CD-1-CLS and CD-1-control mice. (**C**) Averaged fluorescent intensity profile of hAβ distribution along the optic nerve in old DBA/2J or CD-1-CLS compared to respective controls (n = 6-12). (**D**) Total hAβ signal in old DBA/2J or CD-1-CLS compared to respective controls (n = 6-12, $*p < 0.05$, Kruskal-Wallis followed by Dunn's *post hoc* test for DBA/2J model, unpaired two-tailed t-test for CLS model). (**E**) Representative background-subtracted heat-maps of optic nerves from old DBA/2J and D2-control mice 30 min after intravitreal administration of AF-dextran. (**F**) Averaged fluorescent intensity profile of AF-dextran along the optic nerve in old DBA/2J or CD-1-CLS compared to respective controls (n = 6-9). (**G**) Total signal of different sized AF-dextrans in optic nerve from old DBA/2J or CD-1-CLS compared to respective controls (n = 4-9, $*p < 0.05$, $**p < 0.01$, $***p < 0.001$, unpaired two-tailed t-test or Mann-Whitney test). (**H**) Total hAβ or AF-dextran signal in the optic nerves of old DBA/2J mice plotted as a function of RGC density in their retinas (n = 6-8). (**I**) Electron micrographs of the glial lamina region from young D2-control and old DBA/2J mice. (**J**) Schematic of real-time TMA^+ iontophoresis measurement. (**K**) TMA^+ measurements of α (extracellular volume space) and λ (extracellular tortuosity) (n = 6-20, p = 0.765 for α, 0.177 for λ, unpaired two-tailed t-test). (Scale: **B**, **E**: 500µm; **I**: 0.5µm).

Supplementary Materials for

The Ocular Glymphatic Clearance System

Xiaowei Wang, Nanhong Lou, Allison Eberhardt, Peter Kusk, Qiwu Xu, Benjamin Förstera, Sisi Peng, Yujia Yang, Meng Shi, Antonio Ladrón-de-Guevara, Christine Delle, Björn Sigurdsson, Anna L. R. Xavier, Ali Ertürk, Richard T. Libby, Lu Chen*, Alexander S. Thrane, Maiken Nedergaard*.

*Correspondence to: nedergaard@sund.ku.dk or chenlu@berkeley.edu

This PDF file includes:

Supplementary material and methods

Experimental animals

Adult 2-12-month-old C57BL/6J, NG2-DsRed, *Glt1*-eGFP, FVB, DBA/2J, DBA/2J-*Gpnmb*$^{+}$/SjJ and CD-1 mice of either sex (Jackson Laboratory or Charles River Laboratories) and two-month-old Brown Norway rats (Charles River Laboratories) were used. *Aqp4*$^{-/-}$ mice were generated as described (*77*). *Prox1*-GFP mice generated as described (founder mice kindly provided by Young K. Hong at University of Southern California) (*78*). C57BL/6J mice were used if not otherwise noted. All rodents were bred and housed in standard housing conditions at the Universities of Copenhagen, Rochester, or California, Berkeley in temperature-controlled rooms at 24°C with a normal 12-hour light/dark cycle. The animals had free access to food and water. Age-matched mice from both C57BL/6J and DBA/2J-*Gpnmb*$^{+}$/SjJ (D2-controls) strains were used as controls for the DBA/2J strain. We did not observe any differences between C57BL/6J and D2-control mice young or old age (**table S3**), indicating comparable glial lamina integrity between these two groups. The CLS model was adapted from Liu et al. (*46*, *79*). Briefly, CD-1 mice were anesthetized as described below, and a suture was passed transconjunctivally around the equator of the eye with suture tension adjusted to achieve the desired IOP increase. The suture was kept for one month. Age-matched CD-1 mice without the surgical procedure were used as controls for the CLS model. All procedures were approved and in accordance with the guidelines of institutional Animal Care and Use Committee and the National Institutes of Health Guide for the Care and Use of Laboratory Animals at all universities. The experiments were designed to minimize the number of animals utilized.

In vivo intravitreal, suprachoroidal, and intracisternal tracer injection

All rodents were anesthetized with a ketamine/xylazine cocktail (100 mg/kg and 20 mg/kg, respectively). Once reflexes had ceased, rodents were mounted in a stereotactic head frame with body temperature maintained by a homeothermic blanket system (Harvard Apparatus). A conjunctival peritomy was performed to expose the sclera at 11 to 1 o'clock. A 34G needle connected to PE20 tubing and a Hamilton syringe was inserted into the vitreous 1-2 mm posterior to the corneoscleral junction approximately 1-2 mm deep. In a subset of mice, a 30G needle was inserted into the suprachoroidal space about 2 mm behind the limbus (*80*). To map lymphatic drainage three hours following intravitreal tracer injection of hAβ-647, mice were imaged with a fluorescence stereomicroscope (MVX10, Olympus) in the supine position. The cervical region was exposed before imaging. We pre-labeled mouse cervical lymph nodes by bilateral injection of fluorescein into the mouse cheek as described previously (*33*). 1 µl, 0.5% (w/v, diluted in PBS) (*3*, *81*) of one of the following tracers was injected intravitreally, suprachoroidally or intracisternally (**table S4**) over a period of either five or ten min by a syringe pump (11 Plus, Harvard Apparatus): HiLyte Fluor 488-, HiLyte Fluor 555-, or HiLyte Fluor 647-conjugated hAβ (1-40, AnaSpec), FITC-conjugated cadaverine (Thermo Fisher Scientific) (*82*, *83*), FITC-, Texas Red-, Alexa Fluor (AF) 488- or AF 555-conjugated dextrans (3 kDa, 10 kDa, 500 kDa, referred to as AF-dextran for simplicity) (Thermo Fisher Scientific), AF647-conjugated Albumin from Bovine Serum or FITC-ovalbumin (Thermo Fisher Scientific). In a subset of mice, 0.3 µl, 1.67% (w/v) HiLyte Fluor 488-conjugated hAβ (1-40, AnaSpec) was injected to control for the effect of injection volume. We saw no statistical differences in hAβ tracer distribution between the five- and ten-minute injections with respect to fluorescent signal and peak intensity (n = 6-8, p = 0.527-0.649, unpaired two-tailed t-test). A needle holder attached to a hand manipulator (WPI) was used to secure the needle in position for the duration of the experiment. An eye lubricant (GenTeal Lubricant Eye Gel, Alcon) was applied to the cornea during the experiment. Photopic flicker (1 Hz, 100 ms, 5 lumens) from an LED light source (1830 L4, Pelican) was used to stimulate the tracer-injected eye under control of a Master 8 stimulator (A.M.P.I.). We monitored both the lens and retina in all injection experiments and did not observe damage in any animals. A subset of 1 Hz light-stimulated mice was treated with 1% atropine (Sigma-Aldrich) by topical instillation to the stimulated eye. A subset of dark, unstimulated mice was treated with 2% pilocarpine (Sigma-Aldrich) by topical instillation. During the experiment, the pupil sizes of subsets of mice from the dark, unstimulated, 1 Hz light-stimulated, and atropine-treated groups were tracked by an infrared camera (DCC3240N, Thorlabs). Intracisternal injections were performed in anesthetized mice fixed in a stereotactic frame. A 30G needle was inserted into the CM, and 0.5% AF-dextran (Thermo Fisher Scientific) was infused at a rate of 1.5 µl/min over 10 min with a syringe pump (Harvard Apparatus). In a subset of NG2-DsRed mice that received i.v. injection of lectin, perivascular tracer distribution was measured following either intracisternal injection or intravitreal injection. Cumulative line scans perpendicular to blood vessel were collected. Signal was aligned and mapped to the largest vessel within the group.

Ultimate 3D imaging of Solvent-Cleared Organs (uDISCO)

One hour following intravitreal injection of hAβ-HiLyte-647, anesthetized mice were transcardially perfused with heparinized PBS followed by 4% formaldehyde. After 24 hours post-fixation in 4% formaldehyde, uDISCO was performed as previously described (*26*). Subsequently, the transparent mouse heads were imaged at a z-interval of 10 µm using a LaVision BioTec Ultramicroscope II light-sheet microscope with an Olympus MV PLAPO 1x air-objective and MVX10 0.63x zoom body. Amira Software 6.3.0 was used for tracing and 3D-reconstruction of the hAβ signal in eye and optic nerve.

Intravascular tracer administration and quantification

10 µl of isotonic saline containing the K^+-analogue $^{86}Rb^+$ (0.1 µCi/µl, PerkinElmer) was injected into the right internal carotid artery along with ^3H-mannitol (0.1 µCi/µl, American Radiolabeled Chemicals) over two sec through a catheter connected to a syringe pump (Harvard Apparatus). The ipsilateral eye and optic nerve were quickly dissected, and the nerve was separated into proximal and distal parts of equal length. Radioactivity was measured using a Multipurpose Scintillation Counter (Beckman Coulter) following overnight solubilization at 45°C in Soluene (PerkinElmer) and scintillation counting with Hionic Fluor cocktail (PerkinElmer). $^{86}Rb^+$ counts were plotted after subtraction of counts in the contralateral eye and optic nerve. FITC-cadaverine (100 µl, 0.5%,

Thermo Fisher Scientific) was administered to anesthetized C57BL/6J mice through a catheter inserted through the external carotid artery into the right internal carotid artery exposed as described earlier (*84*), and tissue was harvested 10 min later. Fresh eye and nerve were immediately imaged with a naïve control (C57BL/6J without injection) under a fluorescence stereomicroscope (MVX10, Olympus) using a digital camera (C11440, Hamamatsu) controlled by MetaMorph software (Molecular Devices). Retina flat-mounts were prepared as described before (*85*), and images were collected using a confocal microscope following fixation with Bouin solution.

Imaging and quantification of tracer transport

For macroscopic imaging of tracer transport, the freshly harvested nerves obtained from anesthetized mice following removal of brain tissue were imaged using the stereofluorescent microscope described above. A pE LED (PRIOR Lumen 1600-LED) fluorescent light intensity of 95% and exposure time of 1000 ms were kept constant across all groups. Fluorescent intensity was quantified with arbitrary units (A.U.). Following intravitreal injection, the ipsi- and contralateral nerves were imaged simultaneously. After subtracting the mean fluorescent intensity of the control nerve, the fluorescent intensity profile of the tracer-exposed mouse or rat optic nerve was quantified at 3.09 µm or 6.76 µm steps, respectively, using a custom-made MATLAB (MathWorks) script. CD-1 mouse optic nerves were imaged with an Axio Imager M1 epifluorescence deconvolution microscope (Carl Zeiss AG) and quantified at 2.13 µm steps. Fluorescence as a function of distance from the eye was then used for further quantifications. Total fluorescence of tracer transport was obtained by calculating the trapezoidal numerical integration of the function. Peak intensity was the highest value of the fluorescent intensity profile. Movement distance was defined as the length of the wave front of signal in the experimental nerve that exceeded the mean intensity of the control nerves by three standard deviations. For tracer retinal penetration, distance was defined as the length from neurofilament layer (NFL) that exceeds an arbitrary threshold (A.U. = 26). Retinal layers were defined as distance to NFL. A confocal scanning microscope attached to an inverted microscope

(IX81, Olympus) controlled by Olympus Fluoview 500 software was used to map the cellular and subcellular hAβ tracer distribution using the whole-mount preparations or 20 μm cryosections. For mice that received suprachoroidal injections, *in vivo* retinal imaging was recorded by a fundus camera (Micro III, Phoenix Research Labs).

Fluorescence immunocytochemistry

Mice were anesthetized and perfused transcardially with 4% formaldehyde (Sigma-Aldrich). Wheat germ agglutinin (lectin) tagged with AF-647 (Fisher Scientific W32466) was diluted in PBS to a final concentration of 12.5 μg/ml to label the blood vessel lumen in select experiments. Dural whole-mout, retina whole-mount or mouse optic nerve were carefully dissected and were post-fixed in 4% formaldehyde for two hours at room temperature or overnight at 4°C. Serial 20 μm tissue sections were obtained using a cryostat (Leica CM190) following sucrose gradients ending with 30% sucrose. Sections were incubated overnight at 4°C with a single or combination of the following primary antibodies: rabbit anti-mouse LYVE-1, (1:200, Abcam, ab14917-100), rat anti-LYVE1 (ALY7) (1:250, eBioscience 14-0443-83), rabbit anti-RNA-binding protein with multiple splicing (RBPMS) (1:250, GeneTex 118619) (*86*), mouse anti-TUJ1 (1:500, Covance MMS-435P), rabbit anti-APP (1:500, Abcam ab15272), Syrian hamster anti-podoplanin (PDPN) (1:100 eBioscience, clone 8.1.1), rabbit anti-AQP4 (1:500, Millipore AB3594), goat anti-VEGFR3 (1:500, R&D Systems AF743), goat anti-OLIG2 (1:500, R&D Systems AF2418), mouse anti-glutamine synthetase (GS) (1:500, Chemicon MAB302), mouse anti-AP-2α (1:500, DSHB Hybridoma Product 3B5 [deposited by Williams, T.J.]), rat anti-mouse CD68 (1:500, BioRad MCA1957, hydrocephalus brain slice was used as positive control), mouse anti-GFAP (1:500, Millipore MAB360), rabbit anti-caspase-3 (8G10) (1:500, Cell Signaling Technology 9665S, P1 mouse pup brain with ongoing pruning was used as positive control), and goat anti-hOTX2 (1:40, R&D Systems AF1979). The primary antibodies were detected with appropriate AF-488-, 594-, 647-conjugated or Cy2-, Cy3-, Cy5-conjugated secondary antibodies

(1:500, Molecular Probes/Jackson ImmunoResearch) following two hours of incubation at room temperature. Prolong Gold containing DAPI (Invitrogen, P16931) was used for mounting the sections.

Intraocular and intracranial pressure measurement and manipulation

Intraocular pressure (IOP) of the rodent's eye was measured by a rebound tonometer (Icare TONOLAB). Briefly, anesthetized rodents were placed in a prone position. Five to ten measurements at five min following anesthesia induction were taken for each rodent to get the baseline. In a subset of mice, the measurement was performed under light anesthesia with 2% isoflurane for three times for each eye, with each instrument-generated average derived from six effective measurements. In another subset, we also continuously monitored IOP in an experimental group and compared to a sham surgery group in which only the fluid infusion was withheld. In another subset, mouse IOP was measured while their ICP was manipulated from baseline (see below) and normalized to the IOP value without ICP manipulation. In another group, IOP was monitored by intracameral tonometry (*87*) via cannulation to the anterior chamber with a 36G needle. ICP was monitored through a CM catheter sealed to the skull with dental cement (Stoelting Co). Intracameral IOP and ICP were monitored by a pressure transducer (WPI) connected to a pressure monitor (WPI), acquired at 10,000 Hz, digitized, and recorded continuously for the duration of the experiment with a DigiData 1332A and PClampex9.2 software (Axon Instruments) and then downsampled to 100 Hz. To calculate the power of 1 Hz in IOP, signal between 0.99 Hz and 1.01 Hz was used. To elevate the mouse's ICP, we infused 538 ± 76.8μl artificial CSF (aCSF) over 30min into the CM through a Hamilton syringe connected to a syringe pump (Harvard Apparatus). ACSF contained the following (in mM): 155 NaCl, 3.5 KCl, 1 $CaCl_2$, 1 $MgCl_2$, and 2 NaH_2PO_4, pH 7.4, 300 mOsm. To lower ICP, we actively withdrew 37 ± 5.1μl CSF over 30min via a surgical opening in the CM. ICP was monitored in real-time during ICP manipulation. Intravitreal tracer injection was initiated five min after ICP stabilized.

Electron microscopy

D2-control and DBA/2J mice were fixed by transcardial perfusion with 0.5% glutaraldehyde and 4% formaldehyde in 0.1 M phosphate buffer (pH 7.4, 9 ml/min for 25 min). The eye and optic nerve were post-fixed for two hours with 4% formaldehyde, 1% glutaraldehyde in 0.1 M PBS before 50 µm coronal sections were dissected and embedded in Durcupan (Sigma-Aldrich). A powertome XL (RMC Boeckeler) was used to prepare ultrathin sections, and a transmission electron microscope (Hitachi H-7650) attached to a CCD camera (Gatan Inc. ES1000W) was used to examine the glial lamina region of the ONH at a nominal magnification of 4200x.

Real-time tetramethylammonium (TMA^+) iontophoresis

Optic nerves from anesthetized mice were quickly dissected following decapitation and immersed for 60 min in oxygenated aCSF at room temperature. Microelectrodes were fabricated from double-barreled theta-glass using a tetraphenylborate-based ion exchanger. The TMA^+ barrel was backfilled with 150 mM TMA-chloride, and the reference barrel contained 150 mM NaCl and 10 µM AF-594. A series of currents of 20 nA, 40 nA, 80 nA, and 100 nA was applied by a dual-channel microelectrode pre-amplifier. The electrode tips were kept ~150 µm apart. The TMA^+ signal was calculated by subtracting the voltage measured by the reference barrel from the voltage measured by the ion-detecting barrel. Nikolsky equation was used for calibration of the TMA^+ electrodes based on measurements obtained in electrodes containing standards of 0.5, 1, 2, 4, and 8 mM TMA-chloride in 150 mM NaCl. The TMA^+ measurements were acquired relative to similar recordings obtained in 0.3% agarose prepared from a solution containing 0.5 mM TMA^+ and 150 mM NaCl. “Walter” (developed by C. Nicholson) was used to calculate α (volume fraction: ratio of extracellular space volume to total tissue volume) and λ (tortuosity: square root of the ratio of free diffusion coefficient to apparent diffusion coefficient) using the Nikolsky equation (*88*).

Cytokine assay

Thirty minutes after intravitreal injection of hAβ or vehicle in opposite eyes of the same animal, mice were transcardially perfused with ice-cold PBS. Retinas were dissected and homogenized in extraction buffer (20 mM Tris pH 7.4, 150 mM NaCl, 0.5% Tween-20 in PBS) with a 1:100 dilution of Protease Inhibitor Cocktail (Sigma P8340). The soluble fraction following centrifugation was analyzed by Eve Technologies (Alberta, Canada) using the Multiplex Laser Bead platform.

Blood retinal barrier permeability assay

Thirty or 120 minutes after intravitreal injection of hAβ or vehicle in opposite eyes of the same animal, mice were intravenously infused with Evans blue (2%, 2 ml/kg) before fixation and confocal imaging. In a subset of mice, Evans blue leakage from the blood into the retina was measured as described before (*89*).

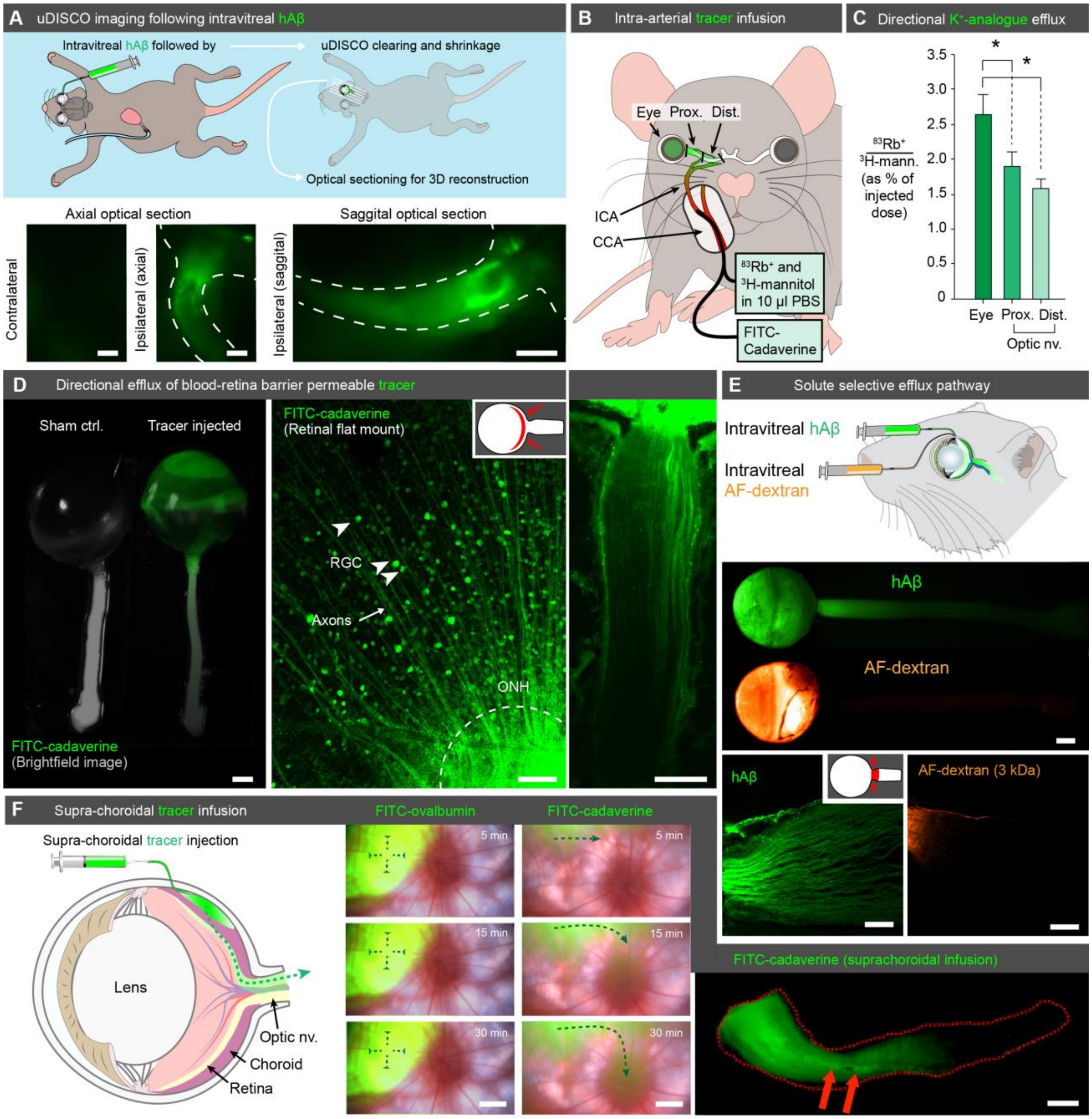

Fig. S1. Characterization of additional tracers and tracer delivery routes. (**A**) Top: Schematic showing hAβ injection followed by uDISCO whole-mouse clearing and shrinkage, along with optical sectioning using light sheet microscopy. Bottom: Representative maximum projections acquired in axial and sagittal plane ipsilateral and contralateral to the hAβ injection (scale: 500 µm). (**B**) Schematic showing non-invasive tracer delivery via injection into the internal carotid artery (ICA). (**C**) Quantification of $^{86}Rb^{+}/^{3}H$-mannitol radioactivity in the ipsilateral eye and optic nerve following ICA injection shows directional flow of the K^{+}-analogue from the eye to the optic nerve ($n = 7$, $*p < 0.05$, one-way ANOVA followed by Dunnett's *post hoc* test). (**D**) Left: Macroscopic imaging following FITC-cadaverine ICA injection showing ipsilateral eye and optic nerve (right) compared to that from a naïve mouse (left). FITC signal (green) is superimposed on bright field (scale: 1 mm). Middle: Confocal image of the mouse retina following ICA injection of FITC-cadaverine showing retinal ganglion cells (RGC) and their axons taking up the blood-retina-barrier-permeable tracer. Right: Confocal image of mouse optic nerve following intravitreal administration of FITC-cadaverine (scale: 100 μm). (**E**) Fluorescent macroscopic (scale: 500 μm) or confocal images (scale: 100 μm) of the eye and optic nerve following intravitreal injection of either the axon-transportable tracer hAβ or the non-transportable tracer AF-dextran (3 kDa). (**F**) Left: Schematic of suprachoroidal tracer delivery and tracer movement. Middle: Representative fundoscopy images following suprachoroidal FITC-ovalbumin or FITC-cadaverine showing tracer movement towards the optic disc in the latter case (scale: 300 μm). Right: Representative confocal image following suprachoroidal FITC-cadaverine injection demonstrating directional transport along the optic nerve, along with enhancement around the central retinal vein (scale: 500 μm).

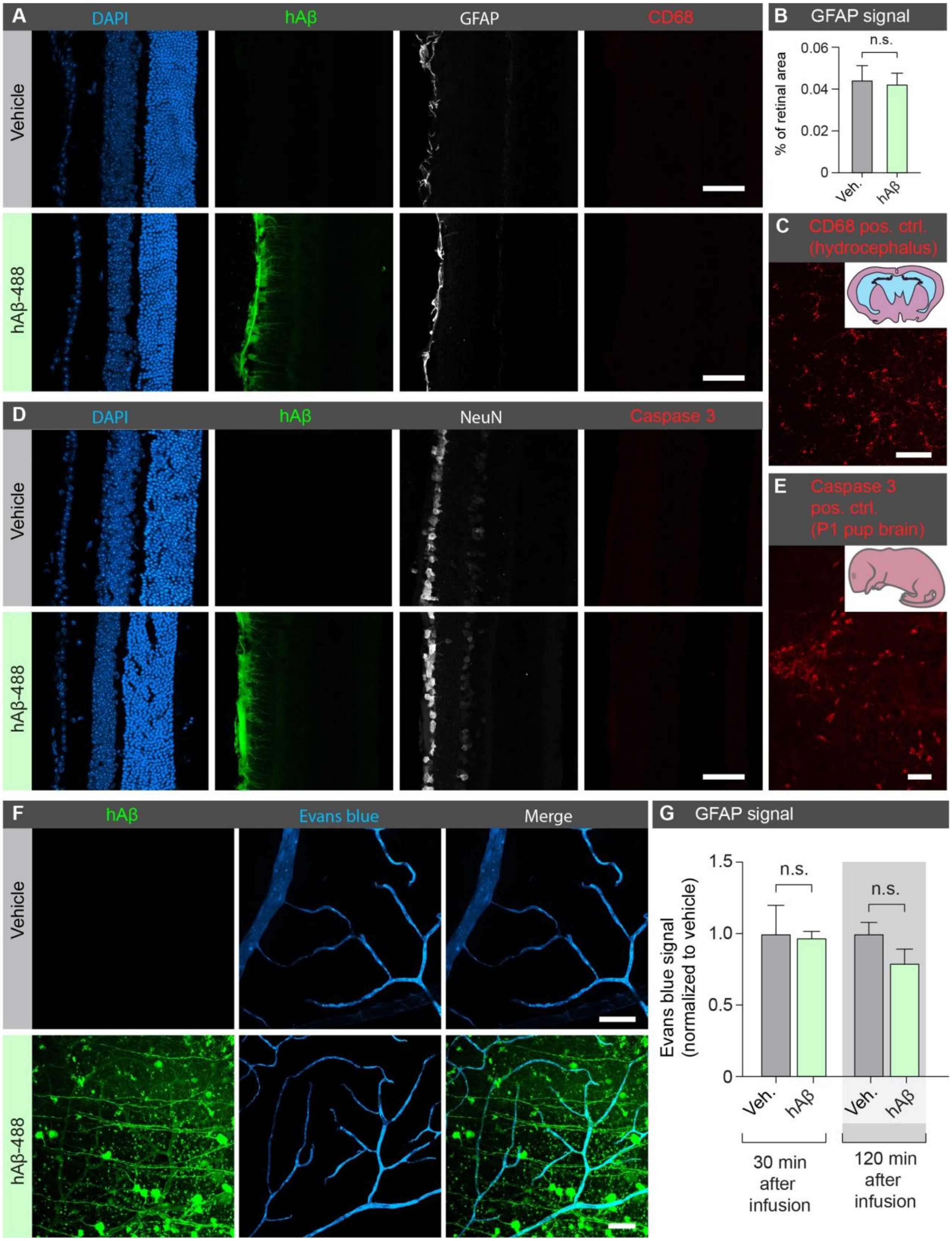

Fig. S2. Brief retinal exposure to trace amounts of hAβ using our intravitreal infusion paradigm does not induce gliosis, microglial activation, apoptosis or blood-retinal barrier disruption. (**A**) Representative confocal transverse retinal sections following intravitreal injection of vehicle or hAβ (green) counterstained for glial fibrillary acidic protein (GFAP, white) and microglial marker CD68 (red). (**B**) Quantification of percentage retinal area positive for GFAP (n = 3, n.s. p = 0.656, Mann-Whitney test). (**C**) Positive control (pos. ctrl.) for CD68 (8 week old hydrocephalic mouse neocortex). (**D**) Representative confocal transverse retinal sections following intravitreal injection of vehicle or hAβ counterstained for neuronal marker NeuN (white) and apoptosis marker caspase 3 (red). (**E**) Positive control for caspase 3 (P1 mouse pup brain). (**F**) Representative confocal flat-mount retinal images following intravascular Evans blue and intravitreal hAβ (green) or vehicle administration. Note that there is no evidence of Evans blue leakage or extravasation. (**G**) Quantification of Evans blue signal normalized to vehicle at different time points after intravitreal administration of hAβ vs. vehicle (n = 3-4, n.s. p = 0.858 for 30 min and p = 0.268 for 120 min, paired t-test). (Scale: **A**, **C**, **D**, **E**, **F**: 50 µm).

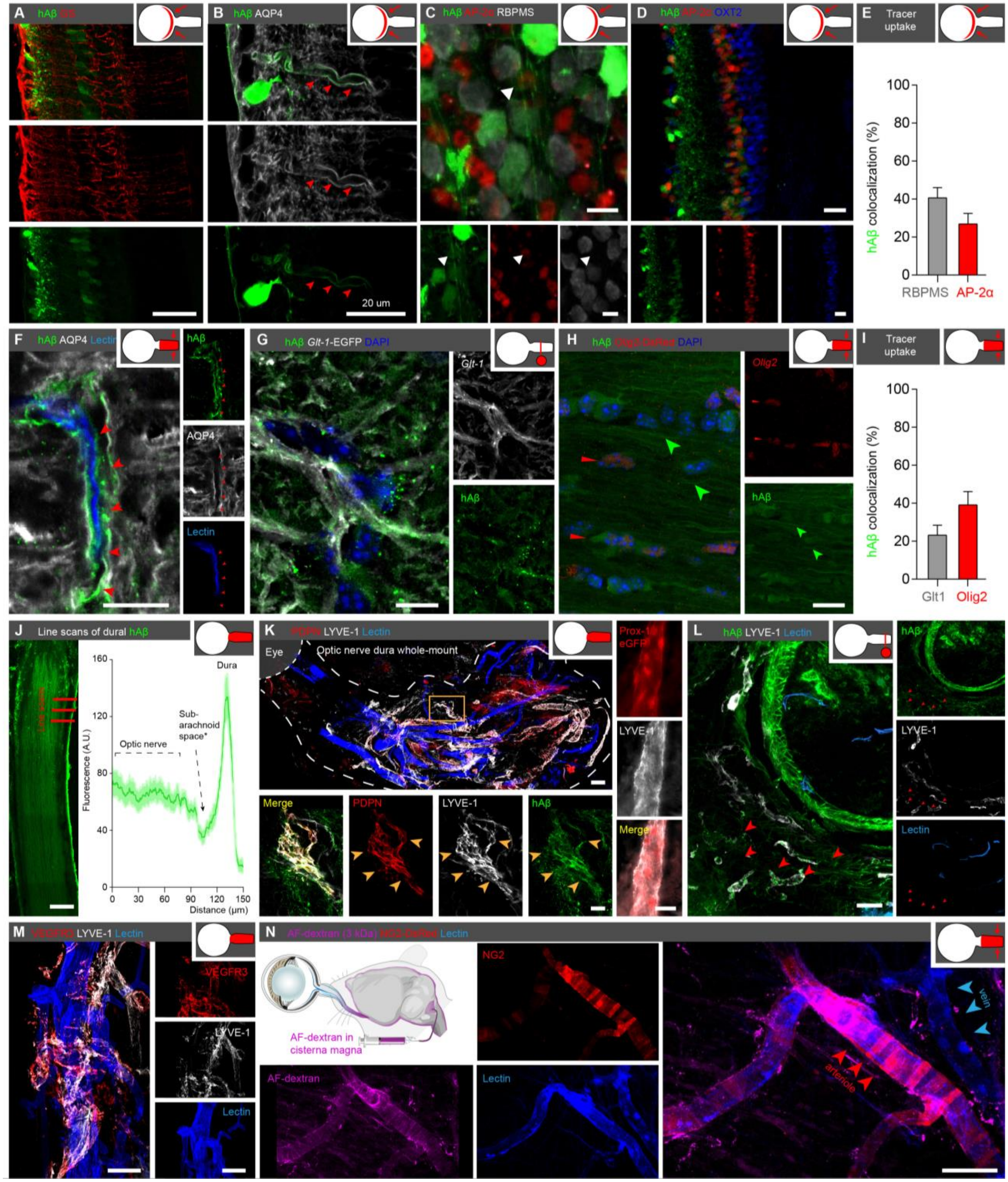

Fig. S3. Detailed analysis of ocular glymphatic clearance route. (**A**) Confocal images of mouse retina counter-stained for glutamine synthetase (GS, scale: 50 µm). (**B-D**) Confocal image of mouse retina counter-stained for aquaporin-4 (AQP4), AP-2α, RNA-binding protein with multiple splicing (RBPMS), and orthodenticle homeobox-2 (OXT2). Note the uptake of hAβ by RPBMS^{+} cells and along the perivascular space (red arrowheads) outlined by AQP4^{+} glial end-feet. Also note sparse uptake by AP-2α^{+} cells (white arrowheads). (**E**) Percentage of retinalcellular uptake (mean ± SEM, n = 7). All images are retinal cross-sections except **C**, which is a retinal flat-mount image (scale: 20 µm). (**F**) Confocal image showing preferential hAβ tracer movement along the AQP4-outlined perivascular space after intravitreal injection in the optic nerve (red arrowheads, scale: 10 µm). (**G-H**) Confocal images showing sparse uptake of hAβ tracer by GLT1-eGFP^{+} and OLIG2^{+} cells after intravitreal injection (scale: 10 µm; green arrows indicate hAβ signal in OLIG2^{+} soma; green arrowheads indicate hAβ signal in axons). (**I**) Percentage of glial uptake in the optic nerve (mean ± SEM, n = 4-12). (**J**) Left: Representative photo-stitched longitudinal section illustrating 150 µm line-scans at the interface of optic nerve and dura. Right: Line graph showing fluorescence intensity (mean ± SEM) of 20 line scans collected from 4 mice 300-900 µm posterior to the glial lamina. *Note that the subarachnoid space was variable and sometimes not present due to tissue processing (scale: 100 µm). (**K**) Left: Whole-mount of dura stripped from the optic nerve following intravitreal hAβ, showing LYVE1^{+}, PDPN^{+}, and hAβ^{+} vessel-like structures (yellow arrowheads), devoid of intravascular lectin (scale: 100 µm in top image, 20 µm in bottom images). Right: Optic nerve dura mater whole-mount immunostaining showing LYVE1- and PROX1- positive lymphatics in *Prox1*-GFP mouse (Images were presented in pseudo colors). (scale: 20 µm). (**L**) Immuno-detection of LYVE1 in cross-section of optic nerve following hAβ tracer intravitreal injection, showing co-labeling of LYVE1^{+}, intravascular lectin-negative structures (yellow arrowheads) with hAβ tracer in the dura and orbital tissue surrounding the optic nerve (scale: 20 µm). (**M**) Dural whole-mount showing LYVE1^{+} and VEGFR3^{+} structures, devoid of intravascular lectin (scale: 100 µm). (**N**) Confocal images of the optic nerve from an NG2-DsRed mouse following cisterna magna (CM) injection shows AF-dextran tracer accumulated preferentially in the periarterial space (red arrowheads) rather than the perivenous space (blue arrowheads) (scale: 50 µm).

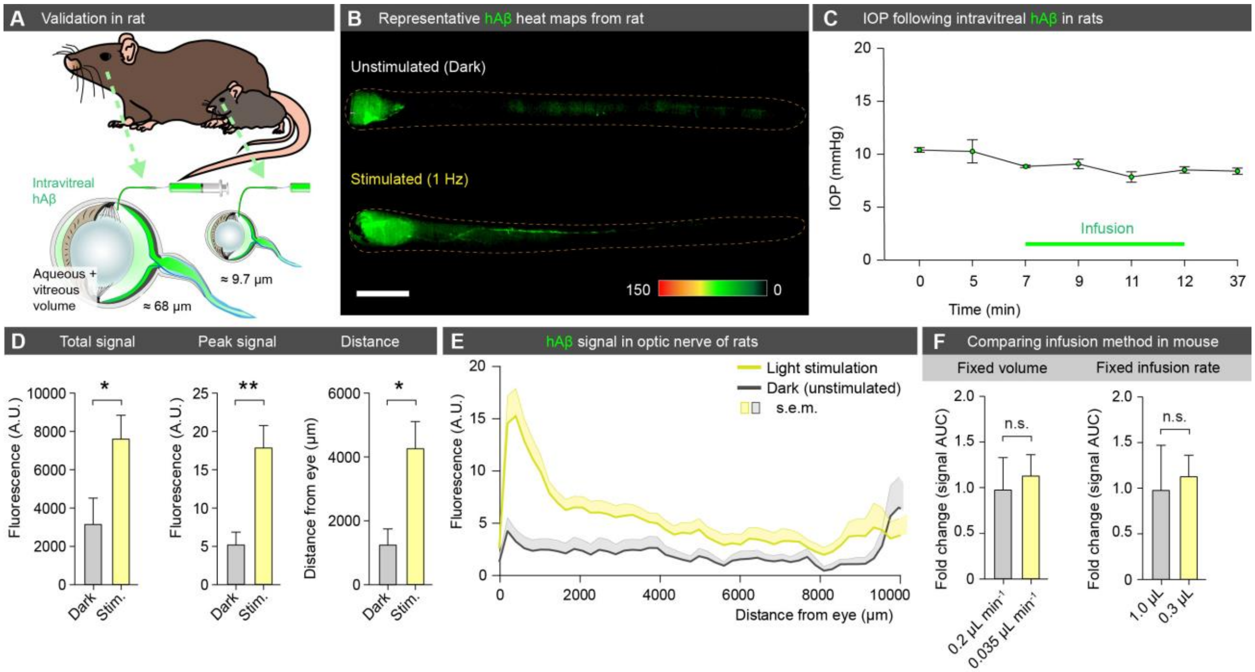

Fig. S4. Validation of tracer delivery model in another species and with different infusion parameters. (**A**) Schematic showing intravitreal hAβ infusion in Brown Norway rat, which has approximately seven times the intraocular fluid volume of a C57BL/6J mouse. (**B**) Representative background-subtracted heat-maps from rats kept in darkness or subjected to 1 Hz light stimulation following intravitreal hAβ infusion, demonstrating a pattern similar to that of a mouse (scale: 1 mm). (**C**) IOP measured by rebound tonometry during the hAβ infusion in rats (n = 3). (**D**) Total hAβ signal, peak hAβ signal, and distance travelled for unstimulated and stimulated (1 Hz) rat eyes (n = 5-7, *p < 0.05, **p < 0.01, unpaired two-tailed t-test). (**E**) Averaged fluorescent intensity profile of hAβ tracer distribution along rat optic nerve (n = 5-7). (**F**) The impact of hAβ infusion volume and rate on overall optic nerve signal (AUC = area under the curve) were compared in mouse (n = 6-11, n.s. p = 0.462 for fixed volume and p = 0.366 for fixed rate, Mann-Whitney test).

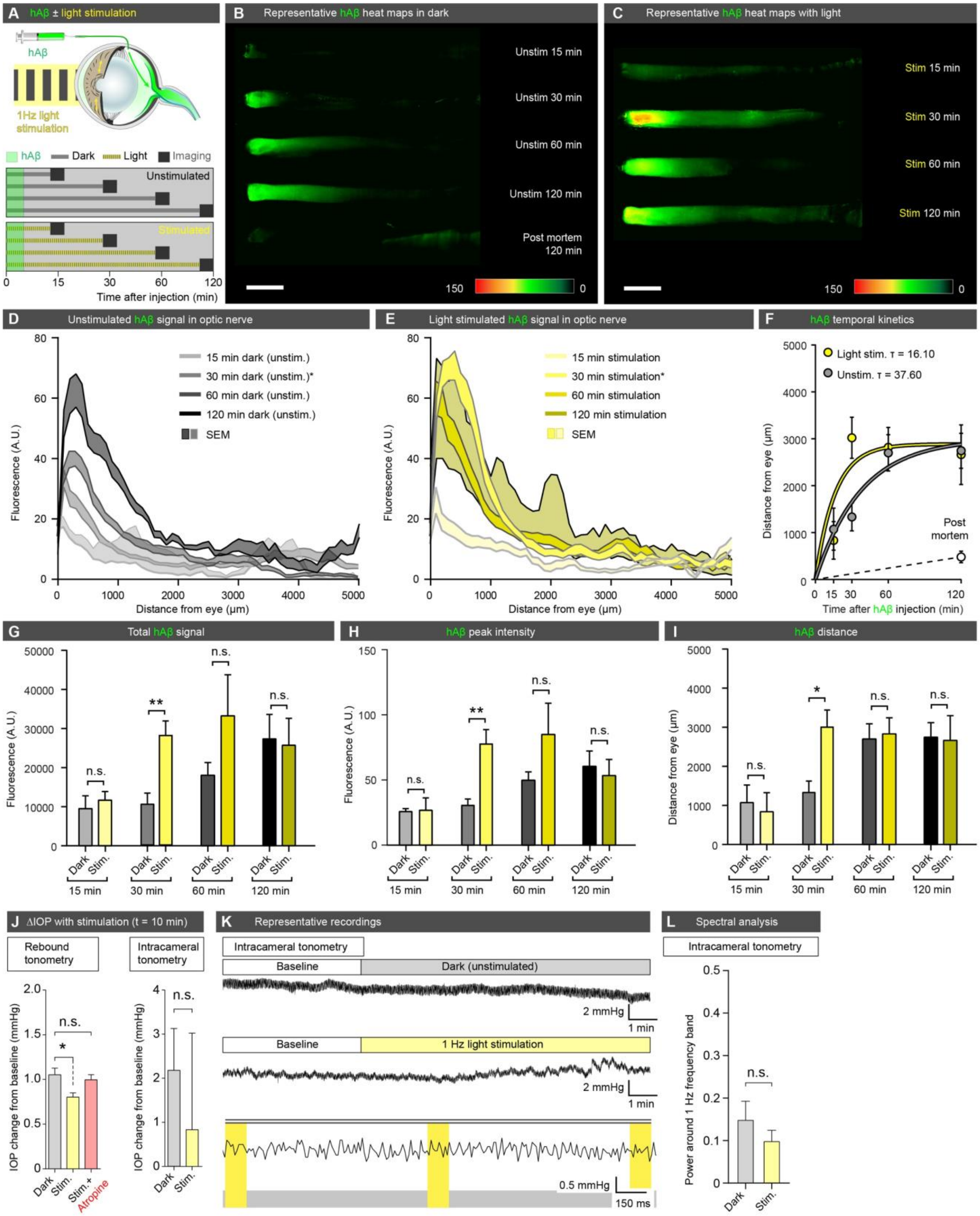

Fig. S5. Light stimulation accelerates hAβ tracer movement along the optic nerve. (**A**) Mice were subjected to either dark or 1 Hz light stimulation (100 ms duration, 5 lumens) and imaged 15, 30, 60, or 120 min after intravitreal hAβ injection. (**B-C**) Representative background-subtracted heat-maps of optic nerves following hAβ tracer injection demonstrate that light stimulation accelerates hAβ tracer clearance via the optic nerve. Almost no hAβ tracer movement is seen postmortem (scale: 1 mm). (**D-E**) Averaged fluorescent intensity profiles of hAβ tracer distribution along the optic nerve in dark, unstimulated and light-stimulated groups at 15-, 30-, 60-, and 120-minute time points (n = 3-8). (**F**) Pseudo-kinetics of the hAβ tracer movement shown by fitting the distance and experiment time to a one-phase decay curve (n = 3-8). Quantification of the time constant (tau, $\boldsymbol{\tau}$) shows light stimulation induces a two-fold acceleration in tracer movement. (**G-I**) Total hAβ tracer signal, peak intensity, and distance travelled in the optic nerve for all the groups. Light stimulation causes significantly increased hAβ tracer transport in the optic nerve 30 min after intravitreal injection (n = 3-8, *$p < 0.05$, **$p < 0.01$, n.s. p = 0.193-0.946, unpaired two-tailed t-test). (**J**) Left: Comparison of the relative change of IOP in light-stimulated (± atropine) vs. control (dark) groups using rebound tonometry (n = 12 for each group, *$p < 0.05$, n.s. p = 0.6973, one-way ANOVA followed by Dunnett's *post hoc* test) measured 10 min after starting the experiments normalized to IOP baseline. Right: Intracameral tonometry (n = 5-6, n.s. p = 0.5453, unpaired two-tailed t-test) of light-stimulated vs. control (dark) groups during the experiment after subtracting baseline level. (**K**) Representative intracameral tonometry of control (dark, top) and light-stimulated groups (middle) following intravitreal tracer injection, in addition to a high temporal resolution view of light-stimulated group (bottom, yellow bars represent individual light stimuli). (**L**) Spectral analysis of intracameral IOP recording shows no significant peak around the 1 Hz frequency band used for light stimulation (n = 5-6, n.s. p = 0.5368, Mann-Whitney test).

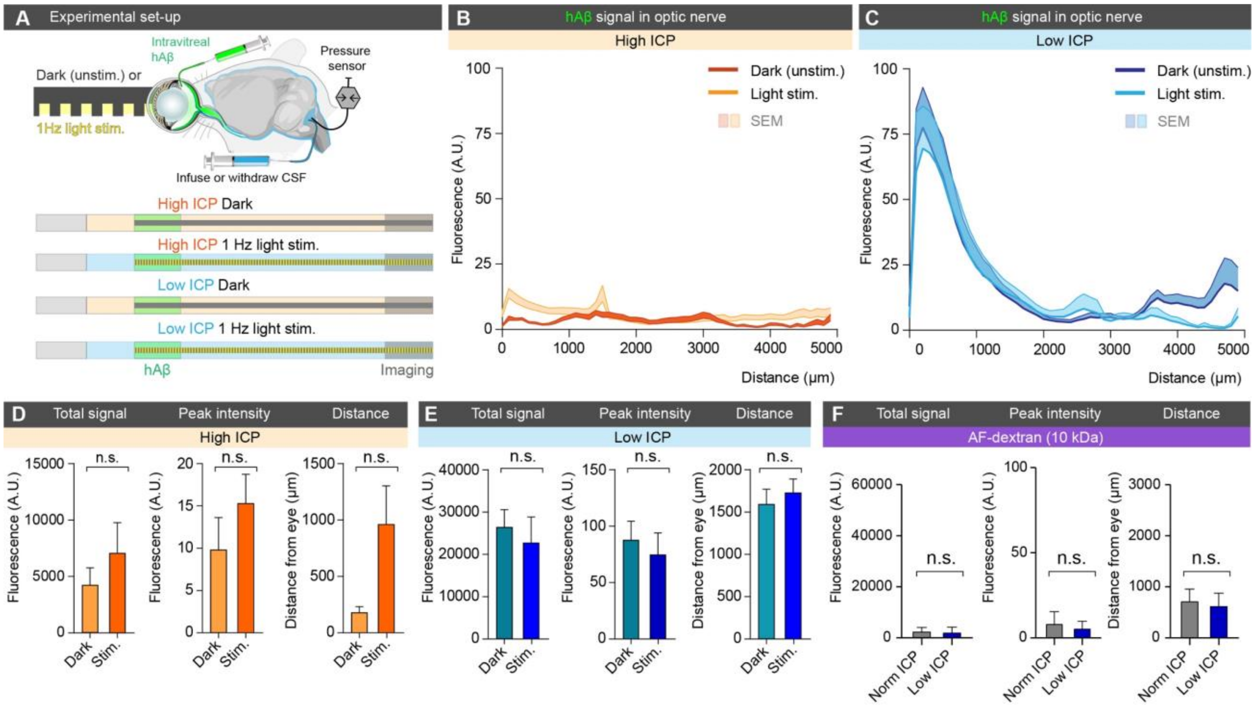

Fig. S6. Influence of the translaminar pressure difference on stimulated and unstimulated tracer movement. (**A**) Schematic of experimental design used for intravitreal injection with concurrent manipulation of intracranial pressure (ICP) and exposure to 1 Hz light stimulation or dark (unstimulated). (**B-C**) Averaged fluorescent intensity profiles of hAβ tracer distribution along the optic nerve in unstimulated and 1 Hz light-stimulated groups under high and low ICP conditions ($n = 6$). (**D-E**) Total hAβ tracer signal, peak intensity, and distance of hAβ tracer transport in the optic nerve following intravitreal injection in either high ICP condition or low ICP condition ($n = 6$, n.s. $p = 0.104$-0.627, unpaired two-tailed *t*-test). (**F**) Total signal, peak signal, and distance travelled for intravitreal AF-dextran (10 kDa) in the setting of normal vs. low ICP ($n = 6$-8, n.s. $p = 0.6620$ for total, 0.4109 for peak, 0.7774 for distance, unpaired two-tailed *t*-test for distance and peak, Mann-Whitney test for total).

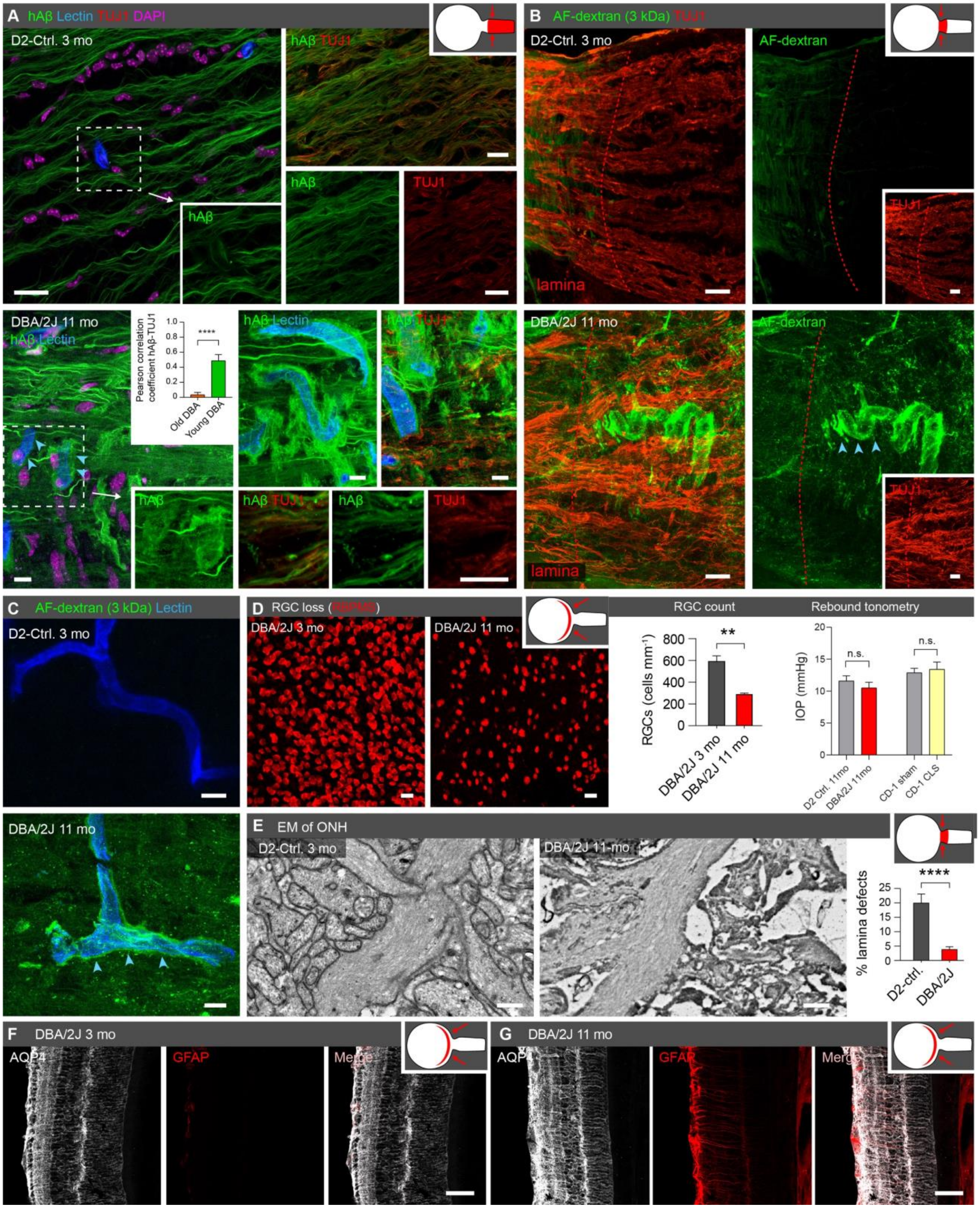

Fig. S7. Tracer efflux pattern in murine glaucoma model indicates leaky lamina that may allow bypass of intra-axonal transport via extracellular route. (**A**) Representative confocal images of the ipsilateral optic nerve following intravitreal hAβ tracer injection from D2-control (top) and 11-month-old DBA/2J mouse (bottom).

Note the mixture of axonal, extracellular, and perivascular hAβ tracer transport (blue arrowheads: perivascular transport, scale: 20 µm). Bar graph shows Pearson correlation coefficient for TUJ1 and hAβ labelling in young vs. old DBA mice (n = 11-20, ****$p < 0.0001$, Mann-Whitney test). (**B**) Confocal images of the optic nerve head stained for axonal marker TUJ1 after intravitreal injection of AF-dextran (3 kDa) in D2-control (top) and old DBA/2J mice (bottom). Note that the dextran tracer does not penetrate the lamina barrier (red dotted line) in control mice, while old DBA/2J mice show extensive dextran leakage into the retrolaminar optic nerve (blue arrowheads: perivascular tracer, scale: 20 µm). (**C**) Higher magnification confocal image showing dextran cannot penetrate the glial barrier in control mice, while dextran tracer in old DBA/2J mice shows a predominantly extra-axonal and perivenous accumulation (blue arrowheads: perivascular tracer, scale: 10 µm). (**D**) Left: Representative confocal images of retina flat-mount demonstrating a loss of RGCs in old DBA/2J mice compared to young DBA/2J animals (scale: 20 µm). Middle: Quantification of RGC number in young DBA/2J vs. old DBA/2J mice (n = 11-33 for IOP and n = 9-10 for RGC count, **$p < 0.01$, n.s. $p = 0.436$ unpaired two-tailed t-test). Right: IOP returned to control level in both glaucoma models at the time of experiment. (n = 7-8, n.s. p = 0.3773 for DBA, n.s. $p = 0.6870$ for CLS, unpaired 2-tailed t-test). (**E**) Left: Representative electron micrographs from the glial lamina region of young D2-control (top) and old DBA/2J mice (bottom) (scale: 0.5 µm) shown here without pseudo-coloring as compared to **Fig. 4I**. Right: Quantification of defects in the glial lamina taken as the percentage pixels out of the total area of the EM image > 2SD above the average parenchymal pixel value, excluding blood-vessels (n = 7-10, ****$p < 0.0001$, unpaired two-tailed t-test). (**F-G**) Representative confocal retinal images stained for aquaporin-4 (AQP4, white) and glial fibrillary acidic protein (GFAP, red) comparing young and aged DBA/2J mice (scale: 50 µm).

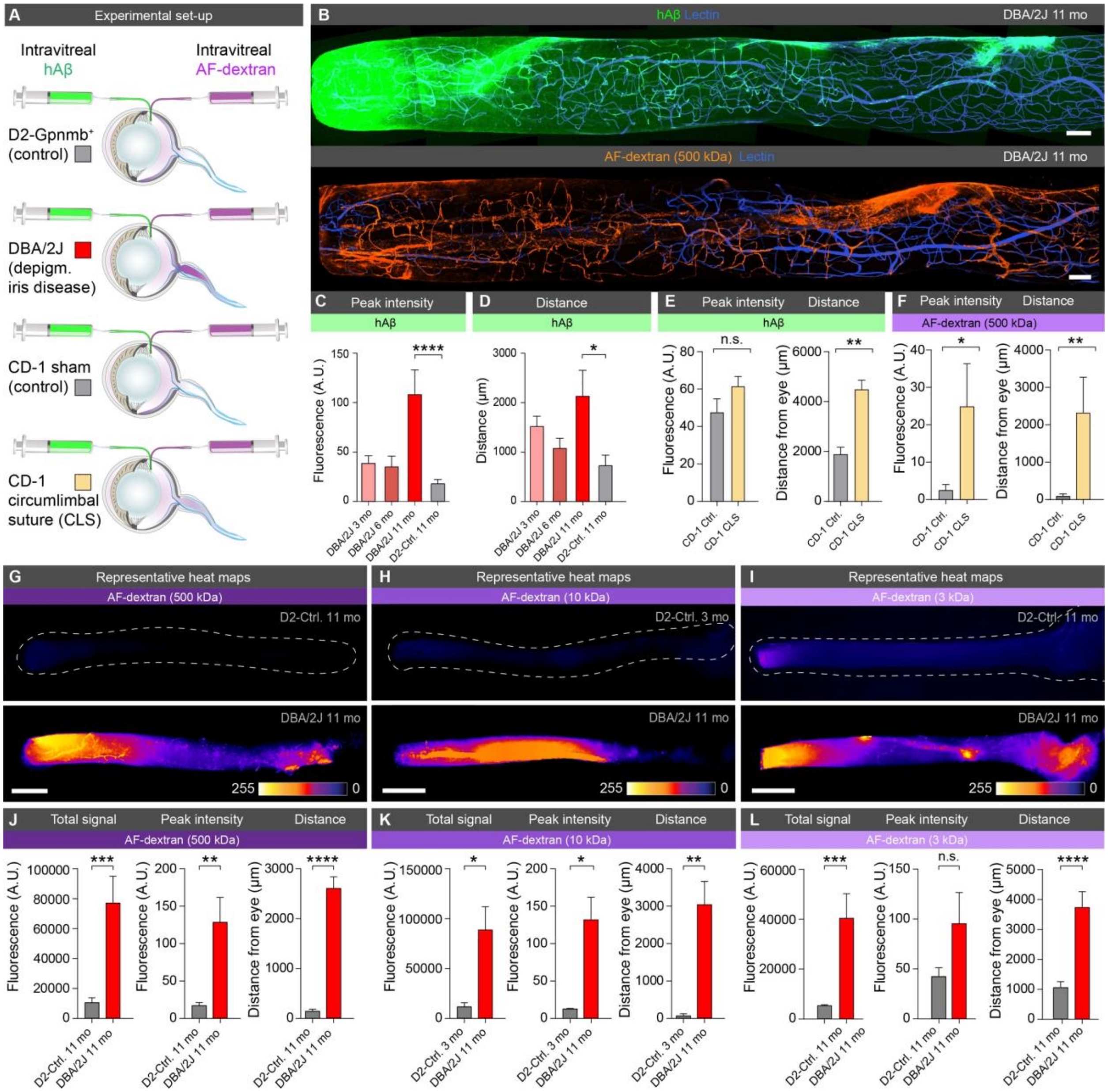

Fig. S8. Murine glaucoma models reveal defects in the lamina barrier allowing escape of large intraocular tracers. (**A**) Schematic of the experimental set-up for intravitreal injection of different size AF-dextran tracers (3, 10, 500 kDa) and hAβ tracer in DBA/2J and chronic circumlimbal suture (CLS) glaucoma models. (**B**) Representative confocal images of the ipsilateral optic nerve following intravitreal injection of hAβ tracer (top) and AF-dextran (bottom) in old DBA/2J mice (scale: 100 µm). (**C-F**) Peak intensity and distance of hAβ and AF-dextran (500 kDa) tracer transport in the optic nerve in 11-month-old DBA/2J, age-matched D2-control, as well as young and mid-age DBA/2J and CLS mice along with CD-1 controls (n = 6-12, *$p < 0.05$, **$p < 0.01$, ****p

< 0.0001, n.s. $p = 0.1255$, Kruskal-Wallis test followed by Dunn's *post hoc* test or unpaired two-tailed t-test, or Mann-Whitney test). (**G-I**) Representative background-subtracted heat-maps of optic nerve following AF-dextran (3, 10, and 500 kDa) tracer injection in D2-control and old DBA/2J mice (scale: 500 µm). (**J-L**) Total hAβ tracer signal, peak intensity, and distance of AF-dextran tracer transport along the optic nerve for 500, 10, and 3 kDa AF-dextran (n = 6-9 [500 kDa groups], n = 4-8 [10 kDa groups], n = 5-6 [3 kDa groups], *$p < 0.05$, **$p < 0.01$, ***$p < 0.001$, n.s. $p = 0.069$, unpaired two-tailed t-test).

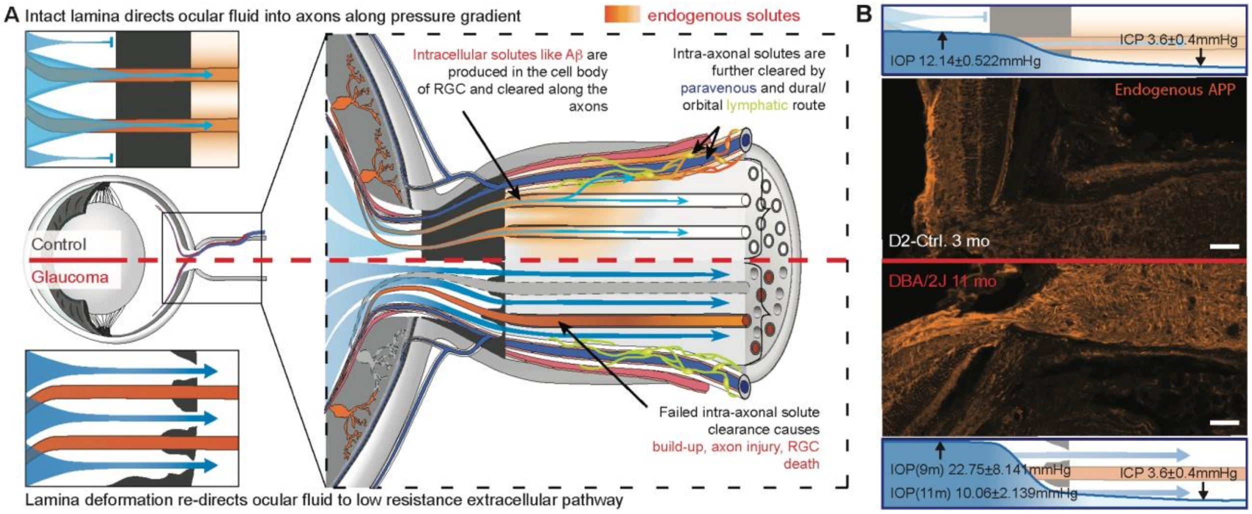

Fig. S9. Schematic model of the ocular glymphatic clearance system and its dysfunction in a murine model of glaucoma. (**A**) In control mice (top), IOP drives intraocular fluid (IOF, blue) into RGC axons prior to the glial cell barrier of lamina cribrosa (black). Intra-axonal transport of solutes (orange) across the lamina is accelerated by IOF uptake by RGC axons. After passing the glial lamina, hAβ is released into the extracellular space, disperses into the perivenous space, and is eventually cleared by dural/orbital lymphatic vessels, where some tracer may also arrive from anterior and peri-papillary choroidal drainage paths. Insert illustrates how IOP in combination with the glial lamina barrier drives IOF into the unmyelinated RGC axons. In old DBA/2J mice (bottom), the barrier function of the glial lamina is lost, resulting in IOF passing directly into the extracellular space of the optic nerve via defects in the lamina, thus bypassing the intra-axonal compartment. The reduction of intra-axonal flow results in accumulation of potentially harmful solutes, such as Aβ (dark orange axons), and axonal degeneration (grey axons). Insert shows IOF bypassing the glial lamina through openings in the barrier. (**B**) Depicts immunolabeling of endogenous (mouse) amyloid precursor protein (APP) in young (top) and old (bottom) DBA mice (scale: 20 µm). Above and below the immunohistogram are diagrams of how the translaminar gradient and lamina barrier differ between control and aged DBA/2J mice. DBA/2J mice IOP lowered at 11 months of age, which is the age we used them for experiment.

Table S1 Tabular summary of all the data

part 1.1 periarterial distribution of intravitreally administered hAβ

	lectin (A.U.)			**NG_2DsRed (A.U.)**			**hAβ (A.U.)**		
distance (μm)	**mean**	**SEM**	**n**	**mean**	**SEM**	**n**	**mean**	**SEM**	**n**
0	13.85816	13.61499	12	7.822567	6.318275	12	9.014658	19.35931	12
0.562124	13.571	13.31677	12	7.74419	6.046415	12	7.3741	15.12819	12
1.239146	13.84533	13.8515	12	7.661401	6.056232	12	6.491163	13.42415	12
1.916056	13.05356	12.35071	12	7.840668	6.274437	12	6.329386	12.91374	12
2.593068	11.84387	9.205582	12	6.87354	6.707695	12	8.159776	13.24441	12
3.270072	10.46714	8.962332	12	6.642627	6.539688	12	6.945194	11.48573	12
3.947077	11.21549	9.170248	12	5.946534	5.882944	12	5.154836	8.032242	12
4.624071	16.75424	19.78461	12	6.414996	5.987301	12	5.230805	9.632612	12
5.300978	14.17471	17.1995	12	5.399294	5.581893	12	4.566525	7.225561	12
5.977989	13.16201	16.12898	12	7.743243	8.851225	12	4.879902	7.811319	12
6.654994	12.78057	15.83949	12	7.095511	7.092478	12	5.122751	7.538446	12
7.332002	13.68776	15.04083	12	4.604011	5.404972	12	8.206811	14.38779	12
8.008898	18.90564	21.49801	12	4.529005	5.763519	12	9.184702	17.2915	12
8.685906	23.22027	33.39856	12	4.873432	6.115847	12	9.749575	19.9073	12
9.362911	21.77728	29.07252	12	6.324265	8.467457	12	10.76072	20.91628	12
10.03991	23.03457	25.77662	12	9.706065	15.29343	12	10.74674	20.75854	12
10.71692	28.68058	31.10882	12	15.55554	26.33889	12	9.997424	18.73794	12
11.39382	31.19563	34.42118	12	24.4714	38.05738	12	9.528738	16.58538	12
12.07083	30.29262	37.35425	12	38.88575	53.11441	12	9.730657	16.72496	12
12.74783	29.25637	38.68872	12	57.23523	71.17689	12	10.55922	19.31983	12
13.42484	28.55813	34.99262	12	77.00992	89.28022	12	10.66045	19.67494	12
14.10175	32.31198	27.33562	12	95.51108	102.5534	12	11.41052	19.51183	12
14.77874	42.35108	28.16131	12	131.6707	96.01762	12	11.56453	18.22736	12
15.45575	70.23546	29.89883	12	183.8491	85.59302	12	12.39589	19.99594	12
16.13275	122.958	45.85615	12	217.5528	59.4105	12	11.24086	17.85952	12
16.80976	179.7498	66.15689	12	217.2014	42.99625	12	11.46219	17.58526	12
17.48668	214.37	59.821	12	215.3	50.51845	12	10.69138	15.34906	12
18.16367	223.8464	66.14324	12	217.2947	46.74246	12	10.92231	14.56915	12
18.84067	226.9528	70.39801	12	222.5605	39.39075	12	9.711449	13.75346	12
19.51768	227.4264	65.60785	12	216.3935	42.80625	12	10.63107	14.8069	12
20.19462	226.3123	59.49748	12	222.2345	33.76373	12	10.11551	13.47803	12
20.87158	235.0929	34.43895	12	225.4488	30.68282	12	11.30533	16.49743	12
21.54859	237.2378	24.78452	12	220.0887	35.78635	12	10.35973	14.8032	12
22.22559	235.687	29.07442	12	221.648	32.33905	12	10.24671	14.60342	12
22.9026	241.7333	24.48665	12	218.9688	46.59445	12	10.90835	14.2294	12
23.57955	244.3028	23.34996	12	226.4228	36.9455	12	10.20518	13.86515	12
24.2565	232.7502	37.83449	12	219.3683	52.88271	12	8.286693	12.622	12

24.93351	239.5671	21.57456	12	221.1297	51.16001	12	7.600427	9.71994	12
25.61051	246.4073	9.677036	12	222.8823	40.52655	12	9.028194	10.45862	12
26.28749	246.6698	11.92448	12	218.9783	45.17551	12	9.493622	10.969	12
26.96441	245.5245	20.0507	12	211.9174	57.57244	12	7.9011	10.62332	12
27.64143	239.6066	36.79408	12	212.2089	46.38769	12	8.444687	10.04492	12
28.31843	234.1474	48.63007	12	222.2784	40.6358	12	9.082532	12.23847	12
28.99543	236.6104	53.063	12	217.413	41.30708	12	10.14543	15.62211	12
29.67242	229.2424	57.56403	12	211.9591	43.95488	12	8.380772	16.61939	12
30.34934	208.0969	79.83583	12	202.6343	51.38956	12	8.593969	17.56105	12
31.02635	191.535	92.9014	12	195.1799	61.4615	12	7.965147	15.60364	12
31.70335	172.6526	90.7747	12	175.715	71.87895	12	7.461236	12.89057	12
32.38036	136.2556	78.72327	12	157.3949	94.05448	12	7.920439	13.00891	12
33.05725	92.96827	61.53722	12	145.7712	95.92253	12	7.310927	12.05961	12
33.73426	59.37674	53.72695	12	128.4729	96.67147	12	6.150775	9.667782	12
34.45066	50.09156	44.45489	12	84.17335	77.88306	12	6.828099	9.831865	12
34.71161	40.06998	37.09428	12	54.49561	75.46189	12	7.280771	10.0357	12
35.74869	34.55371	33.03161	12	44.5134	72.73995	12	7.368074	9.83278	12
36.42517	30.04797	29.68705	12	36.25746	71.52658	12	7.054289	9.884406	12
37.10165	28.04742	29.18178	12	31.60304	66.43328	12	7.651276	14.29674	12
37.77813	30.89303	32.21766	12	27.33126	56.91653	12	8.423257	15.86217	12
38.45461	29.51782	29.67719	12	21.92537	44.50089	12	9.899257	18.55539	12
39.1311	25.25318	25.11213	12	16.58899	31.69322	12	8.315446	14.80848	12
39.80758	18.60425	22.58802	12	11.16124	22.20449	12	8.931766	17.26798	12
40.48406	18.18288	22.13435	12	7.876126	14.60886	12	8.2354	17.65902	12
41.16054	22.21955	23.79705	12	6.353494	9.832897	12	8.384417	17.05462	12
41.83702	25.45881	22.95183	12	6.065352	7.451534	12	3.172656	3.525263	12
42.5135	23.49667	24.78477	12	5.361496	6.236579	12	3.211626	3.320515	12
43.18998	23.27448	29.33677	12	5.885444	5.703302	12	2.441441	2.465064	12
43.86646	21.75401	24.02441	12	5.924212	5.121022	12	2.359172	2.677548	12
44.54295	21.59282	22.44076	12	6.297293	4.798362	12	2.566478	3.141175	12
45.21943	18.84061	14.98275	12	5.870465	5.404015	12	2.475185	2.694219	12
45.89591	26.4878	15.49066	12	5.719899	6.019286	12	1.95706	2.395159	12
46.57239	32.61825	14.74131	12	6.705505	5.839729	12	1.392781	1.963124	12
47.24887	30.34102	19.39092	12	5.024639	4.282923	12	2.30866	3.16191	12
47.92535	33.40644	23.83588	12	5.362946	4.644739	12	2.191842	3.345726	12
48.60183	35.41591	28.32541	12	5.71121	5.145166	12	2.383212	3.984797	12
49.27832	36.97659	31.59639	12	5.740119	5.017553	12	2.676144	4.556079	12
49.9548	37.955	31.78885	12	5.19152	4.975925	12	3.458858	5.049118	12
50.63128	39.29871	32.99458	12	4.929891	5.166483	12	3.770031	5.35325	12
51.30776	49.62167	32.26531	12	6.329653	5.267855	12	2.929341	5.858682	12
51.98424	48.88557	29.29629	12	6.181348	4.63765	12	3.299997	6.599993	12
52.66072	45.30491	21.64169	12	6.00696	3.741468	12	3.583005	7.16601	12
53.3372	41.93009	9.60245	12	5.847176	4.275928	12	4.831487	8.368382	12
54.01369	37.50681	4.449894	12	5.970532	5.030731	12	4.795012	8.305205	12

54.69017	37.05385	7.677812	12	6.258025	7.666482	12	7.105009	10.048	12

part 1.2 Perivenous distribution of intravitreally administered hAβ

distance (μm)	**Lectin (A.U.)**			**NG2DsRed (A.U.)**			**hAβ (A.U.)**		
	mean	SEM	n	mean	SEM	n	mean	SEM	n
0	0.184872	0.078021	18	0.348294	0.119264	18	26.10921	5.878114	18
0.568	0.609935	0.317628	18	0.307979	0.100703	18	26.54736	6.128166	18
1.136	0.971473	0.619904	18	0.234497	0.094115	18	26.77138	6.245928	18
1.705	0.804653	0.505688	18	0.217592	0.090278	18	26.55925	6.055027	18
2.273	0.410722	0.209486	18	0.218935	0.098542	18	26.69456	6.139286	18
2.841	0.18162	0.077484	18	0.238715	0.094972	18	24.15549	6.078374	18
3.409	0.146793	0.051617	18	0.222234	0.084908	18	24.01159	5.865092	18
3.977	0.338376	0.13691	18	0.216962	0.08239	18	24.68588	6.219095	18
4.545	7.243384	5.254383	18	0.27146	0.085233	18	31.24951	7.763357	18
5.114	7.305212	5.400915	18	0.30606	0.087574	18	31.42351	7.735865	18
5.682	6.918488	5.264488	18	0.288782	0.099766	18	28.49942	7.249518	18
6.25	6.860975	5.112357	18	0.300983	0.101507	18	27.84974	6.89921	18
6.818	6.645051	4.756969	18	0.244246	0.093309	18	27.62982	6.758084	18
7.386	5.631887	4.233796	18	0.270425	0.103706	18	27.62433	6.688368	18
7.955	4.407462	3.486699	18	0.304054	0.116408	18	27.3656	6.577402	18
8.523	4.266777	3.28173	18	0.228825	0.094987	18	27.24274	6.540872	18
9.091	4.614999	3.49176	18	0.20846	0.088151	18	27.35109	6.541726	18
9.659	5.667294	3.331027	18	0.228383	0.078036	18	27.4795	6.538259	18
10.227	5.759287	3.345079	18	0.305944	0.089063	18	28.03031	6.993031	18
10.795	6.583042	3.473998	18	0.331468	0.112198	18	27.9622	6.748077	18
11.364	6.428203	3.353871	18	0.349965	0.143819	18	28.26528	6.787627	18
11.932	6.719015	3.448249	18	0.389279	0.182462	18	28.16067	6.733587	18
12.5	7.432564	3.872856	18	0.42667	0.222645	18	28.34545	6.716934	18
13.068	7.67244	3.886354	18	0.442548	0.256905	18	28.67656	6.781263	18
13.636	8.311928	3.770504	18	0.504976	0.268043	18	27.20646	6.767548	18
14.205	8.393799	3.92246	18	0.493346	0.261966	18	27.05631	6.493918	18
14.773	8.613011	3.954204	18	0.524675	0.25723	18	27.0022	6.484901	18
15.341	8.548951	3.847863	18	0.560806	0.247892	18	27.16957	6.569516	18
15.909	8.386315	3.658463	18	0.552636	0.227948	18	27.89737	6.8467	18
16.477	8.555093	3.665608	18	0.543838	0.214622	18	28.60113	7.157644	18
17.045	8.797254	3.706627	18	0.548213	0.21588	18	29.01827	7.216774	18
17.614	9.060307	3.951761	18	0.567856	0.238809	18	28.7158	6.936529	18
18.182	9.132271	3.959307	18	0.648017	0.276274	18	28.42001	6.722707	18
18.75	9.126642	3.836327	18	0.765535	0.323081	18	28.85929	6.835778	18
19.318	9.23738	3.869312	18	0.859636	0.372305	18	28.96881	6.720459	18
19.886	9.461862	3.625427	18	0.878816	0.385679	18	28.78133	6.315832	18
20.455	9.321722	3.38253	18	0.872141	0.394477	18	28.24502	6.093389	18

21.023	9.365897	3.456824	18	0.855455	0.40001	18	28.48272	6.286773	18
21.591	9.455313	3.591303	18	0.854524	0.395467	18	28.40738	6.443814	18
22.159	9.555858	3.759452	18	0.863907	0.381942	18	28.29277	6.400899	18
22.727	9.225192	3.640449	18	0.78079	0.33716	18	28.26207	6.181562	18
23.295	9.338815	3.651143	18	0.777707	0.309036	18	28.20579	6.076416	18
23.864	10.00759	3.89531	18	0.753295	0.292329	18	28.14405	6.173916	18
24.432	9.891471	3.756865	18	0.803016	0.291417	18	28.03642	6.160029	18
25	9.824291	3.798971	18	0.782038	0.287459	18	27.72204	6.1057	18
25.568	10.6032	4.443882	18	0.677995	0.272468	18	27.56766	6.043784	18
26.136	10.58256	4.333478	18	0.679851	0.275977	18	28.2774	6.205231	18
26.705	10.56508	3.994621	18	0.694829	0.258543	18	28.78323	6.340709	18
27.273	11.19165	4.103617	18	0.694601	0.222055	18	28.55345	6.290174	18
27.841	11.074	4.262519	18	0.586327	0.170792	18	28.55481	6.290503	18
28.409	10.69469	4.291286	18	0.474664	0.135844	18	28.77023	6.405405	18
28.977	9.980502	3.681297	18	0.432233	0.12673	18	29.02964	6.568888	18
29.545	8.869029	3.377612	18	0.394932	0.127688	18	29.16882	6.517903	18
30.114	8.538635	3.311377	18	0.345096	0.119653	18	29.04678	6.396119	18
30.682	9.144167	3.231716	18	0.292762	0.09907	18	28.7397	6.244401	18
31.25	8.893184	3.20781	18	0.440972	0.200792	18	28.47706	6.197786	18
31.818	8.674813	3.173008	18	0.477098	0.219689	18	28.82542	6.387041	18
32.386	8.594617	2.951424	18	0.317983	0.101749	18	29.80065	6.758086	18
32.955	8.776044	2.822338	18	0.347147	0.121117	18	31.38671	7.036426	18
33.523	9.130856	2.870814	18	0.442769	0.174311	18	31.85675	7.169849	18
34.091	9.403118	2.925339	18	0.350166	0.122592	18	31.88775	7.302311	18
34.659	9.665301	3.069093	18	0.307364	0.113296	18	32.9273	7.96893	18
35.227	10.31883	3.407603	18	0.323521	0.118456	18	33.27928	8.211049	18
35.795	12.24304	3.967935	18	0.309978	0.117867	18	32.51859	7.761797	18
36.364	14.60851	4.529472	18	0.373934	0.134071	18	32.43769	7.809408	18
36.932	15.33968	4.628077	18	0.393472	0.137545	18	32.5857	7.916626	18
37.50001	15.25136	4.777475	18	0.33971	0.124696	18	32.60572	7.881711	18
38.06819	17.965	5.114989	18	0.317609	0.129407	18	32.78438	7.734643	18
38.63637	22.06918	5.744071	18	0.370337	0.139618	18	32.68586	7.511267	18
39.20455	26.5408	6.447827	18	0.396213	0.138906	18	33.33157	7.472299	18
39.77274	31.87387	7.139598	18	0.357805	0.135468	18	34.0082	7.441673	18
40.34092	37.03637	7.650288	18	0.384577	0.144471	18	34.77238	7.347463	18
40.9091	42.82348	7.888426	18	0.415658	0.152324	18	35.01603	7.165875	18
41.47728	50.19721	7.760706	18	0.375445	0.141738	18	35.60644	7.120407	18
42.04546	59.1459	7.391955	18	0.432056	0.159985	18	36.87261	7.251438	18
42.61365	70.32971	7.090587	18	0.440686	0.160621	18	38.0712	7.429739	18
43.18183	86.76061	6.263657	18	0.419167	0.156716	18	38.86274	7.363275	18
43.75001	105.8267	5.278806	18	0.474542	0.168249	18	40.24178	7.204035	18
44.31819	126.3985	5.185789	18	0.485989	0.169003	18	42.07103	7.033948	18
44.88638	146.5442	7.084827	18	0.551021	0.184538	18	42.93412	6.697086	18
45.45456	160.5883	8.278804	18	0.632352	0.214026	18	44.28206	6.482325	18

46.02274	170.4528	8.389743	18	0.690565	0.23925	18	45.25233	6.26233	18
46.59092	178.059	9.020686	18	0.7624	0.265833	18	45.60366	5.873083	18
47.1591	181.4954	9.662075	18	0.8553	0.299954	18	45.96578	5.604895	18
47.72729	184.0479	10.22662	18	0.918757	0.323126	18	47.05958	5.481903	18
48.29547	188.0004	10.43904	18	1.07791	0.352191	18	48.13453	5.403434	18
48.86365	190.3582	10.60572	18	1.127128	0.375865	18	48.55804	5.283694	18
49.43183	192.3825	10.60579	18	1.114875	0.42908	18	49.28591	5.178863	18
50.00001	193.3792	10.45709	18	1.176081	0.460089	18	50.63686	5.175586	18
50.5682	194.3624	9.842977	18	1.134645	0.426788	18	51.24115	5.058699	18
51.13638	194.1957	9.181246	18	1.119258	0.411644	18	51.3764	5.002338	18
51.70456	193.6897	8.993975	18	1.099164	0.39328	18	51.57748	5.178072	18
52.27274	192.5015	9.018541	18	1.109313	0.412423	18	51.9199	5.348876	18
52.84092	191.197	9.07884	18	1.071302	0.396307	18	52.13673	5.49861	18
53.40911	190.1189	9.1183	18	1.027229	0.369147	18	51.82854	5.240368	18
53.97729	189.7562	9.177058	18	0.961538	0.337721	18	51.43889	5.099764	18
54.54547	188.4863	9.519219	18	1.028013	0.362918	18	51.6123	5.279951	18
55.11365	188.946	9.499803	18	1.167777	0.451407	18	51.6114	5.353719	18
55.68183	189.4412	9.502213	18	1.063888	0.383045	18	52.16731	5.456563	18
56.25002	187.9624	9.787592	18	0.980102	0.321771	18	52.40885	5.463089	18
56.8182	184.644	9.979663	18	0.956495	0.306906	18	52.34692	5.409173	18
57.38638	180.4468	10.44135	18	1.053722	0.330644	18	51.98931	5.34671	18
57.95456	176.2254	10.94657	18	1.090618	0.345074	18	51.47901	5.186513	18
58.52274	173.539	11.28369	18	1.175503	0.392557	18	51.55506	5.118214	18
59.09093	171.2958	11.63003	18	1.278796	0.455611	18	52.05124	5.205906	18
59.65911	169.7767	11.90117	18	1.360706	0.494548	18	52.30715	5.296243	18
60.22729	169.6007	11.86356	18	1.272347	0.431185	18	52.54219	5.322301	18
60.79547	168.4776	12.00375	18	1.18325	0.358266	18	52.8158	5.300677	18
61.36366	167.2833	12.36795	18	1.143459	0.319952	18	53.17776	5.304002	18
61.93184	166.9066	12.77259	18	1.175824	0.337795	18	54.08836	5.395469	18
62.50002	166.2984	13.10547	18	1.17573	0.338611	18	54.75111	5.436702	18
63.0682	165.3169	13.4017	18	1.194193	0.353168	18	55.57803	5.54534	18
63.63638	164.7701	13.71507	18	1.161399	0.370608	18	55.93974	5.575253	18
64.20457	162.6104	13.96364	18	1.171361	0.38544	18	55.87506	5.499039	18
64.77275	161.8698	13.90424	18	1.113514	0.356068	18	56.15213	5.508136	18
65.34093	164.4192	13.84927	18	1.000895	0.313652	18	56.37049	5.49081	18
65.90911	166.5323	13.76194	18	0.933605	0.282323	18	56.39693	5.432745	18
66.47729	166.708	13.90499	18	0.877645	0.261638	18	56.62407	5.419479	18
67.04548	167.6254	13.79844	18	0.79595	0.257753	18	57.20473	5.497776	18
67.61366	170.0052	13.26102	18	0.810418	0.28428	18	57.40676	5.611531	18
68.18184	171.7315	12.99817	18	0.776402	0.273254	18	57.47042	5.716115	18
68.75002	172.7153	12.79941	18	0.839798	0.280045	18	57.25391	5.630681	18
69.3182	173.8801	12.56626	18	0.865467	0.289241	18	57.49633	5.668588	18
69.88639	174.6719	12.50184	18	0.825099	0.271939	18	57.58702	5.753224	18
70.45457	174.6969	12.62963	18	0.815518	0.268454	18	57.56268	5.676654	18

71.02275	175.2841	12.66514	18	0.821503	0.276239	18	57.5384	5.664448	18
71.59093	175.5751	12.74165	18	0.907227	0.301667	18	58.07255	5.801264	18
72.15911	175.8246	12.70697	18	1.031879	0.326708	18	58.08713	5.852541	18
72.7273	175.417	12.61993	18	1.040475	0.309356	18	57.90746	5.926552	18
73.29548	174.7857	12.61491	18	1.108314	0.316353	18	57.44258	5.749913	18
73.86366	174.9197	12.64229	18	1.168293	0.309646	18	58.07621	5.963959	18
74.43184	175.3847	12.66096	18	1.270236	0.351527	18	58.0587	6.154994	18
75.00002	175.7757	12.78761	18	1.326671	0.418742	18	57.74507	6.083676	18
75.56821	174.4061	13.15707	18	1.455965	0.512858	18	57.74406	6.005449	18
76.13639	173.7706	13.37805	18	1.52759	0.574995	18	57.75992	6.029389	18
76.70457	173.6666	13.39202	18	1.596608	0.628049	18	57.59183	5.950701	18
77.27275	173.8581	13.30219	18	1.507114	0.516564	18	58.38737	6.005979	18
77.84094	175.3916	13.02896	18	1.460095	0.441364	18	58.60383	6.049468	18
78.40912	176.4148	12.80921	18	1.351899	0.411019	18	58.27506	6.102754	18
78.9773	176.7712	12.68247	18	1.400631	0.412931	18	58.08673	6.154382	18
79.54548	177.6596	12.43124	18	1.343807	0.398483	18	57.8043	6.153296	18
80.11366	177.9602	12.22932	18	1.351984	0.418663	18	57.43972	6.17998	18
80.68185	177.7127	12.24481	18	1.437127	0.444835	18	57.27688	6.168502	18
81.25003	178.6648	11.67314	18	1.458629	0.478856	18	57.78707	6.313425	18
81.81821	179.1042	11.15055	18	1.532887	0.538121	18	57.9394	6.470703	18
82.38639	178.3916	11.47178	18	1.577294	0.577262	18	57.5579	6.427989	18
82.95457	178.3137	11.577	18	1.739435	0.61855	18	57.20625	6.383847	18
83.52276	178.4008	11.47315	18	1.920052	0.659133	18	57.52446	6.404931	18
84.09094	177.545	11.15003	18	1.94682	0.716921	18	57.44837	6.193099	18
84.65912	177.3114	10.87121	18	2.146238	0.828543	18	57.81834	6.08373	18
85.2273	176.3331	10.9667	18	2.384995	0.943707	18	58.25881	6.189951	18
85.79548	174.9264	11.15654	18	2.625844	1.063796	18	58.38294	6.241944	18
86.36367	174.6092	11.43431	18	2.889778	1.186871	18	58.06946	6.144117	18
86.93185	175.3952	11.63644	18	3.107864	1.303798	18	58.18577	6.144779	18
87.50003	175.7406	11.54837	18	3.318899	1.419803	18	58.18596	6.132078	18
88.06821	177.4421	11.38458	18	3.356165	1.504468	18	58.64534	6.224677	18
88.63639	179.1203	11.34266	18	3.38545	1.564678	18	59.21003	6.286231	18
89.20458	180.9035	11.48601	18	3.406691	1.598792	18	59.12729	6.237346	18
89.77276	182.074	11.4216	18	3.322595	1.61994	18	59.58066	6.361956	18
90.34094	182.2041	10.89747	18	3.313885	1.637025	18	59.69947	6.461735	18
90.90912	180.9252	10.31504	18	3.295961	1.641466	18	60.02674	6.668089	18
91.4773	181.1356	10.1005	18	3.274125	1.626219	18	60.44295	6.823195	18
92.04549	181.5432	10.01621	18	3.257837	1.565705	18	60.45524	6.83694	18
92.61367	182.9038	9.989508	18	3.206829	1.488228	18	60.44559	6.816128	18
93.18185	183.7502	10.04446	18	3.024296	1.378559	18	60.46136	6.889326	18
93.75003	183.6619	10.36645	18	2.845178	1.250003	18	59.94837	6.857568	18
94.31822	183.4191	10.81643	18	2.667703	1.080618	18	59.73334	6.890779	18
94.8864	184.0187	10.78565	18	2.637107	0.94656	18	59.78733	7.001599	18
95.45458	184.1964	10.87685	18	2.448814	0.80892	18	59.39426	6.999136	18

96.02276	184.0907	10.8927	18	2.468289	0.71288	18	58.94249	6.772486	18
96.59094	184.4945	10.96879	18	2.29823	0.659848	18	58.75931	6.609399	18
97.15913	184.4456	11.31586	18	2.23443	0.667691	18	58.93258	6.590837	18
97.72731	184.3936	11.59986	18	2.063379	0.59972	18	59.15005	6.622616	18
98.29549	183.582	11.82249	18	1.917383	0.5401	18	59.31153	6.726784	18
98.86367	181.9114	12.31308	18	1.670863	0.45241	18	59.20773	6.784376	18
99.43185	181.2518	12.74291	18	1.498396	0.406471	18	59.60242	6.767872	18
100	181.4778	12.77971	18	1.439865	0.381715	18	59.95448	6.748089	18
100.5682	181.7439	12.6934	18	1.351068	0.375701	18	60.625	6.844741	18
101.1364	181.345	12.58637	18	1.393292	0.399101	18	60.30946	6.707537	18
101.7046	182.1956	11.8969	18	1.456649	0.440329	18	60.64389	6.683074	18
102.2728	182.2014	11.6087	18	1.297205	0.388531	18	60.9357	6.716697	18
102.8409	180.2494	11.7075	18	1.292656	0.391693	18	60.91437	6.706153	18
103.4091	178.703	11.76224	18	1.388078	0.418028	18	60.62248	6.694396	18
103.9773	178.5462	11.66815	18	1.405745	0.422502	18	60.7669	6.85971	18
104.5455	177.9048	11.67323	18	1.472839	0.473308	18	60.51037	6.990733	18
105.1137	178.1159	11.58885	18	1.476072	0.478044	18	59.87026	6.948835	18
105.6819	178.5282	11.49235	18	1.457018	0.460143	18	60.2039	7.003768	18
106.25	179.2598	11.22557	18	1.467639	0.46331	18	60.99495	7.091331	18
106.8182	178.8222	11.16122	18	1.619528	0.536751	18	61.22286	7.2062	18
107.3864	178.762	11.06467	18	1.87155	0.793705	18	61.02966	7.244174	18
107.9546	178.1996	10.93028	18	2.258817	1.178284	18	60.94408	7.221802	18
108.5228	177.0718	10.75127	18	2.641437	1.487902	18	61.16781	7.270589	18
109.0909	175.0535	10.85263	18	2.836466	1.706612	18	61.2097	7.146976	18
109.6591	173.6843	10.67111	18	2.714862	1.665544	18	61.68909	7.092724	18
110.2273	171.381	10.57071	18	2.433017	1.390508	18	62.27653	7.052635	18
110.7955	169.8217	10.66115	18	2.492445	1.377743	18	62.5941	7.000921	18
111.3637	169.0914	10.72121	18	2.588242	1.479634	18	62.33529	7.018844	18
111.9319	169.3343	10.70117	18	2.551405	1.341401	18	62.47935	7.138824	18
112.5	168.8314	10.69362	18	2.181105	1.002822	18	63.20657	7.47147	18
113.0682	167.6076	10.5309	18	1.607973	0.64198	18	63.61254	7.638413	18
113.6364	165.7155	10.18912	18	1.435784	0.549903	18	63.70898	7.597907	18
114.2046	163.5481	9.991531	18	1.458908	0.559321	18	63.46984	7.50436	18
114.7728	160.9314	10.05227	18	1.503862	0.560893	18	63.3381	7.437972	18
115.341	159.4965	10.18242	18	1.561028	0.571726	18	63.12049	7.464704	18
115.9091	157.897	10.33369	18	1.437559	0.498901	18	63.0414	7.526181	18
116.4773	157.3637	10.43307	18	1.410796	0.471326	18	63.43519	7.593318	18
117.0455	158.8104	10.23738	18	1.504685	0.502491	18	63.45572	7.488907	18
117.6137	158.7931	10.18755	18	1.46211	0.508124	18	64.35308	7.734594	18
118.1819	156.7877	10.85974	18	1.546876	0.581278	18	65.31218	8.016828	18
118.75	155.4081	10.75671	18	1.641238	0.632134	18	65.4616	8.125853	18
119.3182	155.482	10.71366	18	1.797821	0.679227	18	65.41597	8.127885	18
119.8864	155.1328	10.78743	18	1.842528	0.721413	18	65.09665	8.08342	18
120.4546	153.4623	11.11406	18	1.821399	0.776907	18	64.96499	8.108586	18

121.0228	153.373	11.3539	18	1.806702	0.800106	18	64.66257	8.021802	18
121.591	155.0505	11.2765	18	1.811679	0.799809	18	64.79598	8.098334	18
122.1591	155.4898	11.19987	18	1.867172	0.797529	18	64.23005	7.94403	18
122.7273	154.3847	11.32811	18	2.017273	0.860066	18	63.83759	7.867507	18
123.2955	152.2695	11.93741	18	2.121574	0.892535	18	63.41972	7.883275	18
123.8637	153.4881	11.41979	18	2.484673	0.99007	18	63.18276	7.886276	18
124.4319	155.8783	10.79041	18	2.890555	1.201489	18	63.21594	7.993614	18
125	156.5927	10.68028	18	3.412317	1.591196	18	61.85232	7.762283	18
125.5682	154.9385	10.98813	18	4.007746	2.088352	18	61.38847	7.791288	18
126.1364	154.1109	11.36352	18	4.084524	2.101881	18	61.65713	7.849992	18
126.7046	155.1802	11.32437	18	3.215204	1.287973	18	60.97383	7.740209	18
127.2728	152.916	12.01861	18	2.474482	0.761687	18	60.90401	7.815592	18
127.841	151.6632	12.4397	18	2.103824	0.683359	18	60.98212	7.888025	18
128.4091	153.4019	11.82716	18	2.123005	0.707084	18	61.13608	8.010184	18
128.9773	156.5248	11.6186	18	2.190894	0.7405	18	61.16641	8.082894	18
129.5455	160.3545	11.88529	18	2.007592	0.636665	18	61.43485	8.180137	18
130.1137	162.6874	12.12968	18	1.880667	0.581226	18	61.93072	8.272222	18
130.6819	162.2523	12.08323	18	1.96478	0.59955	18	61.96499	8.372336	18
131.25	162.5531	12.03458	18	2.002113	0.655514	18	62.0549	8.452233	18
131.8182	163.3114	12.2238	18	1.97948	0.692232	18	61.78776	8.515696	18
132.3864	163.4418	12.5432	18	1.798988	0.634738	18	61.06754	8.409925	18
132.9546	164.6552	12.71298	18	1.773378	0.60774	18	60.88062	8.320658	18
133.5228	164.7885	12.78156	18	1.86949	0.562415	18	60.73005	8.350873	18
134.091	162.6223	13.00831	18	1.707502	0.444994	18	60.49372	8.300317	18
134.6591	159.3405	13.45684	18	1.495761	0.360316	18	60.58812	8.324686	18
135.2273	157.4971	14.09511	18	1.440234	0.331719	18	60.56344	8.359602	18
135.7955	155.8296	14.3152	18	1.300286	0.334664	18	60.23122	8.361425	18
136.3637	154.4998	14.23402	18	1.327209	0.369918	18	59.992	8.346442	18
136.9319	154.0875	14.10151	18	1.327648	0.38708	18	59.82639	8.250289	18
137.5001	154.4541	13.99147	18	1.357461	0.401376	18	59.52461	8.160524	18
138.0682	154.5472	13.96643	18	1.383127	0.393586	18	59.22015	8.152401	18
138.6364	154.1491	14.12258	18	1.467199	0.417949	18	58.38734	8.065979	18
139.2046	154.0414	14.33034	18	1.574299	0.515932	18	57.50542	7.959691	18
139.7728	152.7758	14.2784	18	1.731423	0.65851	18	57.17116	7.915435	18
140.341	151.1486	14.12149	18	1.98002	0.822578	18	56.68208	7.915759	18
140.9091	149.4212	13.77792	18	2.083157	0.896857	18	56.31532	7.782215	18
141.4773	146.7685	13.39992	18	2.117583	0.924857	18	56.29994	7.787075	18
142.0455	145.0851	13.22803	18	2.313183	1.052221	18	56.3103	7.820112	18
142.6137	144.4504	13.36871	18	2.566188	1.191116	18	56.31096	7.860607	18
143.1819	144.7525	13.56166	18	2.677147	1.273805	18	56.219	8.04741	18
143.7501	144.8728	13.57203	18	2.742106	1.310759	18	56.57374	8.364156	18
144.3182	144.8548	13.39431	18	2.819435	1.309937	18	56.0711	8.459045	18
144.8864	144.0787	13.14178	18	2.83983	1.273415	18	55.455	8.363478	18
145.4546	141.7584	12.80182	18	3.073673	1.336635	18	54.83623	8.388937	18

146.0228	141.0724	12.88086	18	3.173805	1.365509	18	54.54629	8.485261	18
146.591	141.4929	13.22834	18	2.98602	1.294601	18	54.24396	8.517562	18
147.1591	141.5477	13.4464	18	2.877503	1.263656	18	54.00262	8.448405	18
147.7273	142.3921	13.82102	18	2.755147	1.217543	18	53.69414	8.428158	18
148.2955	144.0282	14.26306	18	2.732169	1.164173	18	53.51354	8.417773	18
148.8637	145.0752	14.32859	18	2.792293	1.15324	18	53.60794	8.535132	18
149.4319	146.1963	14.16778	18	2.701305	1.139236	18	53.57712	8.477226	18
150.0001	149.2756	13.98334	18	2.543452	1.097045	18	53.57376	8.465342	18
150.5682	154.7843	14.31981	18	2.475692	1.050748	18	53.71007	8.456156	18
151.1364	160.2515	14.90029	18	2.540102	0.999324	18	53.59245	8.513217	18
151.7046	164.6327	15.27032	18	2.374304	0.933409	18	53.81286	8.573869	18
152.2728	166.9653	15.07533	18	2.112729	0.857206	18	54.39801	8.654609	18
152.841	168.4502	14.6839	18	2.112973	0.797309	18	54.26561	8.595508	18
153.4092	169.8251	14.12601	18	2.204434	0.749575	18	53.67676	8.560297	18
153.9773	171.0419	13.38298	18	2.321776	0.757555	18	53.74582	8.726804	18
154.5455	171.9258	12.93142	18	2.34957	0.71912	18	53.85848	8.888405	18
155.1137	173.5044	12.73251	18	2.135199	0.639981	18	53.50822	9.027802	18
155.6819	174.7038	12.29706	18	1.978047	0.634294	18	53.07827	9.187306	18
156.2501	174.7264	11.74721	18	2.160765	0.753667	18	53.23336	9.235114	18
156.8182	175.4116	11.46982	18	2.391639	0.902215	18	53.01249	9.249211	18
157.3864	175.7512	11.48708	18	2.669289	1.025961	18	52.7446	9.295404	18
157.9546	175.4963	11.50295	18	2.689232	0.972275	18	52.75555	9.657308	18
158.5228	174.3353	11.43884	18	2.462624	0.84645	18	52.31729	9.771208	18
159.091	172.3379	11.46548	18	2.301993	0.748446	18	51.79829	9.688248	18
159.6592	164.7097	10.82252	18	2.278451	0.676894	18	51.55158	9.828139	18
160.2273	157.5655	10.74706	18	2.26925	0.670458	18	50.63049	9.838009	18
160.7955	151.4015	10.83263	18	2.449815	0.837475	18	49.69172	9.750888	18
161.3637	144.7722	10.47765	18	2.751971	1.030292	18	49.26604	9.988514	18
161.9319	138.2769	10.6797	18	3.048777	1.192954	18	49.03037	10.27006	18
162.5001	128.9882	11.24565	18	3.64549	1.577848	18	48.63482	10.41573	18
163.0682	118.0249	11.80545	18	4.298586	2.082363	18	48.62237	10.71119	18
163.6364	107.2585	11.64064	18	4.462591	2.309399	18	48.43318	11.05936	18
164.2046	97.7687	11.30927	18	4.365696	2.422002	18	47.76825	11.36683	18
164.7728	84.49101	11.36545	18	3.954084	2.290723	18	46.10512	11.15066	18
165.341	70.80418	11.1825	18	3.826852	2.307299	18	44.38476	10.88372	18
165.9092	60.16077	10.58343	18	3.695594	2.271299	18	43.1363	10.83567	18
166.4773	51.24344	10.00809	18	3.579744	2.220318	18	42.75166	11.07689	18
167.0455	43.27202	9.299206	18	3.29875	1.94077	18	41.91732	11.19945	18
167.6137	36.0582	8.641864	18	2.7278	1.330743	18	40.79679	11.18021	18
168.1819	30.31899	8.011654	18	2.030295	0.823415	18	40.36463	11.37123	18
168.7501	26.34956	7.688538	18	1.608041	0.6963	18	10.74554	10.44279	18
169.3182	22.42179	7.233626	18	1.573786	0.765745	18	8.906912	8.655962	18
169.8864	19.37078	6.811572	18	1.680718	0.821323	18	9.018814	8.764711	18
170.4546	16.52265	6.509228	18	1.787266	0.862471	18	9.207189	8.94778	18

171.0228	14.61039	6.233014	18	1.828699	0.851536	18	9.388529	9.12401	18
171.591	13.14584	5.930116	18	1.842203	0.819071	18	9.634441	9.362994	18
172.1592	12.04013	5.653711	18	1.767564	0.79648	18	9.768744	9.493513	18
172.7273	10.90624	5.355723	18	1.642016	0.786071	18	9.933706	9.653827	18
173.2955	9.621685	4.859858	18	1.560203	0.771651	18	10.22277	9.934748	18
173.8637	8.474976	4.291876	18	1.441067	0.738678	18	10.13706	9.85145	18
174.4319	7.69849	3.755345	18	1.302808	0.673382	18	9.872769	9.594607	18
175.0001	7.539095	3.258189	18	1.142157	0.61494	18	10.09501	9.810588	18
175.5683	8.015117	3.044045	18	1.494111	0.698838	18	10.0011	9.719327	18
176.1364	9.391996	3.395116	18	2.253395	1.295674	18	9.690319	9.417297	18
176.7046	12.42892	5.236071	18	3.130009	2.073207	18	9.717568	9.443778	18
177.2728	14.72156	7.135425	18	3.593644	2.462874	18	9.44676	9.1806	18
177.841	15.70489	8.217458	18	3.509094	2.356553	18	8.980451	8.72743	18
178.4092	15.09234	7.732298	18	2.854321	1.772614	18	8.812819	8.564521	18
178.9773	13.65942	6.326138	18	2.065772	1.145951	18	8.593318	8.351204	18
179.5455	11.61029	4.783216	18	1.431153	0.811215	18	8.362013	8.126416	18
180.1137	11.15735	4.623385	18	1.22757	0.80992	18	8.319969	8.085556	18
180.6819	10.14663	4.022112	18	1.183179	0.791904	18	8.38522	8.148969	18
181.2501	9.029327	3.464316	18	1.181402	0.744569	18	8.470989	8.232322	18
181.8183	9.149976	3.556265	18	1.128947	0.676055	18	8.475128	8.236344	18
182.3864	10.22068	3.898371	18	1.05411	0.593107	18	8.537227	8.296694	18
182.9546	11.6294	4.557168	18	0.953303	0.497611	18	8.664874	8.420744	18
183.5228	11.45788	4.50216	18	0.875533	0.402882	18	9.038979	8.784309	18
184.091	10.24962	3.952393	18	0.755733	0.311145	18	9.124427	8.867349	18
184.6592	7.6119	3.355018	18	0.627013	0.23472	18	9.179544	8.905465	18
185.2273	7.476284	3.144884	18	0.523676	0.174161	18	8.968438	8.700663	18
185.7955	7.246402	2.928059	18	0.516407	0.164314	18	8.920612	8.654264	18
186.3637	7.04759	2.934952	18	0.570916	0.184439	18	9.275018	8.980498	18
186.9319	8.006494	3.106551	18	0.526856	0.203573	18	9.162998	8.872035	18
187.5001	9.013038	3.528854	18	0.612826	0.221164	18	9.095498	8.806678	18
188.0683	9.900369	4.000217	18	0.772801	0.28163	18	9.071923	8.783852	18
188.6364	23.22397	12.40872	18	0.660379	0.261982	18	9.099442	8.810497	18
189.2046	10.94666	4.531415	18	0.642917	0.283315	18	9.243824	8.950294	18
189.7728	10.4592	4.333954	18	0.70074	0.294602	18	9.494287	9.192804	18
190.341	11.16594	4.579408	18	0.678946	0.287304	18	9.437731	9.138044	18
190.9092	11.24407	4.543419	18	0.621942	0.264081	18	9.238444	8.945085	18
191.4773	23.25705	12.25176	18	0.554613	0.234485	18	9.164542	8.873529	18
192.0455	11.5158	4.563237	18	0.488508	0.206408	18	9.620705	9.315208	18
192.6137	12.61028	5.137402	18	0.509498	0.194252	18	9.65404	9.347484	18
193.1819	14.53309	6.093887	18	0.600652	0.19692	18	9.648009	9.320862	18
193.7501	14.52548	6.120352	18	0.559261	0.185755	18	10.0157	9.676085	18
194.3183	13.14669	5.298714	18	0.550895	0.189635	18	10.16824	9.823457	18
194.8864	11.51335	4.590276	18	0.574037	0.205108	18	10.19734	9.851569	18
195.4546	11.85479	4.683899	18	0.600394	0.219835	18	10.03409	9.693849	18

196.0228	12.01412	4.709603	18	0.603993	0.225233	18	9.908115	9.572149	18
196.591	11.92796	4.701173	18	0.639819	0.231468	18	9.835076	9.501586	18
197.1592	8.652213	4.228119	18	0.418443	0.156305	18	10.16036	9.761762	18
197.7274	4.429108	2.664497	18	0.462678	0.166294	18	12.82689	12.28081	18
198.2955	4.374405	2.625794	18	0.47102	0.170827	18	13.01089	12.45698	18
198.8637	5.617515	3.509114	18	0.38247	0.159071	18	13.43023	12.80522	18
199.4319	6.434244	3.819411	18	0.350259	0.137437	18	13.80512	13.09668	18
200.0001	6.131552	3.604903	18	0.348858	0.149887	18	13.85864	13.14746	18
200.5683	6.50239	3.851919	18	0.363394	0.160874	18	13.92672	13.21204	18
201.1364	6.3709	3.721457	18	0.349764	0.153589	18	13.86089	13.14959	18
201.7046	5.978802	3.427316	18	0.321766	0.138763	18	13.78085	13.07366	18
202.2728	5.914548	3.405793	18	0.284088	0.122797	18	13.87194	13.16007	18
202.841	1.034413	0.458041	18	0.354864	0.137827	18	11.38568	10.73452	18
203.4092	1.00615	0.425314	18	0.381742	0.148177	18	11.46236	10.80681	18
203.9774	1.078617	0.414163	18	0.418968	0.170082	18	11.51725	10.85857	18
204.5455	0.96812	0.366233	18	0.469103	0.197371	18	11.54708	10.88669	18
205.1137	0.749875	0.303428	18	0.479046	0.20624	18	11.53876	10.87885	18
205.6819	0.519251	0.250604	18	0.486981	0.207514	18	11.55516	10.89431	18
206.2501	0.414431	0.25292	18	0.506013	0.195833	18	11.58846	10.9257	18
206.8183	0.465489	0.275299	18	0.48469	0.157812	18	11.61625	10.9519	18
207.3864	0.584414	0.338198	18	0.600318	0.178534	18	11.63844	10.97282	18
207.9546	0.771124	0.448758	18	0.806757	0.242003	18	11.66287	10.99586	18
208.5228	0.938835	0.561678	18	0.994261	0.303238	18	11.68854	11.02007	18
209.091	1.046426	0.632642	18	1.20369	0.370351	18	11.72608	11.05546	18
209.6592	1.121371	0.673469	18	1.406723	0.436037	18	11.7663	11.09338	18
210.2274	1.547828	0.80215	18	1.316919	0.465724	18	13.39739	12.40358	18
210.7955	1.569297	0.82249	18	1.392634	0.493501	18	13.4455	12.44811	18
211.3637	1.542485	0.831838	18	1.409878	0.495166	18	13.4777	12.47793	18
211.9319	0.084882	0.039011	18	1.6163	0.536377	18	14.78514	13.49693	18
212.5001	0.128788	0.060178	18	1.677251	0.555657	18	14.8201	13.52884	18
213.0683	0.145792	0.066971	18	1.611941	0.523677	18	14.86785	13.57243	18

Part 1.3 Periarterial distribution of intracisternally administered Dextran tracer

distance (μm)	**Lectin (A.U.)**			**NG_2DsRed (A.U.)**			**Dextran (A.U.)**		
	mean	**SEM**	**n**	**mean**	**SEM**	**n**	**mean**	**SEM**	**n**
0	0	0	8	0	0	8	13.36156	11.8044	8
0.6263	0	0	8	0.865131	0.865131	8	12.60258	7.463995	8
1.2526	0	0	8	0.602401	0.602401	8	18.92277	14.57065	8

1.8789	0	0	8	0.206584	0.206584	8	21.64619	15.38742	8
2.5052	0	0	8	0.049033	0.049033	8	23.78959	10.00627	8
3.1315	0	0	8	-0.01078	0.010777	8	39.18436	22.31034	8
3.7578	0	0	8	-0.00359	0.003588	8	37.00375	19.23305	8
4.3841	0	0	8	-0.15945	0.136316	8	27.17741	15.07486	8
5.0104	1.11477	1.302265	8	3.027027	1.886209	8	28.01056	13.00258	8
5.6367	1.1951	1.278373	8	3.526368	2.187015	8	35.95775	13.34659	8
6.263	3.21674	2.038304	8	2.066363	2.152029	8	53.57844	15.48311	8
6.8893	5.11763	2.653112	8	2.632991	1.800098	8	74.9667	26.73986	8
7.5156	3.19	1.709694	8	1.898986	1.219404	8	87.82342	27.33698	8
8.1419	3.25716	1.938525	8	2.118125	1.366436	8	99.94927	27.05008	8
8.7682	3.33594	2.193608	8	2.208729	1.940659	8	111.3572	28.62795	8
9.3945	4.14534	2.190633	8	2.534787	3.261247	8	142.6298	33.64894	8
10.0208	4.36563	2.568925	8	19.71022	10.90451	8	154.422	34.22724	8
10.6471	5.41562	3.614116	8	74.6695	34.02893	8	161.8688	31.06331	8
11.2734	8.81875	4.820042	8	101.0108	42.87625	8	158.48	26.55124	8
11.8997	12.8655	6.157897	8	111.3945	43.4312	8	145.2031	27.56214	8
12.526	16.3521	6.92571	8	121.558	41.35164	8	140.4124	33.51748	8
13.1523	26.5138	9.362271	8	165.498	33.59461	8	139.4968	37.18206	8
13.7786	78.7337	20.48965	8	187.0351	33.13617	8	133.54	36.01916	8
14.4049	167.974	26.35069	8	189.6502	30.16785	8	127.2638	30.27485	8
15.0312	218.206	12.49231	8	197.7567	24.87416	8	120.5285	27.27977	8
15.6575	246.487	3.336043	8	204.2662	19.41616	8	115.5826	27.42485	8
16.2838	253.612	1.424968	8	220.2142	14.52253	8	118.5816	30.28026	8
16.9101	252.714	0.943118	8	222.7659	16.16312	8	119.7699	34.47908	8
17.5364	251.066	2.66851	8	229.8279	17.0922	8	114.599	31.88959	8
18.1627	252.745	0.821908	8	229.6728	17.48802	8	109.6902	28.26656	8
18.789	253.375	0.754451	8	232.029	17.24663	8	107.7748	26.75979	8
19.4153	253.375	0.754451	8	236.0609	15.84044	8	111.0552	25.33637	8
20.0416	253.375	0.754451	8	237.6399	14.65936	8	118.0426	23.09466	8
20.6679	253.375	0.754451	8	236.8807	14.93581	8	116.7774	20.79952	8
21.2942	253.375	0.754451	8	237.0995	15.44284	8	110.7565	17.96436	8
21.9205	253.375	0.754451	8	235.6695	15.94543	8	101.1308	16.22041	8
22.5468	253.375	0.754451	8	237.5434	16.74245	8	101.8392	13.92732	8
23.1731	253.381	0.752804	8	236.9981	17.13488	8	103.6942	14.40303	8
23.7994	253.379	0.753349	8	234.0374	17.2008	8	103.8433	13.79226	8
24.4257	253.328	0.768093	8	234.5749	16.67109	8	105.0733	17.78034	8
25.052	248.966	4.662643	8	233.2726	15.86065	8	105.8036	18.89273	8
25.6783	250.831	2.835975	8	237.4752	14.33864	8	107.0646	20.27976	8
26.3046	253.711	0.741612	8	238.1528	13.50647	8	113.2891	22.5343	8
26.9309	253.379	0.753547	8	239.7028	12.78628	8	118.4053	23.30427	8
27.5572	253.375	0.754451	8	243.037	11.96723	8	122.052	23.33926	8
28.1835	253.375	0.754451	8	244.4774	10.415	8	128.3235	22.39474	8
28.8098	253.375	0.754451	8	244.6151	8.964651	8	122.0457	23.54082	8

29.4361	253.375	0.754451	8	243.3976	8.275757	8	119.0037	22.85485	8
30.0624	253.375	0.754451	8	246.6115	7.952567	8	121.5931	22.50185	8
30.6887	253.375	0.754451	8	246.0184	8.587506	8	110.1467	21.27805	8
31.315	253.375	0.754451	8	244.3355	10.08481	8	106.3148	19.50034	8
31.9413	253.375	0.754451	8	242.3356	10.34219	8	107.9479	16.8756	8
32.5676	253.319	0.739173	8	241.7111	9.616026	8	119.7079	16.05037	8
33.1939	253.394	0.76057	8	239.6324	10.52485	8	137.2086	22.30084	8
33.8202	253.615	0.854599	8	238.9165	11.1353	8	132.0683	23.36515	8
34.4465	253.603	0.776632	8	241.4382	10.44947	8	126.9828	23.30162	8
35.0728	252.599	0.851088	8	244.3475	9.315268	8	118.4704	18.534	8
35.6991	249.17	3.452282	8	247.5921	7.260598	8	118.3141	20.05292	8
36.3254	234.656	11.83179	8	247.4227	6.631592	8	124.4224	23.08158	8
36.9517	206.441	22.37778	8	239.8092	11.96091	8	135.6303	25.09439	8
37.578	149.861	27.5264	8	218.6942	18.31058	8	145.322	24.07544	8
38.2043	77.3754	18.01698	8	174.5309	33.71721	8	159.1661	21.6653	8
38.8306	24.8956	8.523702	8	145.9824	35.05808	8	178.5502	22.88984	8
39.4569	12.5756	6.769377	8	91.76886	37.01784	8	165.5155	20.72878	8
40.0832	10.6474	5.561238	8	81.64788	38.66001	8	147.3404	25.53903	8
40.7095	9.74852	4.845275	8	78.33929	39.29271	8	154.8358	28.07727	8
41.3358	9.47175	4.562684	8	73.30183	37.80572	8	167.1276	32.51952	8
41.9621	9.63984	4.704474	8	61.16658	31.93953	8	162.76	33.87184	8
42.5884	9.6198	5.182933	8	55.94915	30.96079	8	150.3025	34.76562	8
43.2147	6.72101	3.381747	8	54.21395	31.13822	8	141.9549	33.38859	8
43.841	4.79724	2.231178	8	45.70247	24.49276	8	132.9531	28.27265	8
44.4673	3.85393	2.309852	8	36.9666	16.35748	8	122.4303	28.89044	8
45.0936	3.4936	2.16919	8	21.15652	7.733051	8	108.8145	28.49937	8
45.7199	7.79113	4.767888	8	14.5786	8.181239	8	96.86048	29.15078	8
46.3462	3.53763	1.998637	8	18.43116	8.33251	8	89.48521	35.70068	8
46.9725	3.77059	2.021248	8	21.74551	9.138192	8	93.58468	38.10214	8
47.5988	3.57997	1.677006	8	19.57124	9.197021	8	76.37006	28.09032	8
48.2251	2.85442	1.591292	8	18.07294	9.408157	8	57.01776	22.44609	8
48.8514	3.54755	1.502625	8	18.08751	9.1569	8	48.06415	19.40271	8
49.4777	3.91168	2.273751	8	11.16434	8.338809	8	39.72827	20.93481	8
50.104	2.28938	2.289383	8	0.717398	0.717398	8	29.47001	25.46104	8
50.7303	0.8182	0.818198	8	0.840926	0.840926	8	25.56019	21.99376	8
51.3566	0.13443	0.134428	8	1.070603	1.070603	8	22.42951	20.07539	8
51.9829	0.22028	0.220279	8	0.941307	0.941307	8	22.37958	20.33413	8
52.6092	0.35427	0.354274	8	1.008783	1.008783	8	24.3517	20.63157	8
53.2355	0	0	8	0	0	8	4.236662	4.695302	8
53.8618	0	0	8	0	0	8	4.647055	2.951447	8
54.4881	0	0	8	0	0	8	4.89925	1.21232	8
55.1144	0	0	8	0	0	8	5.273026	5.160665	8
55.7407	0	0	8	0	0	8	7.791955	7.903945	8
56.367	0	0	8	0	0	8	11.17131	11.20213	8

56.9933	0	0	8	0	0	8	12.44804	12.45108	8

part 1.4 Perivenous distribution of intracisternally administered Dextran

distance (µm)	Lectin (A.U.)			NG_2DsRed (A.U.)			Dextran (A.U.)		
	mean	**SEM**	**n**	**mean**	**SEM**	**n**	**mean**	**SEM**	**n**
0	0.441751	0.448218	9	2.509289	4.346216	9	5.789813	7.649998	9
0.626292	0.307496	0.442467	9	2.610956	4.522308	9	5.767184	7.576018	9
0	0.312005	0.337551	9	2.891559	5.008327	9	5.95818	7.798406	9
0.626292	0.623197	0.674439	9	3.057142	5.295125	9	5.775117	7.497714	9
1.252583	0.981777	1.393639	9	3.0534	5.288644	9	5.485246	7.049577	9
1.878875	0.859529	1.296127	9	2.564157	4.44125	9	5.534172	7.08046	9
2.505167	0.61284	0.93091	9	2.16233	3.745266	9	5.740754	7.324939	9
3.131459	0.355556	0.511581	9	2.25098	3.898812	9	6.080582	7.753419	9
3.75775	0.191488	0.26505	9	3.694244	4.271705	9	8.869846	8.271488	9
4.384042	0.222344	0.326266	9	3.809535	4.40329	9	8.929757	8.361837	9
5.010334	0.207893	0.280676	9	3.897169	4.506515	9	8.915887	8.398088	9
5.636626	0.167388	0.187913	9	3.805937	4.394887	9	8.907825	8.457617	9
6.262917	0.159682	0.184747	9	3.713238	4.309626	9	8.849077	8.515831	9
6.889209	0.201642	0.319408	9	3.521806	4.184329	9	8.549314	8.334356	9
7.515501	0.201558	0.37718	9	3.353798	4.019174	9	8.16302	8.003055	9
8.141792	0.135123	0.270246	9	3.338226	3.906983	9	8.064703	7.918165	9
8.768084	0.717162	1.38557	9	4.406742	4.230991	9	10.35299	8.358062	9
9.394376	0.919497	1.76212	9	4.398005	4.267475	9	10.62664	8.564515	9
10.02067	1.262433	2.394741	9	4.664413	4.450781	9	10.66904	8.599026	9
10.64696	1.664049	2.921356	9	4.665329	4.373852	9	10.47551	8.432721	9
11.27325	2.143963	3.32637	9	4.542423	4.263655	9	10.47105	8.391359	9
11.89954	2.578653	3.752497	9	4.474169	4.227818	9	10.76456	8.603186	9
12.52583	2.47492	3.103035	9	4.300944	4.093267	9	11.02447	8.794828	9
13.15213	1.851907	2.080553	9	3.771351	3.847761	9	9.380953	9.214451	9
13.77842	1.915901	2.494697	9	3.88989	3.62223	9	9.614117	9.469893	9
14.40471	2.050452	2.897007	9	4.274523	3.752023	9	9.687945	9.600333	9
15.031	2.086825	2.932008	9	4.167452	4.085555	9	8.103439	9.293927	9
15.65729	2.278023	3.189416	9	4.446057	4.137464	9	7.972518	9.069465	9
16.28358	2.473332	3.40597	9	4.537626	4.015342	9	7.907733	8.900959	9
16.90988	2.674771	3.741456	9	4.498301	3.789938	9	7.878403	8.778571	9
17.53617	2.847299	3.910048	9	4.39412	3.58135	9	7.901351	8.766441	9
18.16246	3.279791	3.788662	9	3.969649	3.423349	9	7.933523	8.809733	9
18.78875	2.843659	3.491722	9	3.79505	3.586059	9	7.986445	8.902009	9
19.41504	2.557915	3.334907	9	3.765886	3.828971	9	8.093846	9.045584	9
20.04134	2.981548	3.438388	9	3.729906	4.065918	9	7.966977	8.878411	9
20.66763	3.060885	3.475214	9	3.646841	4.168564	9	7.784676	8.598545	9
21.29392	2.822977	3.587091	9	3.420311	4.165973	9	7.863502	8.581437	9

21.92021	2.829319	3.998765	9	3.416639	4.191293	9	8.026104	8.66499	9
22.5465	2.56432	4.496522	9	3.179304	3.956153	9	8.885792	8.397125	9
23.17279	2.941425	5.410664	9	3.136938	3.952999	9	9.211058	8.57134	9
23.79909	3.427562	6.717454	9	3.164624	4.000478	9	9.38801	8.650286	9
24.42538	4.059014	8.181243	9	3.282012	4.080289	9	9.366285	8.495258	9
25.05167	3.585814	8.859809	9	3.153618	3.81278	9	10.54195	8.538976	9
25.67796	3.895266	9.412868	9	3.15816	3.722668	9	10.91733	8.658453	9
26.30425	4.346951	9.806878	9	3.055079	3.65248	9	11.21312	8.704223	9
26.93054	4.278963	10.46896	9	3.013754	3.652189	9	11.4915	8.796286	9
27.55684	4.652472	11.04509	9	3.355607	3.8118	9	11.72168	9.001983	9
28.18313	5.034437	11.84183	9	3.594313	4.064793	9	11.94569	9.282517	9
28.80942	5.495525	13.31192	9	3.649117	4.327997	9	12.10929	9.401268	9
29.43571	6.193831	15.24187	9	3.656241	4.301761	9	12.23399	9.513788	9
30.062	7.403419	17.0343	9	3.69029	3.891572	9	12.57759	9.841963	9
30.68829	8.49604	18.78532	9	3.671402	3.774569	9	12.90889	10.01368	9
31.31459	9.385362	20.59504	9	3.936826	3.789597	9	13.09348	10.14121	9
31.94088	9.339339	22.11627	9	4.08818	3.730865	9	13.30868	10.36819	9
32.56717	9.216262	22.88669	9	4.035114	3.749288	9	13.45607	10.68136	9
33.19346	9.262568	23.18302	9	4.00952	3.925187	9	13.76095	11.27326	9
33.81975	9.424942	23.28131	9	4.067381	4.043126	9	13.93439	11.62072	9
34.44604	9.386575	23.10965	9	3.943983	4.063444	9	14.12513	11.85075	9
35.07234	9.093863	23.02995	9	3.830251	3.977071	9	14.28742	12.03208	9
35.69863	9.036557	23.34792	9	3.793514	3.880934	9	14.41944	12.18704	9
36.32492	9.585848	23.87188	9	3.749546	3.886674	9	14.7463	12.53721	9
36.95121	10.17766	24.53528	9	3.965251	4.090605	9	15.02542	12.76101	9
37.5775	11.55212	26.99901	9	4.137366	4.290221	9	15.11424	13.04625	9
38.2038	10.6918	26.73752	9	4.093697	4.281661	9	15.23973	13.58923	9
38.83009	11.9084	27.31295	9	4.046127	4.185227	9	15.34854	13.69168	9
39.45638	11.45642	27.47611	9	4.230542	4.248394	9	15.54479	13.78148	9
40.08267	12.20146	26.85011	9	4.340367	4.289359	9	15.84965	14.02956	9
40.70896	14.98089	26.99684	9	4.217448	4.13384	9	16.06569	14.32032	9
41.33525	17.70267	30.06219	9	4.078453	4.106178	9	15.99168	14.42072	9
41.96155	20.38085	31.44033	9	4.136246	4.227947	9	16.11987	15.40412	9
42.58784	23.36971	31.64359	9	4.322834	4.233982	9	16.24531	16.20086	9
43.21413	26.46712	31.97217	9	4.52817	4.148806	9	16.30089	16.74363	9
43.84042	30.75813	33.18363	9	4.680468	3.957037	9	16.50902	17.33524	9
44.46671	36.83866	34.88115	9	4.804672	3.784248	9	17.2219	18.00068	9
45.093	46.90327	35.15311	9	5.329765	4.180525	9	17.19991	18.34064	9
45.7193	60.56512	34.99736	9	6.146306	5.409219	9	17.12914	18.71004	9
46.34559	77.54737	33.88789	9	6.78769	6.776359	9	17.06672	18.66051	9
46.97188	102.3368	32.25976	9	7.025306	7.25173	9	16.71302	18.0658	9
47.59817	132.5586	39.70317	9	6.765235	6.738327	9	16.23056	17.01957	9
48.22446	158.923	44.86958	9	6.37895	5.542231	9	16.38448	17.15669	9
48.85075	174.9224	53.00773	9	6.056644	4.927182	9	17.09126	18.38823	9

49.47705	185.0377	58.22572	9	5.503256	4.4365	9	17.67066	19.92909	9
50.10334	190.7278	58.97533	9	5.329144	4.076108	9	17.63849	19.96669	9
50.72963	192.5227	58.54597	9	4.966096	3.809972	9	17.19807	19.00608	9
51.35592	193.7644	53.91139	9	4.591611	3.792147	9	16.82251	18.391	9
51.98221	191.4856	51.30761	9	4.548293	3.985938	9	16.87965	18.87554	9
52.60851	188.3282	50.82112	9	4.477858	4.105856	9	16.93192	19.27799	9
53.2348	184.8592	48.5895	9	4.556689	4.236786	9	16.89576	19.23897	9
53.86109	182.2056	47.66169	9	4.653276	4.249765	9	16.77473	18.88927	9
54.48738	179.3049	52.04319	9	4.733441	4.210922	9	16.5582	18.31151	9
55.11367	178.928	55.44724	9	4.906999	4.237494	9	16.14566	17.46008	9
55.73996	177.7441	56.63709	9	4.7998	4.131136	9	15.80875	16.93962	9
56.36626	179.7897	51.39461	9	4.811806	3.983392	9	15.67978	16.98374	9
56.99255	180.0241	49.1011	9	4.814034	3.992507	9	15.79949	17.26947	9
57.61884	178.8721	51.43007	9	4.773701	3.997488	9	16.08293	17.34835	9
58.24513	177.2636	54.01947	9	4.832709	4.021099	9	16.38007	17.47237	9
58.87142	176.8524	54.74599	9	5.292946	4.082516	9	16.33179	17.09038	9
59.49771	176.6544	52.99966	9	5.597387	3.927107	9	16.02963	16.51604	9
60.12401	174.9929	51.39746	9	5.602188	3.899682	9	15.77286	16.11476	9
60.7503	172.5931	51.95167	9	5.971466	4.082024	9	15.38894	15.35397	9
61.37659	171.2408	54.37939	9	6.027993	4.194499	9	15.18869	15.10477	9
62.00288	170.9937	54.07304	9	5.736422	4.146113	9	14.8645	14.84505	9
62.62917	171.3539	51.59462	9	5.346498	3.955978	9	14.39511	14.25319	9
63.25546	171.0708	50.76	9	4.863926	3.714394	9	13.84301	13.32325	9
63.88176	171.856	53.34961	9	4.532399	3.848372	9	13.63653	12.9968	9
64.50805	172.0273	54.55369	9	4.589122	4.194719	9	13.29848	12.62037	9
65.13434	172.8348	56.06612	9	4.628388	4.381614	9	13.08294	12.36329	9
65.76063	174.8725	58.6552	9	4.525651	4.449891	9	13.1547	12.47732	9
66.38692	174.5176	60.81725	9	4.494065	4.491556	9	13.16392	12.37739	9
67.01321	172.5886	63.69212	9	4.470367	4.416097	9	13.3164	12.36132	9
67.63951	171.9221	63.42142	9	4.53637	4.44088	9	13.32714	12.2232	9
68.2658	170.6994	62.67505	9	4.505133	4.384165	9	13.16933	11.94954	9
68.89209	167.8651	61.45396	9	4.260177	4.166726	9	13.28259	12.04772	9
69.51838	168.2621	59.94678	9	4.208329	4.010102	9	13.3772	12.17732	9
70.14467	167.2304	62.24864	9	4.242837	4.116596	9	13.52405	12.4109	9
70.77097	168.0947	61.95577	9	4.219577	4.140909	9	13.69232	12.74824	9
71.39726	170.2224	60.0727	9	4.145329	4.09509	9	13.55922	12.66935	9
72.02355	167.6083	60.50099	9	4.418146	4.207443	9	13.13657	12.17229	9
72.64984	166.4574	60.41461	9	4.594878	4.194531	9	12.98714	12.03916	9
73.27613	164.9576	61.59343	9	4.620979	4.104621	9	12.92746	11.94837	9
73.90242	163.4734	61.12004	9	4.606349	4.064911	9	12.92631	11.56226	9
74.52872	162.7763	58.10453	9	4.736617	4.023738	9	13.41054	11.7905	9
75.15501	163.78	55.98771	9	4.643063	3.743161	9	13.32704	11.45701	9
75.7813	168.6979	50.83908	9	4.5362	3.610521	9	13.16329	11.02821	9
76.40759	171.3687	49.07363	9	4.723298	3.786014	9	12.96679	10.87739	9

77.03388	172.506	46.83767	9	5.149852	4.074637	9	13.25533	11.22238	9
77.66017	171.9024	43.05481	9	5.381442	4.290546	9	13.40309	11.15172	9
78.28647	169.8648	42.58357	9	5.40215	4.195131	9	13.30153	11.07959	9
78.91276	169.9471	42.83728	9	5.279211	3.985521	9	13.23441	11.08555	9
79.53905	171.9674	43.31237	9	5.210161	3.852887	9	13.26495	11.20391	9
80.16534	175.2613	44.59196	9	5.226072	3.851517	9	13.14972	11.04065	9
80.79163	176.3235	45.44353	9	5.127283	3.928087	9	13.26401	10.96141	9
81.41792	174.8709	46.83606	9	5.005761	3.954934	9	13.37555	10.88179	9
82.04422	174.1237	44.88291	9	5.181153	3.803803	9	13.41978	10.84761	9
82.67051	174.495	42.85118	9	5.084186	3.721366	9	13.73282	11.13534	9
83.2968	177.2149	42.56758	9	5.123624	3.757747	9	13.86071	11.09022	9
83.92309	176.3832	42.91982	9	5.440451	4.011317	9	14.10372	11.00219	9
84.54938	173.796	43.62771	9	5.553949	4.263098	9	14.27258	11.00457	9
85.17567	172.5656	44.52343	9	5.316902	4.171841	9	14.20108	10.84462	9
85.80197	170.688	45.75851	9	4.920174	3.916983	9	14.1057	10.78378	9
86.42826	172.5505	46.32138	9	4.519208	3.856909	9	13.97094	10.71708	9
87.05455	173.7061	47.05263	9	4.41925	4.085578	9	14.12732	10.78459	9
87.68084	173.471	47.56188	9	4.345998	4.189112	9	14.43295	11.01289	9
88.30713	170.957	48.26622	9	4.46448	4.18103	9	14.35097	10.92366	9
88.93343	169.8627	48.12065	9	4.40518	4.161382	9	14.54941	11.21938	9
89.55972	169.7218	48.60473	9	4.328467	4.234505	9	14.87623	11.57418	9
90.18601	168.2268	50.28545	9	4.356854	4.272726	9	15.20187	11.85864	9
90.8123	165.7734	53.03822	9	4.510353	4.440612	9	15.43399	12.23931	9
91.43859	161.4062	56.3816	9	4.655647	4.497477	9	15.36524	12.14974	9
92.06488	158.0411	60.0601	9	4.596101	4.332261	9	15.36876	12.17746	9
92.69118	155.2521	62.87186	9	4.510148	4.202308	9	15.4764	12.48066	9
93.31747	151.4013	64.62821	9	4.669316	4.429288	9	15.46385	12.76066	9
93.94376	147.0958	66.038	9	4.861636	4.77412	9	15.3922	12.78182	9
94.57005	143.6572	66.4193	9	4.86794	4.89588	9	15.09589	12.54688	9
95.19634	141.6903	67.28672	9	4.77967	4.806106	9	14.91255	12.40384	9
95.82263	140.7837	68.59062	9	4.824492	4.822336	9	14.86617	12.29329	9
96.44893	140.9203	67.29226	9	4.678001	4.704428	9	14.59269	11.73684	9
97.07522	138.3542	66.99959	9	4.583782	4.433725	9	14.46503	11.60933	9
97.70151	135.1441	68.41276	9	4.469755	4.230099	9	14.41959	11.82649	9
98.3278	134.8116	68.07793	9	4.180677	4.025928	9	14.67088	12.0349	9
98.95409	135.3773	68.5054	9	4.078429	3.938773	9	14.75849	11.96661	9
99.58038	135.0298	68.29207	9	4.193191	4.058764	9	14.78845	12.05872	9
100.2067	133.5449	67.22272	9	4.272156	4.06892	9	14.66719	11.99929	9
100.833	131.3823	66.20915	9	4.272432	4.050362	9	14.53356	11.88506	9
101.4593	130.3999	65.23497	9	4.331388	4.110324	9	14.56502	11.84499	9
102.0856	130.1198	65.48509	9	4.287741	4.043383	9	14.70979	11.90589	9
102.7118	128.9374	67.20862	9	4.132253	3.920575	9	14.68076	11.91246	9
103.3381	126.4931	68.61889	9	4.024138	3.791815	9	14.5076	11.71929	9
103.9644	124.1871	68.54061	9	4.043039	3.849673	9	14.26779	11.35518	9

104.5907	120.722	67.87601	9	4.1696	3.958305	9	13.98621	11.00025	9
105.217	118.3002	67.88506	9	4.002849	3.725344	9	13.83239	11.03656	9
105.8433	115.3706	67.69452	9	3.931469	3.702113	9	13.73566	10.88727	9
106.4696	114.0062	67.44694	9	3.970439	3.702665	9	13.61629	10.5371	9
107.0959	113.6609	66.3016	9	4.165843	3.529638	9	13.69453	10.54312	9
107.7222	113.9582	64.95092	9	4.444229	3.567993	9	14.00644	10.78127	9
108.3485	113.3949	65.64092	9	4.535558	3.607628	9	13.82305	10.68813	9
108.9748	113.2511	65.7188	9	4.631303	3.689937	9	13.68807	10.58599	9
109.6011	114.4616	63.96789	9	4.714331	3.750527	9	13.88013	10.77699	9
110.2273	116.9111	62.36977	9	4.77628	3.6803	9	13.84315	10.69708	9
110.8536	116.6206	64.40172	9	4.618636	3.546199	9	13.69785	10.52038	9
111.4799	117.6097	68.27926	9	4.480649	3.630605	9	13.5756	10.20814	9
112.1062	122.0619	69.45846	9	4.54851	3.658647	9	13.45549	10.03221	9
112.7325	125.952	67.85763	9	4.488324	3.60894	9	13.53882	10.19645	9
113.3588	130.0289	66.10284	9	4.349577	3.661571	9	13.81951	10.56387	9
113.9851	133.8155	65.08076	9	4.368132	3.810932	9	14.00514	10.73195	9
114.6114	135.4788	66.0569	9	4.584247	3.989862	9	13.93258	10.5493	9
115.2377	138.605	66.60472	9	4.588832	4.090763	9	13.71407	10.13726	9
115.864	143.9511	67.30829	9	4.453262	3.99856	9	13.62804	10.03731	9
116.4903	144.5363	69.13787	9	4.236689	3.836415	9	13.56387	9.940883	9
117.1166	144.9859	72.02146	9	4.204714	3.800111	9	13.72391	10.10323	9
117.7428	145.0464	73.11048	9	4.286609	4.052366	9	13.89153	10.35244	9
118.3691	145.27	73.5831	9	4.486765	4.278978	9	13.77708	10.42408	9
118.9954	145.4257	73.85075	9	4.508853	4.216601	9	13.56751	10.58333	9
119.6217	143.4482	73.88376	9	4.526533	4.225607	9	13.30195	10.69173	9
120.248	141.9371	73.67413	9	4.590553	4.303306	9	12.91802	10.53451	9
120.8743	145.6068	69.68374	9	4.381989	4.258347	9	12.63363	10.47547	9
121.5006	146.2256	67.32438	9	4.518237	4.350627	9	12.72034	10.81083	9
122.1269	145.1099	63.25592	9	4.611096	4.456369	9	12.54624	10.96789	9
122.7532	144.0401	59.8004	9	4.594461	4.473417	9	12.25769	10.94578	9
123.3795	142.0969	60.32188	9	4.649442	4.44722	9	12.00042	10.99261	9
124.0058	141.8699	59.30282	9	4.710841	4.57938	9	11.8906	11.17842	9
124.6321	142.6067	58.39541	9	4.833191	4.669976	9	11.96096	11.33933	9
125.2583	142.0861	57.58723	9	4.898607	4.695598	9	12.22716	11.65708	9
125.8846	141.3061	57.67316	9	4.911049	4.679442	9	12.52905	12.1776	9
126.5109	141.447	57.8303	9	4.779026	4.456386	9	12.56277	12.13402	9
127.1372	141.5529	57.29838	9	4.8583	4.431618	9	12.32535	11.86006	9
127.7635	144.9934	56.8593	9	5.136255	4.587759	9	12.02102	11.68573	9
128.3898	149.1595	57.30399	9	5.528702	4.823156	9	11.88442	11.66363	9
129.0161	151.7776	58.50984	9	5.748954	4.804083	9	11.83881	11.6296	9
129.6424	151.5416	59.01907	9	6.045927	4.688518	9	11.73098	11.54034	9
130.2687	154.5238	59.05477	9	6.376916	4.880084	9	11.80715	11.54822	9
130.895	159.2168	56.78713	9	6.651395	5.302518	9	12.06918	11.69282	9
131.5213	160.873	54.03517	9	7.164101	6.218896	9	12.19752	12.05218	9

132.1476	162.2739	52.47954	9	7.615975	7.171515	9	12.22568	12.16193	9
132.7738	160.7334	52.82243	9	7.723217	7.719816	9	12.37068	12.32761	9
133.4001	158.3262	52.52339	9	7.648478	7.627404	9	12.37916	12.44904	9
134.0264	158.951	49.67353	9	7.566325	7.357876	9	12.31423	12.47443	9
134.6527	163.0139	45.65559	9	7.244479	6.946823	9	12.16617	12.05979	9
135.279	167.4736	44.38557	9	7.077035	6.507713	9	12.08255	11.86995	9
135.9053	169.1197	44.89783	9	6.979582	6.5084	9	11.83761	11.54553	9
136.5316	171.5177	46.35383	9	6.92989	6.423186	9	11.58242	11.13343	9
137.1579	174.9821	48.6882	9	6.942145	6.206247	9	11.40793	10.90442	9
137.7842	175.4496	52.60399	9	6.864927	5.860022	9	11.22792	10.57448	9
138.4105	170.5499	57.23343	9	7.001329	5.588334	9	11.12826	10.47945	9
139.0368	166.7597	60.22018	9	7.062189	5.228911	9	11.19012	10.52917	9
139.6631	165.1811	61.18461	9	6.878496	4.974138	9	11.23808	10.4478	9
140.2893	159.8542	64.9351	9	6.634508	4.822657	9	11.19275	10.09572	9
140.9156	156.7074	64.91174	9	6.777231	5.034852	9	11.17936	9.963481	9
141.5419	156.5246	64.37884	9	6.537115	5.108113	9	11.21569	9.836073	9
142.1682	159.2977	65.11357	9	6.321828	4.986897	9	11.18688	9.63494	9
142.7945	158.9513	67.25964	9	6.598943	5.178392	9	11.07969	9.422153	9
143.4208	158.7322	68.00134	9	6.439781	5.117713	9	11.22449	9.410755	9
144.0471	159.4846	67.22425	9	6.128406	4.713059	9	11.37103	9.467613	9
144.6734	160.2074	65.86334	9	5.735098	4.238156	9	11.40928	9.569899	9
145.2997	159.9212	65.87267	9	5.689813	4.209587	9	11.42498	9.524561	9
145.926	158.4583	68.57592	9	5.519308	4.199763	9	11.26961	9.217198	9
146.5523	158.5066	70.44531	9	5.372157	4.18039	9	11.2749	9.273176	9
147.1786	159.9856	71.08212	9	5.391348	4.210463	9	11.08607	9.276494	9
147.8048	162.9717	71.40738	9	5.420989	4.272095	9	10.73393	8.942513	9
148.4311	165.4483	69.64531	9	5.69593	4.448439	9	10.46103	8.662568	9
149.0574	167.346	67.27396	9	5.714142	4.589944	9	10.09504	8.207691	9
149.6837	167.3324	65.01529	9	5.476789	4.393399	9	10.00624	8.072846	9
150.31	166.1785	62.50981	9	5.393831	4.185619	9	10.04736	8.071211	9
150.9363	164.2843	58.79165	9	5.254176	4.045269	9	10.02783	8.038496	9
151.5626	165.8916	55.57316	9	5.337407	4.118754	9	9.913318	7.966686	9
152.1889	166.7965	55.99396	9	5.35449	4.154569	9	9.863348	7.920049	9
152.8152	166.7782	56.14151	9	5.328118	4.146106	9	10.01069	7.93252	9
153.4415	166.5211	53.31312	9	5.355039	4.297199	9	10.07774	7.79623	9
154.0678	163.082	50.72679	9	5.32885	4.432058	9	10.04214	7.744993	9
154.6941	164.1105	48.03594	9	5.353667	4.511313	9	9.887125	7.68298	9
155.3203	165.4189	48.1807	9	5.321217	4.325031	9	9.826115	7.632041	9
155.9466	165.2065	51.18667	9	5.243782	4.15202	9	9.786334	7.603568	9
156.5729	168.3011	51.5112	9	5.125711	4.123624	9	9.784732	7.714697	9
157.1992	165.7745	55.47559	9	5.112501	4.079632	9	9.833338	7.798911	9
157.8255	161.6864	61.62226	9	5.052954	4.084451	9	9.696257	7.712953	9
158.4518	159.4476	67.18667	9	4.987725	4.330216	9	9.336089	7.434129	9
159.0781	158.5074	71.30867	9	4.883855	4.472061	9	8.967776	7.132368	9

159.7044	159.5493	73.06089	9	4.77167	4.458367	9	8.729305	7.056489	9
160.3307	158.2782	76.27366	9	4.746285	4.389403	9	8.797712	7.208014	9
160.957	155.7305	76.26757	9	4.748324	4.359616	9	8.80319	7.216086	9
161.5833	152.9151	74.36479	9	4.678913	4.432563	9	8.700471	7.132722	9
162.2096	147.7895	72.76475	9	4.819478	4.529205	9	8.632729	7.081979	9
162.8358	139.9585	68.17855	9	5.070578	4.637695	9	8.514352	7.001236	9
163.4621	132.4822	63.24311	9	5.355742	4.629539	9	8.479009	6.949726	9
164.0884	124.4831	59.61288	9	5.426911	4.611403	9	8.472344	6.955476	9
164.7147	112.7623	55.8667	9	5.28535	4.60192	9	8.267018	6.776211	9
165.341	100.7222	53.53796	9	5.048286	4.395329	9	8.166287	6.700348	9
165.9673	87.70733	50.3991	9	5.068339	4.180442	9	8.125956	6.703864	9
166.5936	75.24453	47.91402	9	5.074476	4.267443	9	8.18065	6.860325	9
167.2199	64.4345	44.21567	9	5.20672	4.419332	9	8.325739	7.06648	9
167.8462	53.38801	38.01562	9	5.175671	4.477754	9	8.474617	7.267762	9
168.4725	41.08123	32.54932	9	5.244857	4.58881	9	8.77302	7.524842	9
169.0988	30.87935	28.91222	9	5.280116	4.797324	9	9.116993	7.880835	9
169.7251	25.46936	26.11578	9	5.346904	4.991151	9	9.39299	8.300196	9
170.3513	21.51981	24.80192	9	5.381959	4.998054	9	9.948143	9.100836	9
170.9776	18.52586	22.41995	9	5.342079	4.714725	9	10.22331	9.362858	9
171.6039	15.57709	18.46427	9	5.244216	4.572627	9	10.2548	9.286475	9
172.2302	13.30011	13.67458	9	5.055046	4.48441	9	10.08238	9.060789	9
172.8565	11.34419	10.90676	9	4.831363	4.349292	9	9.763846	8.732121	9
173.4828	10.23053	11.30819	9	4.712059	4.279148	9	9.523755	8.519818	9
174.1091	9.19688	12.38546	9	4.926341	4.483953	9	9.571829	8.57778	9
174.7354	8.517506	11.84044	9	5.143418	4.721254	9	9.628019	8.614835	9
175.3617	7.173624	9.461163	9	5.193864	4.782384	9	9.519065	8.475638	9
175.988	6.053674	8.598181	9	5.286186	4.731238	9	9.349731	8.392651	9
176.6143	5.418019	7.645411	9	5.192984	4.695733	9	8.954022	8.157308	9
177.2406	4.818797	6.836768	9	5.034689	4.785879	9	8.71358	8.000529	9
177.8669	5.159339	7.756998	9	5.062758	4.747934	9	8.577946	7.837457	9
178.4931	6.380731	9.802475	9	5.052133	4.663659	9	8.430399	7.678236	9
179.1194	5.753354	8.476021	9	5.187822	4.6249	9	8.316783	7.569395	9
179.7457	5.178414	7.167093	9	5.113091	4.51477	9	8.123049	7.414761	9
180.372	4.740665	6.528936	9	5.022895	4.411764	9	7.938583	7.202051	9
180.9983	4.1769	5.795011	9	5.077709	4.401882	9	7.818119	7.08641	9
181.6246	4.171334	5.785553	9	5.027072	4.355969	9	7.866219	7.166752	9
182.2509	4.488773	6.956159	9	4.956301	4.274144	9	7.873278	7.194634	9
182.8772	4.464891	6.481549	9	4.917045	4.248504	9	7.87762	7.202753	9
183.5035	4.156578	4.730916	9	4.989489	4.227036	9	7.924028	7.218925	9
184.1298	3.469108	4.293842	9	5.000601	4.156479	9	7.786618	7.137199	9
184.7561	3.593595	6.876171	9	4.988417	4.257702	9	8.893449	7.094459	9
185.3824	3.358751	5.967337	9	4.824472	4.103527	9	8.959105	7.152991	9
186.0086	3.469445	5.347684	9	4.802532	3.999623	9	8.795574	7.062186	9
186.6349	3.663422	5.123564	9	4.658745	3.876012	9	8.695856	7.014566	9

187.2612	3.29617	5.058677	9	4.718871	4.002925	9	8.706707	7.034143	9
187.8875	4.577009	7.096113	9	4.973969	4.224325	9	8.740356	6.986037	9
188.5138	5.042666	6.594565	9	5.100576	4.34904	9	8.813783	6.985714	9
189.1401	3.866797	4.488133	9	5.144255	4.430482	9	8.789947	6.954634	9
189.7664	4.224438	7.205377	9	5.039462	4.344752	9	8.65455	6.804583	9
190.3927	3.630397	6.773754	9	4.885947	4.165491	9	8.606428	6.708912	9
191.019	2.948415	5.447839	9	4.807398	4.080032	9	8.668724	6.762696	9
191.6453	2.813852	4.555845	9	4.726983	4.026061	9	8.845148	6.952563	9
192.2716	3.707735	4.636233	9	4.514568	3.890247	9	9.020919	7.102817	9
192.8979	3.707521	3.803029	9	4.524011	3.818264	9	9.077001	7.053497	9
193.5241	3.879323	2.989212	9	4.761442	3.834126	9	8.989616	6.874112	9
194.1504	4.337817	3.114761	9	5.060385	3.875152	9	8.922284	6.734701	9
194.7767	3.197545	2.806434	9	5.089677	3.739545	9	8.837618	6.647646	9
195.403	2.295463	2.115322	9	5.128928	3.644029	9	8.975042	6.722296	9
196.0293	1.464478	1.265591	9	5.364095	3.889307	9	10.20306	6.250124	9
196.6556	1.87132	2.166267	9	5.342491	3.932353	9	10.04571	6.26316	9
197.2819	2.782132	3.450606	9	5.485271	3.951068	9	10.05467	6.332577	9
197.9082	2.50295	3.585108	9	5.380072	3.905731	9	10.05954	6.524996	9
198.5345	2.094219	3.310439	9	5.376612	3.865949	9	9.799922	6.463784	9
199.1608	1.649911	3.211866	9	5.312428	4.206208	9	9.373654	6.860976	9
199.7871	1.583985	2.831431	9	5.352627	4.212847	9	9.174102	6.828976	9
200.4134	1.400315	1.919289	9	5.371204	4.22462	9	9.030529	6.761611	9
201.0396	1.217939	1.394396	9	5.437671	4.28158	9	8.979797	6.715325	9
201.6659	1.913683	2.495282	9	5.324514	4.886037	9	7.233684	5.932581	9
202.2922	2.591647	3.544404	9	5.367671	4.927591	9	7.323514	5.998639	9
202.9185	2.799829	4.309378	9	5.257526	4.815502	9	7.371233	6.052525	9
203.5448	2.440065	3.859027	9	5.325849	4.86915	9	7.334147	6.056418	9
204.1711	2.044734	2.839277	9	5.587464	5.101437	9	7.232948	6.016508	9
204.7974	2.143894	2.784377	9	5.722343	5.23164	9	7.226921	5.970167	9
205.4237	2.493931	2.992977	9	5.658285	5.221922	9	7.33287	6.030582	9
206.05	2.885112	3.223427	9	5.566674	5.215104	9	7.420399	6.128618	9
206.6763	3.005446	2.934953	9	5.575447	5.27518	9	7.292632	6.044832	9
207.3026	2.75038	2.410967	9	5.73086	5.389741	9	6.879457	5.719561	9
207.9289	2.306661	1.98855	9	5.841133	5.432909	9	6.684581	5.544548	9
208.5551	2.083986	1.738241	9	5.892916	5.426279	9	6.59172	5.471477	9
209.1814	2.663778	1.736529	9	5.916969	5.412708	9	6.220769	5.203181	9
209.8077	3.462027	2.032317	9	5.930961	5.402244	9	6.006969	5.109466	9

Part 2 Double injections in the vitreous body and cisterna magna

	CM: BSA (A.U.)			ITV: hAβ (A.U.)		
distance from eyeball(μm)	**mean**	**SEM**	**n**	**mean**	**SEM**	**n**

0	1.6556	0.56157	12	29.8419	3.310624	12
100	0	0	12	40.54825	8.26459	12
200	0.005365	0.005365	12	36.35475	6.660122	12
300	0.11678	0.11678	12	30.99542	4.683882	12
400	0.2178	0.2178	12	27.127	4.056111	12
500	0.28974	0.28974	12	24.11317	3.232383	12
600	0.36984	0.36984	12	21.71367	2.672561	12
700	0.42616	0.42616	12	19.51517	2.237113	12
800	0.56536	0.37808	12	17.42833	1.835801	12
900	0.76967	0.4134	12	15.52333	1.622953	12
1000	0.87235	0.5171	12	13.98192	1.498723	12
1100	0.91588	0.64631	12	12.78242	1.373503	12
1200	1.0755	0.78324	12	12.06667	1.227525	12
1300	1.2774	0.99295	12	11.51175	1.202571	12
1400	1.6421	1.1314	12	10.94625	1.153111	12
1500	1.9205	1.3017	12	10.8415	1.097503	12
1600	2.359	1.5045	12	10.567	1.071609	12
1700	2.6643	1.5876	12	10.73575	1.162462	12
1800	2.9051	1.6734	12	10.49542	1.147988	12
1900	3.0715	1.7526	12	10.30817	1.112188	12
2000	3.386	1.808	12	10.03267	1.133445	12
2100	4.245	1.9162	12	9.50725	1.095853	12
2200	5.2658	2.1553	12	9.594916	1.074903	12
2300	7.0034	2.5282	12	9.636833	1.140316	12
2400	8.4017	2.8736	12	9.06175	1.033215	12
2500	10.15	3.2103	12	9.01125	1.063772	12
2600	11.981	3.4063	12	8.92125	1.066624	12
2700	13.616	3.5686	12	8.898417	1.171541	12
2800	13.823	3.6019	12	8.360583	1.095755	12
2900	14.965	3.6637	12	8.09875	1.195545	12
3000	17.326	4.4013	12	8.018	1.295684	12
3100	19.488	4.6871	12	7.80025	1.311005	12
3200	20.423	4.4279	12	7.574833	1.291925	12
3300	21.811	4.3626	12	7.517	1.282632	12
3400	23.655	4.1217	12	7.34175	1.265718	12
3500	24.715	3.9942	12	7.11975	1.354047	12
3600	26.31	4.3713	12	7.602833	1.350946	12
3700	29.557	5.0043	12	8.884	1.918899	12
3800	31.089	4.5883	12	7.927667	1.445457	12
3900	33.153	4.4648	12	7.9055	1.437301	12
4000	35.285	4.3805	12	7.50325	1.38073	12
4100	37.517	4.3808	12	7.69	1.456474	12
4200	40.969	4.7326	12	7.64775	1.415313	12
4300	39.494	4.8594	12	7.46	1.381845	12

4400	41.057	5.2666	12	7.522	1.387245	12
4500	43.481	5.2945	12	7.707	1.408456	12
4600	48.044	6.003	12	6.8315	1.325829	12
4700	50.752	5.8133	12	6.842417	1.342486	12
4800	56.502	5.937	12	6.404667	1.332338	12
4900	55.322	6.1401	12	7.589083	1.288809	12

Part 3 Colocalization of different intravitreally administered tracer with TUJ1 staining

	dextran	**hAβ**
Pearson correlation coefficient	-0.12	0.65
	0.17	0.67
	-0.15	0.7
	-0.12	0.73
	0.1	0.49
	0.1	0.53
	0.14	0.65
	0.01	0.27
	0.13	0.3
		0.25
		0.12

Part 4. IOP of AQP4+/+ and AQP4 -/- mice

AQP4+/+ (mmHg)	AQP4-/-(mmHg)
19.33333	18.66667
18.66667	16
17	13
16	12.66667
19	18
10.66667	15
19	9.666667
17	20.66667
17	16
11.66667	11.33333
15.66667	14.66667
11	16.33333
20.66667	9
18	13
20.33333	15
14.66667	17
13.66667	11
8	15.66667
15.66667	13
12	13.66667
23	13
7	14.33333
17.66667	8.666667
7	14.33333
14.66667	19
13.66667	14.66667
15.66667	17.33333
7	22
7	16
14.66667	12
16	16.66667
17.33333	13
12.33333	15.66667
7	8
	12.33333

Part 5.1 hAβ tracer distribution in AQP4+/+ and AQP4-/- mice retina

	AQP4+/+ (A.U.)			AQP4-/- (A.U.)		
distance from RNFL (μm)	**mean**	**SEM**	**n**	**mean**	**SEM**	**n**
0.025146	43.46967	6.600804	9	29.20929	5.826537	7
2.3286	58.169	8.786117	9	39.741	5.981125	7

4.6402	75.00133	10.23663	9	49.23971	7.011494	7
6.952	84.24122	10.35063	9	54.13014	7.525359	7
9.2637	90.73511	10.55676	9	56.08229	7.681028	7
11.575	93.42422	11.14912	9	56.24086	7.95089	7
13.887	93.80878	11.6201	9	56.06157	8.379235	7
16.199	91.64567	12.06675	9	54.39514	8.819277	7
18.511	87.50756	12.25819	9	52.10571	8.697332	7
20.822	83.964	12.61583	9	49.12143	8.172097	7
23.134	79.16833	12.87826	9	46.168	8.002808	7
25.445	75.13389	12.57089	9	43.67829	7.605358	7
27.757	70.80622	12.18439	9	39.47329	7.509145	7
30.068	67.158	11.97526	9	34.62543	7.365673	7
32.38	62.003	11.50491	9	32.191	7.11459	7
34.692	58.20789	11.02736	9	31.42143	6.980209	7
37.004	54.58556	10.41764	9	29.47014	6.313101	7
39.315	51.75889	9.729142	9	28.62357	6.110663	7
41.627	48.07133	8.676702	9	27.532	5.856273	7
43.939	44.95611	7.707502	9	26.08086	5.662622	7
46.251	42.63244	7.329907	9	24.83029	5.326404	7
48.562	40.50544	7.113323	9	23.197	4.632961	7
50.874	39.137	6.758556	9	22.03057	4.276815	7
53.186	36.99856	6.550517	9	21.273	4.110574	7
55.498	35.75656	6.119001	9	20.51429	4.001658	7
57.809	34.60389	5.74567	9	19.96529	3.782729	7
60.121	33.58733	5.632462	9	19.69571	3.755955	7
62.433	32.88989	5.67451	9	19.354	3.766213	7
64.745	31.78011	5.249931	9	18.81671	3.451931	7
67.056	30.94733	4.976838	9	18.11543	3.214874	7
69.368	30.70167	4.946909	9	17.924	3.040371	7
71.679	30.47544	4.654792	9	17.75514	2.941945	7
73.991	30.30056	4.608541	9	17.46257	2.855149	7
76.302	30.111	4.62371	9	17.30199	2.769684	7
78.614	30.51089	4.851071	9	17.41586	2.807644	7
80.926	30.49156	4.893424	9	17.30547	2.80661	7
83.238	30.35211	4.885469	9	17.24413	2.789392	7
85.549	30.21478	4.942257	9	17.11107	2.844248	7
87.861	29.857	4.903747	9	16.94053	2.956656	7
90.173	29.229	4.993882	9	16.79103	3.12678	7
92.485	28.53667	5.10192	9	16.68763	3.239254	7
94.796	28.06256	5.334756	9	16.60329	3.480909	7

97.108	27.57378	5.559734	9	16.85113	3.791721	7
99.42	27.22056	5.756471	9	17.23351	4.164455	7
101.73	26.91278	5.773143	9	17.38784	4.390974	7
104.04	26.22644	5.704474	9	17.1829	4.377961	7
106.36	25.84444	5.642387	9	16.98133	4.36782	7
108.67	25.56367	5.728102	9	16.64527	4.330554	7
110.98	25.061	5.58296	9	16.46894	4.302959	7
113.29	24.36589	5.405857	9	16.47764	4.426892	7
115.6	23.68237	5.384769	9	16.26036	4.403811	7
117.91	23.07944	5.325372	9	15.79037	4.323248	7
120.22	22.65713	5.066216	9	15.13753	4.097497	7
122.54	22.30263	4.894731	9	14.42039	3.829536	7
124.85	21.79791	4.698794	9	14.14289	3.775134	7
127.16	21.41481	4.559357	9	14.14334	3.809179	7
129.47	21.50044	4.666504	9	14.15879	3.879592	7
131.78	21.14422	4.615035	9	14.14317	3.891623	7
134.1	20.81067	4.437077	9	14.32669	3.871491	7
136.41	20.45844	4.077142	9	14.48064	3.840137	7
138.72	20.22622	3.738073	9	14.58406	3.883058	7
141.03	19.96156	3.511085	9	14.7367	3.954475	7
143.34	19.85389	3.284748	9	14.77924	3.922449	7
145.65	19.68044	3.14885	9	14.81154	3.964581	7
147.96	19.28744	3.058735	9	14.9382	3.978161	7
150.27	19.07578	2.994378	9	15.15464	4.030869	7
152.59	18.99722	2.997697	9	15.1666	4.089266	7
154.9	18.87722	2.943546	9	15.17606	4.203902	7
157.21	18.70388	2.910136	9	15.05953	4.264499	7
159.52	18.46529	2.829524	9	14.69679	4.35389	7
161.83	17.8606	2.764174	9	14.40913	4.497375	7
164.14	17.27522	2.616212	9	14.20426	4.672946	7
166.46	16.45969	2.46211	9	13.97763	4.804002	7
168.77	15.62117	2.239773	9	13.651	4.895252	7
171.08	14.80349	2.073481	9	13.26564	4.908974	7
173.39	13.72363	1.914833	9	12.90666	4.914309	7
175.7	12.85246	1.746758	9	12.62381	4.961749	7
178.01	12.01223	1.625971	9	12.41103	4.952648	7
180.33	11.35463	1.517278	9	12.16226	4.995632	7
182.64	10.75418	1.371218	9	11.95459	5.015723	7
184.95	10.15422	1.159307	9	11.80971	5.097815	7
187.26	9.847511	1.07571	9	11.61157	5.147175	7

189.57	9.582911	0.985525	9	11.36629	5.217033	7
191.88	9.264589	0.881868	9	11.09521	5.301363	7
194.2	8.928033	0.791897	9	10.94163	5.418953	7
196.51	8.709522	0.69724	9	10.9878	5.505398	7
198.82	8.641778	0.689767	9	10.91583	5.550673	7
201.13	8.580189	0.665991	9	10.96801	5.658253	7
203.44	8.389533	0.599578	9	10.98544	5.690983	7
205.75	8.392278	0.574167	9	11.06557	5.761118	7
208.07	8.4037	0.545524	9	11.17039	5.844528	7
210.38	8.476022	0.532767	9	11.28399	5.907255	7
212.69	8.528767	0.567101	9	11.4446	5.957808	7
215	8.567478	0.587737	9	11.62573	6.039287	7
217.31	8.483411	0.546463	9	11.76066	6.178154	7
219.62	8.584833	0.56801	9	11.75123	6.163308	7
221.94	8.679922	0.556433	9	11.9593	6.242378	7
224.25	8.9944	0.586351	9	11.95946	6.320685	7
226.56	9.3343	0.666137	9	11.9886	6.37672	7
228.87	9.728556	0.739081	9	12.17024	6.451475	7
231.18	9.881322	0.799027	9	12.45369	6.498621	7
233.49	10.25106	0.917694	9	12.82196	6.533315	7
235.81	10.59962	1.08917	9	13.26809	6.646099	7
238.12	11.22217	1.205367	9	13.695	6.702003	7
240.43	12.11629	1.369248	9	13.97624	6.775416	7
242.74	12.93528	1.564636	9	14.48451	6.957539	7
245.05	13.66992	1.688261	9	14.94851	7.00295	7
247.37	14.64737	1.819608	9	15.49303	7.087481	7
249.68	15.94993	1.964749	9	16.18029	7.133459	7
251.99	16.88723	1.973229	9	16.9735	7.190913	7
254.3	17.92763	2.001458	9	17.78904	7.206343	7
256.61	18.8174	2.020247	9	18.67174	7.228536	7
258.92	19.98256	2.102562	9	19.37091	7.224441	7
261.23	21.21656	2.087458	9	20.34643	7.231371	7
263.55	22.97767	1.995798	9	21.3768	7.253757	7
265.86	24.94056	2.036317	9	22.30056	7.286927	7
268.17	26.11989	1.988118	9	23.38204	7.390376	7
270.48	27.285	2.125937	9	24.02143	7.308584	7
272.79	28.48844	2.250853	9	24.88914	7.432319	7
275.11	28.86889	2.172667	9	25.69629	7.445021	7
277.42	29.80967	2.36794	9	26.40571	7.549001	7
279.73	30.48644	2.447038	9	26.87586	7.633961	7

282.04	30.50722	2.501251	9	26.95229	7.669233	7
284.34	30.16089	2.55441	9	26.90471	7.650667	7

Part 5.2 hAβ tracer distribution in AQP4+/+ and AQP4-/- mice retina layers

retinal layers	**AQP4+/+ (A.U.)**						**AQP4-/- (A.U.)**					
NFL	465.2	399.6	940.5	718.8	1148.8	791.3	179.2	338.2	507.0	328.0	760.4	772.3
IPL	815.2	1201.0	751.2	896.1	2208.3	1415.7	1139.0	424.4	1066.1	444.1	1098.4	1523.0
INL	248.2	247.3	278.1	272.4	574.0	323.5	1054.3	138.9	685.4	147.9	326.3	448.1
OPL	636.7	42.6	411.3	54.6	124.1	133.2	112.4	71.7	125.0	95.6	208.7	137.2
ONL	2734.2	176.6	1635.9	194.6	322.8	244.0	357.7	466.1	416.1	378.0	323.6	250.0
IS	347.4	282.9	388.4	441.0	358.9	290.4	1374.0	160.6	771.0	121.8	407.1	216.3

Part 5.3 hAβ retinal penetration distance

AQP4+/+ (μm)	**AQP4-/- (μm)**
51.2292	27.9432
97.8012	34.929
139.716	32.6004
102.4584	65.2008
51.2292	90.8154
41.9148	37.2576
179.3022	39.5862
169.9878	
54.17953	

Part 6.1 Optic nerve hAβ signal in AQP4 +/+ and AQP4 -/- mice

	AQP4+/+ (A.U.)			**AQP4-/- (A.U.)**		
distance (μm)	**mean**	**SEM**	**n**	**mean**	**SEM**	**n**
0	39.898	4.8528	25	24.915	3.1385	24
100	48.922	7.5161	25	25.698	3.333	24
200	43.484	6.8627	25	23.878	3.5678	24
300	38.216	5.6076	25	22.475	3.6073	24
400	33.076	4.5873	25	20.684	3.3354	24
500	28.226	3.5855	25	18.507	2.9103	24
600	23.973	2.8655	25	16.478	2.4677	24
700	20.437	2.1987	25	14.507	2.0898	24
800	17.154	1.7665	25	12.476	1.7913	24

900	14.862	1.4979	25	10.838	1.5504	24
1000	12.855	1.3448	25	9.3377	1.3693	24
1100	11.342	1.2052	25	8.2593	1.2697	24
1200	10.13	1.1185	25	7.3411	1.2006	24
1300	9.2032	1.0838	25	6.8609	1.1566	24
1400	8.4445	1.0268	25	6.3363	1.1355	24
1500	8.0023	1.0254	25	5.9143	1.0998	24
1600	7.5812	1.0232	25	5.612	1.0296	24
1700	7.4847	1.0591	25	5.4307	1.0141	24
1800	7.2912	1.0717	25	5.2151	0.97843	24
1900	7.1141	1.0788	25	4.9129	1.0156	24
2000	6.8103	1.0837	25	4.6985	0.99184	24
2100	6.3277	1.0702	25	4.4241	0.97394	24
2200	6.3081	1.0783	25	4.4559	0.985	24
2300	6.0923	1.1356	25	4.0603	1.006	24
2400	5.723	1.0637	25	3.9905	1.0276	24
2500	5.7105	1.0603	25	3.7664	1.014	24
2600	5.6029	1.0196	25	3.5697	0.99525	24
2700	5.5948	1.0514	25	3.3991	0.99584	24
2800	5.2041	1.0303	25	3.0211	0.97274	24
2900	5.1991	1.0444	25	2.7164	0.97085	24
3000	4.9289	1.1043	25	2.3347	0.95776	24
3100	4.7411	1.1209	25	2.0886	0.9206	24
3200	4.428	1.1262	25	2.1073	0.93215	24
3300	4.1177	1.1121	25	2.3521	0.96013	24
3400	3.7919	1.1228	25	2.5063	1.0116	24
3500	3.5972	1.1296	25	2.4211	1.03	24
3600	3.7373	1.1787	25	2.7431	1.0545	24
3700	4.2958	1.4278	25	3.0685	1.0363	24
3800	3.967	1.1986	25	3.299	1.0496	24
3900	3.9333	1.1796	25	3.358	1.0358	24
4000	3.8655	1.1205	25	3.6305	1.0725	24
4100	4.3786	1.0855	25	4.324	1.1499	24
4200	4.3636	1.0692	25	3.8971	1.076	24
4300	4.4228	1.0408	25	3.8844	1.1088	24
4400	4.3208	1.1024	25	3.6623	1.1452	24
4500	4.1342	1.1694	25	3.6662	1.1199	24
4600	3.9432	1.0702	25	3.5715	1.1935	24
4700	3.6145	1.1826	25	3.1994	1.2171	24
4800	3.2325	1.1322	25	3.3506	1.2531	24
4900	4.2564	1.1063	25	3.9265	1.1659	24

Part 6.2 Distance of hAβ tracer transport in optic nerve in AQP4+/+ and AQP4-/- mice

AQP4+/+ (μm)	AQP4-/- (μm)
790.1234568	1203.703704
1697.530864	2074.074074
1620.37037	1120.37037
2935.185185	43.20987654
1509.259259	2114.197531
2787.037037	1033.950617
1444.444444	1379.62963
2870.37037	1024.691358
805.5555556	783.9506173
4000	4629.62963
1033.950617	89.50617284
4441.358025	962.962963
2694.444444	780.8641975
2083.333333	987.654321
962.962963	1246.91358
935.1851852	2410.493827
796.2962963	836.4197531
1126.54321	725.308642
1083.333333	163.5802469
932.0987654	1854.938272
2395.061728	2879.62963
1246.91358	774.691358
1932.098765	848.7654321
1141.975309	

Part 6.3 Total hAβ signal in optic nerve in AQP4+/+ and AQP4-/- mice

AQP4+/+ (A.U.)	AQP4-/- (A.U.)
5996.9383	12022.8023
14042.8163	17459.4733
15289.3308	10011.7278
26571.3568	5107.1513
22957.3458	19209.3093
18669.7658	7690.2153
9854.8918	13678.4783
21273.6208	10936.6158
9055.6183	3772.9133
20649.4933	26949.3173
12790.5843	640.2663
24792.5508	9769.9813
16140.8518	4788.1238
21091.2458	5387.4553
11014.4273	10237.3758

6993.8038	20785.4953
6181.3763	5016.1523
14259.0283	5792.2193
8673.0203	1034.6748
5879.9483	26594.4218
29871.6848	23718.8133
13390.2643	6067.2398
37722.7808	6787.4613
16432.2668	

Part 6.4 Peak hAβ signal intensity in optic nerve in AQP4+/+ and AQP4-/- mice

AQP4+/+ (A.U.)	AQP4-/- (A.U.)
18.95104895	41.68872378
30.06993007	22.76223776
41.55557692	32.30769231
56.43356643	3.72027972
116.4673427	30.78237413
35.1048951	24.23076923
24.02097902	64.05594406
32.5844528	16.43356643
14.79020979	14.10839161
25.58628671	49.02097902
73.56643357	8.006993007
41.74917133	17.83216783
18.4965035	34.26573427
33.54135664	23.16382867
50.6993007	24.86013986
27.58741259	44.71795804
33.70629371	18.53146853
88.46153846	39.48633706
27.83216783	10.6602986
22.66077972	87.06293706
131.6433566	41.41057692
61.25874126	24.44055944
157.3426573	29.05594406
65.73426573	

Part 7.1 ICP manipulation

	high ICP (mmHg)		low ICP (mmHg)		norm ICP (mmHg)	
time(min)	**mean**	**SEM**	**mean**	**SEM**	**mean**	**SEM**
0	3.62129	0.14107	3.52478	0.44829	3.62129	0.14107

0.11	3.58353	0.16369	3.46883	0.44759	3.58353	0.16369
0.22	3.65486	0.13963	3.46883	0.51033	3.65486	0.13963
0.33	3.62129	0.13613	3.41288	0.50849	3.62129	0.13613
0.44	3.68004	0.13767	3.35693	0.45038	3.68004	0.13767
0.55	3.60031	0.14253	3.52478	0.56005	3.60031	0.14253
0.66	3.48282	0.19786	3.46883	0.49539	3.48282	0.19786
0.77	3.76816	0.20089	3.41288	0.44549	3.76816	0.20089
0.88	3.64647	0.14563	3.46883	0.49539	3.64647	0.14563
0.99	3.62129	0.1457	3.46883	0.49539	3.62129	0.1457
1.1	3.81851	0.16245	3.46883	0.49539	3.44086	0.15532
1.21	3.62129	0.14107	3.52478	0.54647	3.3905	0.13155
1.32	3.62129	0.14843	3.58073	0.51764	3.44086	0.13833
1.43	3.57513	0.18593	3.52478	0.54647	3.47443	0.1448
1.54	3.57933	0.14958	3.46883	0.49539	3.49121	0.14693
1.65	3.59611	0.13479	3.46883	0.49539	3.3905	0.14239
1.76	3.6087	0.1314	3.52478	0.46475	3.40729	0.21688
1.87	3.59192	0.12415	3.46883	0.49539	3.37372	0.13367
1.98	3.59611	0.12439	3.46883	0.4721	3.3905	0.14816
2.09	3.62968	0.12679	3.58073	0.51764	3.44086	0.13063
2.2	3.6129	0.1275	3.52478	0.46475	3.35693	0.12908
2.31	3.60451	0.13078	3.52478	0.46475	3.35693	0.13443
2.42	3.6129	0.13276	3.58073	0.45591	3.37372	0.14834
2.53	3.60031	0.13823	3.52478	0.46475	3.37372	0.15125
2.64	3.6087	0.12924	3.52478	0.52544	3.44086	0.13721
2.75	3.6129	0.13811	3.69263	0.54818	3.28979	0.13439
2.86	3.62129	0.12439	3.63668	0.51582	3.45764	0.1256
2.97	3.62129	0.13192	3.52478	0.52544	3.37372	0.15565
3.08	3.6171	0.13588	3.52478	0.52544	3.35693	0.12374
3.19	3.64647	0.13576	3.58073	0.57928	3.35693	0.13136
3.3	3.64647	0.13457	3.69263	0.54818	3.3905	0.12398
3.41	3.64227	0.11698	3.69263	0.54818	3.37372	0.15129
3.52	3.62129	0.12374	3.63668	0.57112	3.35693	0.15949
3.63	3.62968	0.13208	3.69263	0.54818	3.37372	0.15139
3.74	3.65486	0.13329	3.74857	0.53723	3.35693	0.12923
3.85	3.66745	0.13469	3.74858	0.54417	3.3905	0.12276
3.96	3.65906	0.13063	3.69263	0.54818	3.34015	0.15802
4.07	3.66325	0.12111	3.74858	0.66811	3.35693	0.13588
4.18	3.67165	0.11523	3.69263	0.54818	3.37372	0.13443
4.29	3.58353	0.16233	3.69263	0.55499	3.35693	0.13701
4.4	3.59611	0.15532	3.69263	0.54818	3.34015	0.1531
4.51	3.6087	0.13473	3.69263	0.55499	3.37372	0.15604
4.62	3.65066	0.13529	3.97237	0.62151	3.34015	0.15704

4.73	3.56674	0.17266	3.80452	0.52485	3.37372	0.12406
4.84	3.58353	0.16369	3.80452	0.45591	3.37372	0.16217
4.95	3.59192	0.13913	3.58073	0.49539	3.35693	0.15389
5.06	3.65066	0.12889	3.58073	0.49539	3.35693	0.12924
5.17	4.75006	0.24447	3.30098	0.79163	3.37372	0.12624
5.28	5.60188	0.37801	2.96529	0.87287	3.30658	0.14199
5.39	6.58379	0.54612	2.96529	0.73759	3.35693	0.15116
5.5	7.49855	0.74135	3.02124	0.78488	3.32336	0.16096
5.61	8.50143	0.86841	3.02124	0.88392	3.35693	0.19874
5.72	9.412	0.93403	2.68555	0.59422	3.32336	0.12259
5.83	10.4485	0.95968	2.6296	0.59052	3.27301	0.18329
5.94	11.2457	1.01536	2.57365	0.59211	3.34015	0.15777
6.05	12.1101	1.03968	2.57365	0.58573	3.35693	0.1275
6.16	12.7396	1.0915	2.5177	0.57331	3.37372	0.123
6.27	13.2473	1.06887	2.4058	0.52305	3.35693	0.13617
6.38	13.6501	1.07715	2.12606	0.55273	3.34015	0.15523
6.49	14.1369	1.05611	2.18201	0.57331	3.35693	0.14057
6.6	14.5397	1.05809	2.23796	0.51764	3.34015	0.20026
6.71	14.7453	1.11717	2.12606	0.53196	3.35693	0.12479
6.82	15.0013	1.06209	2.18201	0.5533	3.35693	0.12736
6.93	15.2447	1.06899	2.23796	0.57928	3.34015	0.16542
7.04	15.2908	1.04324	2.23796	0.52485	3.35693	0.1314
7.15	15.3496	1.04952	2.18201	0.51094	3.35693	0.12037
7.26	15.5678	1.02179	1.95821	0.4701	3.35693	0.14417
7.37	15.6223	1.10117	2.07011	0.50849	3.32336	0.12766
7.48	15.5678	1.08058	2.01416	0.52723	3.25622	0.13856
7.59	15.6097	1.1059	1.84631	0.57982	3.35693	0.22727
7.7	15.6223	1.05644	1.73442	0.59685	3.35693	0.14639
7.81	15.7104	1.07844	1.73442	0.59685	3.35693	0.12219
7.92	15.6979	0.99025	1.79036	0.56616	3.35693	0.14958
8.03	15.7314	1.01091	1.67847	0.61289	3.35693	0.14843
8.14	15.6937	1.03392	1.62252	0.49349	3.34015	0.13913
8.25	15.6349	1.02152	1.56657	0.46407	3.34015	0.14025
8.36	15.7356	1.04371	1.34277	0.46676	3.32336	0.13753
8.47	15.6517	1.02055	1.45467	0.52485	3.28979	0.13818
8.58	15.593	0.96283	1.39872	0.55781	3.32336	0.16162
8.69	15.6391	1.05889	1.45467	0.57276	3.35693	0.16433
8.8	15.6181	1.05102	1.23088	0.43048	3.35693	0.19568
8.91	15.6097	0.99889	1.23088	0.48775	3.30658	0.15627
9.02	15.6979	1.03259	1.34277	0.45038	3.25622	0.14823
9.13	15.6307	1.01506	1.23088	0.50292	3.27301	0.13473
9.24	15.6265	0.97848	1.34277	0.48259	3.34015	0.13109

9.35	15.8531	1.00385	1.28682	0.50105	3.34015	0.14154
9.46	15.8028	0.98043	1.39872	0.45384	3.35693	0.14577
9.57	15.8447	1.01218	1.34277	0.52723	3.32336	0.13768
9.68	15.6979	0.98389	0.67139	0.58144	3.30658	0.14057
9.79	15.6811	0.9991	0.83923	0.56671	3.34015	0.24113
9.9	15.7146	0.94352	0.78328	0.4721	3.27301	0.13985
10.01	15.7818	0.98151	0.67139	0.37781	3.27301	0.13108
10.12	15.5972	1.01439	0.67139	0.37781	3.32336	0.12111
10.23	15.7902	0.95599	0.55949	0.37448	3.27301	0.12439
10.34	15.6937	0.97452	0.55949	0.35385	3.30658	0.13895
10.45	15.6475	1.00001	0.61544	0.31748	3.25622	0.14958
10.56	15.5846	0.9391	0.50354	0.35474	3.18909	0.14823
10.67	15.6727	0.98054	0.44759	0.29605	3.32336	0.14625
10.78	15.6181	1.00959	0.33569	0.3467	3.37372	0.13215
10.89	15.5972	1.01571	0.44759	0.32043	3.37372	0.13016
11	15.6391	1.01116	0.39164	0.29286	3.37372	0.15301
11.11	15.6853	1.0226	0.39164	0.35119	3.35693	0.13208
11.22	15.509	1.00754	0.44759	0.32043	3.35693	0.1286
11.33	15.6433	1.02259	0.27974	0.29286	3.34015	0.1279
11.44	15.6433	1.00143	0.16785	0.30949	3.1723	0.15012
11.55	15.5888	1.01512	0.27974	0.30542	3.12195	0.15039
11.66	15.6433	0.98973	0.27974	0.30542	3.35693	0.14396
11.77	15.572	1.01782	0.39164	0.29286	3.37372	0.1159
11.88	15.5678	1.08741	0.33569	0.30025	3.40729	0.13457
11.99	15.7734	1.03258	0.2238	0.2238	3.45764	0.14693
12.1	15.6685	1.03524	0.1119	0.14154	3.47443	0.13576
12.21	15.7063	1.04658	0.33569	0.12258	3.35693	0.14549
12.32	15.807	1.01044	0.2238	0.18724	3.30658	0.13228
12.43	15.7776	0.99342	0.2238	0.16597	3.34015	0.14888
12.54	15.7608	1.02111	0.39164	0.18216	3.32336	0.15198
12.65	15.6559	0.988	0.33569	0.22932	3.27301	0.16555
12.76	15.7692	1.00827	0.33569	0.15013	3.27301	0.12177
12.87	15.6223	0.97175	0.50354	0.14374	3.35693	0.13753
12.98	15.6433	1.01916	0.44759	0.14154	3.32336	0.15704
13.09	15.6685	0.92811	0.39164	0.10316	3.35693	0.13811
13.2	15.7272	0.97341	0.44759	0.14154	3.30658	0.13013
13.31	15.6853	0.95741	0.50354	0.11466	3.34015	0.13782
13.42	15.6853	0.99108	0.44759	0.1119	3.35693	0.15471
13.53	15.6979	0.94402	0.44759	0.14154	3.32336	0.15125
13.64	15.6181	0.92258	0.50354	0.14374	3.32336	0.19273
13.75	15.5804	0.88267	0.44759	0.14154	3.37372	0.12624
13.86	15.6811	0.89499	0.50354	0.16785	3.27301	0.14797

13.97	15.5048	0.90434	0.50354	0.1889	3.28979	0.16099
14.08	15.4377	0.89364	0.50354	0.1889	3.28979	0.13078
14.19	15.5762	0.8875	0.50354	0.1889	3.35693	0.13177
14.3	15.3999	0.84124	0.55949	0.18724	3.37372	0.13382
14.41	15.593	0.84644	0.55949	0.18724	3.37372	0.15441
14.52	15.5132	0.8142	0.50354	0.1889	3.35693	0.14014
14.63	15.53	0.88186	0.55949	0.16597	3.32336	0.20152
14.74	15.5132	0.92892	0.61544	0.21956	3.30658	0.11584
14.85	15.4377	0.96315	0.72734	0.20173	3.35693	0.13716
14.96	15.316	0.90561	0.61544	0.16021	3.34015	0.14438
15.07	15.3118	0.87138	0.61544	0.16021	3.34015	0.12415
15.18	15.4503	0.89358	0.67139	0.17335	3.34015	0.12341
15.29	15.5048	0.90554	0.67139	0.17335	3.35693	0.14999
15.4	15.5762	0.94507	0.72734	0.16021	3.37372	0.13182
15.51	15.6265	0.92311	0.61544	0.13474	3.42407	0.13093
15.62	15.7188	1.01502	0.72734	0.20173	3.3905	0.22579
15.73	15.6349	0.99068	0.67139	0.15013	3.37372	0.13201
15.84	15.5342	0.96855	0.50354	0.18891	3.34015	0.13075
15.95	15.5426	0.97875	0.67139	0.15013	3.35693	0.19543
16.06	15.5678	0.98067	0.72734	0.16021	3.34015	0.18593
16.17	15.5006	0.9138	0.67139	0.15013	3.35693	0.12889
16.28	15.53	0.9918	0.67139	0.15013	3.34015	0.1391
16.39	15.5888	0.95039	0.61544	0.13474	3.32336	0.13706
16.5	15.4797	0.91785	0.61544	0.13474	3.34015	0.13999
16.61	15.4545	0.91078	0.44759	0.18724	3.23944	0.15341
16.72	15.5804	0.94245	0.50354	0.18891	3.32336	0.14082
16.83	15.572	0.9673	0.39164	0.16021	3.30658	0.15558
16.94	15.4839	0.9296	0.50354	0.18891	3.34015	0.14945
17.05	15.5594	0.92167	0.44759	0.18724	3.35693	0.15742
17.16	15.593	0.95054	0.39164	0.23605	3.27301	0.13529
17.27	15.5006	0.91247	0.44759	0.18724	3.25622	0.13162
17.38	15.4419	0.92457	0.44759	0.23999	3.25622	0.14522
17.49	15.4839	0.97479	0.33569	0.24516	3.15552	0.12573
17.6	15.2363	0.90738	0.39164	0.21956	3.27301	0.13621
17.71	15.2699	0.89813	0.39164	0.25146	3.20587	0.1392
17.82	15.4503	0.91974	0.44759	0.20633	3.18909	0.21921
17.93	15.4209	0.92457	0.44759	0.26949	3.12195	0.13934
18.04	15.4629	0.92093	0.39164	0.25146	3.18909	0.13928
18.15	15.379	0.8603	0.27974	0.30542	3.13873	0.11523
18.26	15.4041	0.85922	0.27974	0.21956	3.1723	0.13
18.37	15.4587	0.91244	0.27974	0.29286	3.23944	0.14253
18.48	15.379	0.899	0.33569	0.24516	3.23944	0.14393

18.59	15.4755	0.88239	0.2238	0.20633	3.20587	0.15895
18.7	15.5762	0.88542	0.33569	0.21231	3.18909	0.13869
18.81	15.4964	0.91356	0.27974	0.18216	3.15552	0.12893
18.92	15.5006	0.92029	0.27974	0.18216	3.20587	0.13424
19.03	15.5006	0.85899	0.2238	0.16597	3.18909	0.14982
19.14	15.4293	0.89603	0.27974	0.18216	3.13873	0.13329
19.25	15.4671	0.89888	0.27974	0.13474	3.35693	0.1317
19.36	15.4083	0.89182	0.39164	0.18216	3.10516	0.12955
19.47	15.2111	0.87553	0.33569	0.17335	3.12195	0.14143
19.58	15.3328	0.86692	0.33569	0.17335	3.12195	0.14752
19.69	15.2908	0.87664	0.39164	0.20173	3.07159	0.14532
19.8	15.4629	0.86218	0.33569	0.17335	3.05481	0.12719
19.91	15.3244	0.9	0.33569	0.17335	3.05481	0.12663
20.02	15.2573	0.82132	0.39164	0.18216	3.13873	0.15032
20.13	15.3706	0.88801	0.33569	0.17335	3.13873	0.13457
20.24	15.3286	0.84532	0.39164	0.20173	3.15552	0.13258
20.35	15.3118	0.88513	0.33569	0.17335	3.1723	0.13109
20.46	15.3538	0.84406	0.33569	0.17335	3.05481	0.14918
20.57	15.3748	0.91442	0.39164	0.20173	3.08838	0.16266
20.68	15.5216	0.91025	0.39164	0.21956	3.28979	0.15908
20.79	15.3957	0.94823	0.39164	0.20173	3.35693	0.12487
20.9	15.3664	0.92542	0.44759	0.20633	3.35693	0.13394
21.01	15.4377	0.96204	0.33569	0.21231	3.28979	0.15707
21.12	15.4922	0.9604	0.44759	0.2238	3.28979	0.12439
21.23	15.4125	0.97095	0.39164	0.20173	3.20587	0.12951
21.34	15.593	0.93586	0.44759	0.18724	3.05481	0.14097
21.45	15.4461	0.94682	0.50354	0.14374	3.03802	0.14985
21.56	15.3328	0.95624	0.55949	0.14154	3.12195	0.15487
21.67	15.4922	0.93485	0.55949	0.20633	3.18909	0.18446
21.78	15.4755	0.93677	0.55949	0.20633	3.13873	0.11715
21.89	15.3748	0.96172	0.55949	0.20633	3.23944	0.13804
22	15.2824	0.92694	0.50354	0.18891	3.12195	0.15973
22.11	15.3748	0.91611	0.50354	0.18891	3.07159	0.13276
22.22	15.3076	0.89875	0.55949	0.18724	3.08838	0.12496
22.33	15.3118	0.93916	0.61544	0.20173	3.03802	0.141
22.44	15.274	0.91078	0.61544	0.20173	3.42407	0.1596
22.55	15.295	0.91126	0.67139	0.22932	3.3905	0.18208
22.66	15.2866	0.93679	0.67139	0.22932	3.44086	0.19712
22.77	15.1314	0.87367	0.61544	0.20173	3.47443	0.13062
22.88	15.2992	0.88434	0.55949	0.18724	3.47443	0.1694
22.99	15.2279	0.90539	0.67139	0.22932	3.40729	0.16196
23.1	15.2069	0.88843	0.61544	0.20173	3.40729	0.12439

23.21	15.295	0.92603	0.67139	0.22932	3.37372	0.11392
23.32	15.1985	0.8521	0.61544	0.23605	3.3905	0.14323
23.43	15.2153	0.87501	0.67139	0.22932	3.42407	0.14605
23.54	15.1608	0.87464	0.61544	0.27974	3.35693	0.12915
23.65	15.1356	0.86505	0.67139	0.22932	3.35693	0.21254
23.76	15.0642	0.8504	0.55949	0.2238	3.37372	0.13847
23.87	15.1272	0.91389	0.67139	0.22932	3.37372	0.13013
23.98	14.9761	0.88011	0.72734	0.18216	3.42407	0.17327
24.09	15.0475	0.87962	0.61544	0.21956	3.27301	0.14958
24.2	15.0307	0.82854	0.61544	0.21956	3.47443	0.13
24.31	14.9425	0.86312	0.72734	0.18216	3.3905	0.14549
24.42	14.8796	0.88037	0.61544	0.23605	3.35693	0.1387
24.53	14.909	0.84526	0.67139	0.22932	3.35693	0.14577
24.64	14.9425	0.87307	0.55949	0.20633	3.3905	0.14445
24.75	14.9929	0.85201	0.61544	0.23605	3.37372	0.13499
24.86	14.8922	0.8462	0.61544	0.23605	3.35693	0.14143
24.97	14.9635	0.86443	0.61544	0.23605	3.37372	0.1584
25.08	14.93	0.87563	0.61544	0.23605	3.34015	0.14227
25.19	14.9761	0.9366	0.61544	0.23605	3.3905	0.17266
25.3	14.9761	0.95743	0.67139	0.22932	3.35693	0.13869
25.41	14.8754	0.97583	0.67139	0.24516	3.35693	0.14507
25.52	14.9384	0.97179	0.67139	0.24516	3.35693	0.13721
25.63	14.9761	0.98091	0.55949	0.25517	3.35693	0.12982
25.74	14.9887	0.97175	0.55949	0.25517	3.34015	0.15571
25.85	15.06	1.03646	0.61544	0.23605	3.37372	0.20369
25.96	14.9887	0.96677	0.61544	0.29286	3.34015	0.14057
26.07	14.9635	1.0001	0.50354	0.25639	3.37372	0.14242
26.18	14.93	1.0203	0.55949	0.25517	3.37372	0.16233
26.29	15.0223	0.94187	0.61544	0.23605	3.35693	0.127
26.4	15.3915	0.93928	0.61544	0.21956	3.37372	0.13953
26.51	15.2447	0.95328	0.67139	0.27409	3.37372	0.14673
26.62	15.2699	0.98138	0.67139	0.19381	3.28979	0.14775
26.73	15.4083	0.95314	0.55949	0.25517	3.35693	0.14403
26.84	15.4377	0.97982	0.55949	0.20633	3.32336	0.13957
26.95	15.3538	0.93272	0.67139	0.22932	3.34015	0.14196
27.06	15.3706	0.98472	0.55949	0.25517	3.30658	0.13783
27.17	15.3244	0.95677	0.61544	0.26598	3.28979	0.13469
27.28	15.358	0.96874	0.55949	0.25517	3.35693	0.13789
27.39	15.3286	0.97518	0.67139	0.22932	3.35693	0.13192
27.5	15.4797	0.95102	0.61544	0.26598	3.37372	0.14902
27.61	15.3622	0.94617	0.55949	0.25517	3.35693	0.15222
27.72	15.4419	0.97161	0.61544	0.29286	3.34015	0.15116

27.83	15.3957	0.96885	0.50354	0.24129	3.35693	0.11454
27.94	15.4671	0.96031	0.50354	0.24129	3.34015	0.1256
28.05	15.3076	0.96912	0.55949	0.25517	3.35693	0.15186
28.16	15.2489	0.94884	0.61544	0.26598	3.35693	0.11698
28.27	15.379	0.98401	0.50354	0.29711	3.32336	0.13532
28.38	15.4041	0.94211	0.55949	0.25517	3.28979	0.13383
28.49	15.4377	0.92373	0.61544	0.25146	3.32336	0.14972
28.6	15.3244	0.93836	0.55949	0.20633	3.28979	0.16682
28.71	15.3286	0.93741	0.55949	0.20633	3.35693	0.16481
28.82	15.2699	0.91205	0.72734	0.26598	3.32336	0.11835
28.93	15.3706	0.96478	0.67139	0.26003	3.28979	0.12774
29.04	15.4545	0.92233	0.61544	0.21956	3.34015	0.1434
29.15	15.3286	0.92483	0.61544	0.21956	3.34015	0.13192
29.26	15.3202	0.8885	0.61544	0.25146	3.30658	0.13628
29.37	15.4083	0.88582	0.67139	0.22932	3.37372	0.13494
29.48	15.316	0.87469	0.67139	0.26003	3.28979	0.15085
29.59	15.2824	0.87875	0.61544	0.21956	3.32336	0.14163
29.7	15.2153	0.89621	0.61544	0.21956	3.30658	0.16975
29.81	15.3538	0.83515	0.55949	0.20633	3.34015	0.13017
29.92	15.2363	0.85034	0.61544	0.25146	3.32336	0.16049
30.03	15.2027	0.82439	0.67139	0.26003	3.37372	0.15474
30.14	15.4629	0.85215	0.67139	0.26003	3.37372	0.13823
30.25	15.3328	0.84157	0.55949	0.20633	3.35693	0.1281
30.36	15.3286	0.8482	0.55949	0.28308	3.28979	0.14556
30.47	15.2153	0.8335	0.50354	0.24129	3.35693	0.15441
30.58	15.2363	0.83869	0.50354	0.24129	3.34015	0.15665
30.69	15.2069	0.79629	0.55949	0.20633	3.32336	0.18734
30.8	15.3328	0.83208	0.67139	0.30025	3.34015	0.12186
30.91	15.295	0.81823	0.61544	0.26598	3.35693	0.17152
31.02	15.3244	0.82645	0.61544	0.25146	3.37372	0.15808
31.13	15.3664	0.82576	0.61544	0.25146	3.37372	0.12679
31.24	15.3748	0.80416	0.61544	0.25146	3.44086	0.11791
31.35	15.2824	0.78943	0.61544	0.25146	3.37372	0.13561
31.46	15.3412	0.8171	0.61544	0.25146	3.34015	0.14078
31.57	15.337	0.8136	0.61544	0.25146	3.35693	0.11999
31.68	15.3202	0.80554	0.61544	0.21956	3.34015	0.21709
31.79	15.2405	0.82335	0.72734	0.23605	3.35693	0.12842
31.9	15.4377	0.81959	0.67139	0.26003	3.35693	0.13306
32.01	15.3915	0.83556	0.72734	0.20173	3.30658	0.16048
32.12	15.2111	0.83047	0.67139	0.19381	3.34015	0.13479
32.23	15.274	0.86783	0.61544	0.20173	3.30658	0.12826
32.34	15.2321	0.91525	0.61544	0.23605	3.30658	0.13139

32.45	15.2363	0.88837	0.50354	0.20784	3.30658	0.12137
32.56	15.2866	0.88562	0.50354	0.24129	3.34015	0.14687
32.67	15.2573	0.90839	0.55949	0.28308	3.37372	0.19169
32.78	15.1104	0.86319	0.67139	0.30025	3.30658	0.1421
32.89	15.1272	0.87786	0.67139	0.27409	3.28979	0.12711
33	15.2027	0.90113	0.67139	0.30025	3.30658	0.14911
33.11	15.0349	0.85419	0.67139	0.30025	3.22265	0.14107
33.22	15.0516	0.86655	0.61544	0.29286	3.25622	0.16369
33.33	15.1943	0.91025	0.67139	0.26003	3.20587	0.13963
33.44	15.0684	0.89589	0.67139	0.26003	3.20587	0.13613
33.55	15.0684	0.9417	0.61544	0.23605	3.18909	0.13767
33.66	15.0055	0.83573	0.44759	0.2238	3.18909	0.14253
33.77	14.93	0.86313	0.55949	0.26949	3.13873	0.19786
33.88	14.9803	0.83553	0.39164	0.26598	3.20587	0.20089
33.99	14.9593	0.8965	0.44759	0.2238	3.20587	0.14563
34.1	15.0055	0.90697	0.44759	0.26949	3.22265	0.1457
34.21	15.0013	0.91838	0.39164	0.26598	3.22265	0.15532
34.32	14.9467	0.86005	0.50354	0.28419	3.20587	0.13155
34.43	15.06	0.87765	0.39164	0.25146	3.23944	0.13833
34.54	14.9887	0.87345	0.39164	0.25146	3.12195	0.1448
34.65	15.0139	0.87581	0.44759	0.20633	3.22265	0.14693
34.76	14.9635	0.87652	0.33569	0.19381	3.1723	0.14239
34.87	15.0642	0.90969	0.33569	0.17335	3.34015	0.21688
34.98	14.9635	0.9079	0.39164	0.21956	3.22265	0.13367

Part 7.2 IOP response to ICP manipulation (normalized to normal ICP condition)

time post ICP manipulation (min)	**high ICP (mmHg)**		**normal ICP (mmHg)**		**low ICP (mmHg)**	
	mean	**SEM**	**mean**	**SEM**	**mean**	**SEM**
0	1	0	1	0	1	0
3	1.16609	0.0115726	1.04319	0.0351081	0.81498	0.071040774
6	1.18801	0.0343862	0.99912	0.0461922	0.97272	0.128807801
9	0.98684	0.0186081	1.06779	0.0912208	0.78451	0.053116006
12	1.08277	0.0191888	1.08573	0.1117882	0.86058	0.025221505
15	0.91151	0.0292021	0.98129	0.0878287	0.71753	0.042716948
18	0.78353	0.0152803	0.94105	0.0767137	0.68888	0.030103736
21	1.04212	0.0275989	1.12068	0.0929466	0.91405	0.043408788
24	1.12257	0.0024076	1.1266	0.1088791	0.94881	0.084536786
27	1.13609	0.0055212	1.21651	0.1210071	1.00782	0.075953863
30	1.07532	0.0132238	0.97961	0.0541602	0.92562	0.062126913

Part 8.1 Optic nerve hAβ signal with manipulation of translaminar pressure difference

	high ICP (A.U.)			norm ICP (A.U.)			low ICP (A.U.)		
distance (μm)	**mean**	**SEM**	**n**	**mean**	**SEM**	**n**	**mean**	**SEM**	**n**
0	1.9183	1.5576	8	16.067	3.1964	7	34.18	4.935	6
100	3.4664	1.5433	8	33.553	6.0246	7	76.685	16.202	6
200	3.7967	1.7381	8	32.298	5.7787	7	72.94	14.688	6
300	3.3692	1.6106	8	30.156	6.4518	7	67.164	13.281	6
400	3.3867	1.7362	8	28.24	6.1144	7	62.66	13.173	6
500	3.5518	1.6892	8	25.451	5.2348	7	57.91	13.401	6
600	3.397	1.5504	8	21.622	4.7944	7	49.207	11.963	6
700	3.4743	1.6502	8	18.436	4.0721	7	40.825	9.9443	6
800	3.9916	1.8649	8	15.29	3.395	7	35.014	8.404	6
900	4.1667	1.7862	8	13.119	2.7212	7	30.873	7.4173	6
1000	4.7142	1.8401	8	11.289	2.5203	7	26.924	6.2191	6
1100	5.3146	2.2139	8	10.157	2.331	7	23.681	5.6084	6
1200	5.4283	2.2487	8	9.227	2.1599	7	21.055	4.7811	6
1300	5.8509	2.2536	8	8.9013	2.0296	7	18.609	4.3276	6
1400	6.1253	2.3387	8	8.3618	2.1489	7	16.284	3.9126	6
1500	6.188	2.4659	8	7.9456	2.0864	7	14.453	3.5849	6
1600	6.443	2.4986	8	7.6425	2.0556	7	12.846	3.0977	6
1700	6.4939	2.6451	8	7.3768	2.0215	7	11.02	3.0345	6
1800	6.1209	2.6152	8	7.1991	2.0486	7	8.7276	2.7974	6
1900	5.7556	2.5922	8	6.8472	2.0664	7	8.4159	2.3149	6
2000	5.8343	2.6558	8	6.7831	2.1032	7	7.2051	2.0422	6
2100	6.1938	2.679	8	6.6047	1.8645	7	7.2191	1.7336	6
2200	6.1162	2.725	8	6.4379	1.8775	7	6.8	1.7012	6
2300	6.0705	2.6412	8	6.0575	1.8002	7	6.7272	1.4888	6
2400	6.1228	2.6125	8	6.076	1.6888	7	6.9722	1.3701	6
2500	6.6245	2.8827	8	6.0268	1.7752	7	6.8296	1.3603	6
2600	6.9175	3.0492	8	6.471	1.744	7	7.8192	1.7439	6
2700	7.0092	3.0833	8	6.946	1.7473	7	7.1511	2.0876	6
2800	7.3479	3.1701	8	7.1113	1.7359	7	6.5984	2.0094	6
2900	7.5584	3.1615	8	7.179	1.7912	7	6.9736	2.0664	6
3000	7.6735	3.307	8	7.4815	1.7714	7	6.9848	1.8078	6
3100	7.5875	3.3604	8	7.5367	1.7797	7	7.5029	1.5205	6
3200	7.1721	3.1994	8	7.5643	1.9164	7	7.1262	1.0415	6
3300	6.8548	3.0581	8	7.6526	2.1117	7	7.9792	1.3342	6
3400	5.8867	2.6072	8	8.2677	2.2801	7	9.1705	1.3712	6
3500	5.5644	2.2424	8	7.8745	2.4311	7	10.562	2.1553	6

3600	4.5808	1.8502	8	8.4946	2.6838	7	12.119	2.9927	6
3700	4.3731	1.6766	8	7.8224	2.8002	7	12.743	2.8404	6
3800	3.8964	1.4962	8	7.4724	2.8886	7	11.825	2.5188	6
3900	3.9149	1.7194	8	7.5766	2.9431	7	11.956	2.9883	6
4000	3.9336	1.9657	8	7.5586	3.3523	7	10.496	3.2896	6
4100	3.3226	1.8177	8	7.5783	3.4692	7	10.359	3.41	6
4200	3.8248	1.6512	8	7.4373	3.4181	7	10.258	3.5976	6
4300	3.5129	1.3733	8	7.468	3.696	7	10.443	3.7832	6
4400	4.3838	1.5852	8	6.7275	3.9083	7	10.53	4.1713	6
4500	4.747	1.463	8	6.6161	4.108	7	13.753	6.2464	6
4600	4.4077	1.6888	8	6.4069	4.3596	7	17.874	7.7699	6
4700	4.8172	1.9327	8	5.9632	3.2455	7	18.444	8.5119	6
4800	5.3385	2.1358	8	4.2657	2.572	7	18.467	8.8739	6
4900	4.2746	1.8106	8	3.6658	2.4215	7	15.682	8.306	6

Part 8.2 Distance of hAβ transport in optic nerve with manipulation of translaminar pressure difference

high ICP (μm)	normal ICP (μm)	low ICP (μm)
45.6022	191.358	1768.519
9.7719	1756.173	1543.21
185.6661	1361.111	858.0247
78.1752	2243.827	2222.222
35.8303	839.5062	1598.765
156.3504	1632.716	1552.469
87.9471	3267.072	
32.573		

Part 8.3 Total hAβ signal in optic nerve with manipulation of translaminar pressure difference

high ICP (A.U.)	normal ICP (A.U.)	low ICP (A.U.)
12527.17	5863.765	43632.05
22827.64	14516.89	31913.44
157.486	9557.693	27494.46
6320.898	21450.28	40357.79
14761.57	3579.067	14934.28
4871.55	32439.78	19454.46
101.1027	21796.62	
653.3475		

Part 8.4 Peak hAβ signal in optic nerve with manipulation of translaminar pressure difference

high ICP (A.U.)	normal ICP (A.U.)	low ICP (A.U.)
0.029155	18.57143	144.5335
8.177843	44.54082	90.23324
2.015306	16.34694	56.42857
0.034985	46.86589	111.0787
13.40816	28.64431	36.32653
11.56268	46.91691	68.46939
2.768222	58.86297	
3.48105		

Part 9.1 Optic nerve hAβ signal in eye exposed to darkness, darkness with pilocarpine treatment, 1Hz light stimulation, 1Hz light stimulation with atropine treatment

	30min 1Hz stim + atropine (A.U.)			30min 1Hz stim (A.U.)			30min dark unstim (A.U.)			30min dark unstim+ pilocarpine (A.U.)		
Distance from eyeball (μm)	mean	SEM	n	mean	SEM	n	mean	SEM	n	mean	SEM	n
0	10.7078	8.65483	6	17.5417	5.77423	6	11.3333	2.58945	6	5.46173	1.32193	19
100	19.851	5.66007	6	53.1528	7.71268	6	30.5833	5.77985	6	18.4036	2.35938	19
200	14.7488	4.0899	6	63.8611	8.41347	6	24.2639	5.35454	6	18.085	3.0038	19
300	11.002	3.02224	6	66.0694	7.42791	6	23.5694	4.33722	6	17.8397	2.94863	19
400	8.50597	2.75839	6	66.0972	9.60423	6	20.4861	4.69261	6	15.9828	2.60673	19
500	6.68494	2.46047	6	58.9306	9.44952	6	18.2778	4.07594	6	13.7577	2.28336	19
600	5.00513	1.92861	6	55.6944	10.1799	6	15.7222	3.37644	6	11.772	2.14563	19
700	4.09239	1.66618	6	49.5583	9.98108	6	12.5833	2.61052	6	9.85806	2.05999	19
800	3.71195	1.53844	6	40.9694	9.18224	6	11.4028	1.79746	6	8.72854	2.09169	19
900	3.58936	1.5477	6	32.0861	7.14408	6	10.5139	1.45315	6	8.25099	2.27192	19
1000	3.42722	1.6453	6	26.95	6.16075	6	8.84722	1.47842	6	7.77737	2.51996	19
1100	3.27181	1.55552	6	23.0917	5.1383	6	8.31945	1.15944	6	7.47505	2.69199	19
1200	3.11399	1.55439	6	19.325	3.75968	6	7.325	1.15643	6	7.30509	2.80422	19
1300	2.67543	1.38492	6	17.2361	3.00517	6	7.1	1.15259	6	7.1128	2.80667	19
1400	2.52494	1.34947	6	15.0278	2.66679	6	6.63611	0.92492	6	6.86145	2.68872	19
1500	2.23251	1.24978	6	13.4028	2.45982	6	6.13056	1.12035	6	6.62321	2.63889	19
1600	2.18309	1.21911	6	10.9444	2.8918	6	5.13333	1.00979	6	6.42839	2.55692	19
1700	2.11752	1.09299	6	10.2222	3.08663	6	4.93056	0.73741	6	6.23874	2.4748	19
1800	2.26259	1.05531	6	8.84722	2.79173	6	4.75278	0.95707	6	5.94568	2.38547	19
1900	2.58559	1.23198	6	7.84722	2.47623	6	4.40833	1.0662	6	5.35867	2.11856	19
2000	2.59839	1.32339	6	8.02778	2.32925	6	4.29167	1.00476	6	5.0419	1.88474	19

2100	2.27521	1.3244	6	7.83333	2.54754	6	4.54722	1.2918	6	4.39592	1.5881	19
2200	1.84278	1.11669	6	7.13889	2.31263	6	3.35556	1.29208	6	3.91053	1.31362	19
2300	2.05871	1.10336	6	8.15278	2.59677	6	4	1.16087	6	3.64892	1.18826	19
2400	1.50371	0.66622	6	8.09722	3.57889	6	4.43056	1.16591	6	3.63569	1.26687	19
2500	1.59387	0.85904	6	8.61111	3.23427	6	4.56111	1.0781	6	3.45256	1.30318	19
2600	1.99187	0.78087	6	7.70833	3.09025	6	4.71944	0.98284	6	3.17906	1.30669	19
2700	2.1519	0.74808	6	6.97222	2.61662	6	4.11944	1.16173	6	3.08235	1.28273	19
2800	1.94736	0.69579	6	6.5	2.26393	6	4.23611	1.18495	6	3.10566	1.25849	19
2900	1.8117	0.66184	6	6.94445	2.57081	6	4.66667	1.1967	6	3.18508	1.27465	19
3000	1.96129	0.66761	6	7.69445	2.85947	6	4.23611	1.18787	6	3.27841	1.30767	19
3100	1.97447	0.67754	6	8.71667	3.46931	6	4.61389	1.24496	6	3.42237	1.38964	19
3200	2.15539	0.74992	6	9.18056	2.77836	6	4.41667	1.52487	6	3.30747	1.37574	19
3300	2.12384	0.67528	6	8.09722	1.62511	6	4.73333	1.50216	6	3.16881	1.37526	19
3400	2.01449	0.78773	6	5.91667	1.88347	6	5.98611	1.55313	6	3.16545	1.32095	19
3500	2.65691	0.89682	6	6.59722	2.66076	6	6.42222	1.49333	6	3.40986	1.41475	19
3600	2.97391	0.96603	6	6.18056	1.87838	6	7.47222	2.27826	6	3.65022	1.52923	19
3700	2.6931	1.04678	6	6.58333	2.035	6	7.375	2.21167	6	5.20475	1.81766	19
3800	1.86516	0.71816	6	6.03889	1.56358	6	7.18056	2.49478	6	4.99253	1.70001	19
3900	1.32933	0.85216	6	4.93056	1.7417	6	7.16945	2.33712	6	4.94939	1.79883	19
4000	1.6733	1.22429	6	5.20833	1.82709	6	7.80278	2.47191	6	4.96931	1.90197	19
4100	1.28853	1.07446	6	5.53056	2.41256	6	7.67778	2.73005	6	5.19208	2.20899	19
4200	1.99085	1.18075	6	6.79564	2.08878	6	7.16389	2.96756	6	4.85609	2.09311	19
4300	2.72631	1.44639	6	6.18982	1.89285	6	6.35	2.83681	6	4.64808	1.81764	19
4400	2.79333	1.79865	6	4.60648	2.02125	6	5.9	3.13455	6	4.88203	1.59695	19
4500	2.51345	1.93315	6	4.0537	1.93068	6	6.77778	3.39711	6	4.94689	1.36626	19
4600	4.78237	2.01393	6	3.88611	1.78351	6	5.675	2.70932	6	4.53253	1.17172	19
4700	5.97514	1.80642	6	4.81945	2.43836	6	4.45833	2.31847	6	3.959	1.02707	19
4800	6.1686	1.83425	6	3.58333	2.07825	6	3.68056	1.72898	6	3.74957	0.99821	19
4900	6.44213	1.93096	6	4.5246	2.62235	6	3.75198	1.57936	6	4.00772	0.96465	19

Part 9.2 Distance of hAβ transport in the optic nerve after eye exposure to darkness, darkness with pilocarpine treatment, 1Hz light stimulation, 1Hz light stimulation with atropine treatment

30min dark unstim (μm)	30min 1Hz stim (μm)	30min 1Hz stim+ atropine (μm)	30min dark unstim+ pilocarpine (μm)
191.358	3975.309	555.5556	482.0804
1756.173	1981.481	9.259259	2416.917
1361.111	2104.938	129.6296	918.5586
2243.827	3206.79	2197.531	1338.75
839.5062	2299.383	589.5062	1022.792
1632.716	4567.901	379.6296	648.2027
			211.7245

811.0677
889.2429
1485.329
4413.58
3388.889
2462.963
709.8765
3401.235
2151.235
3388.889
1716.049
3388.889

Part 9.3 Total hAβ signal in the optic nerve after eye exposure to darkness, darkness with pilocarpine treatment, 1Hz light stimulation, 1Hz light stimulation with atropine treatment

30min dark unstim (A.U.)	30min 1Hz stim (A.U.)	30min 1Hz stim+ atropine (A.U.)	30min dark unstim+ pilocarpine (A.U.)
2841.144	40343.54	2686.602	774.337
13867.49	33003.37	3088.446	25632.54
9367.861	14767.07	1701.827	1722.297
11913.5	20571.5	10006.11	3759.509
3197.173	31318.49	6656.685	2040.062
21509.13	28347.37	3773.71	1230.576
			1359.269
			3079.156
			2786.769
			10578.63
			35267.28
			12884.28
			9011.042
			5142.953
			12562.24
			10882.64
			15964.85
			9123.013
			17224.59

Part 9.4 Peak hAβ signal in the optic nerve after eye exposure to darkness, darkness with pilocarpine treatment, 1Hz light stimulation, 1Hz light stimulation with atropine treatment

30min dark unstim (A.U.)	30min 1Hz stim (A.U.)	30min 1Hz stim+ atropine (A.U.)	30min dark unstim+ pilocarpine (A.U.)
17.60641	103.0321	10.72303	12.67347
43.75364	105.8309	2.059767	55.1895
16.50437	46.72012	11.81633	10.65306
36.67638	60.10204	34.03061	14.1035
27.76968	100.2332	30.96939	11.42274
42.3105	53.79009	21.24636	10.65306
			9.918367
			17.81633
			19.38776
			59.73761
			39.16181
			20.16327
			26.02041
			20.22595
			14.42857
			16.1895
			33.31633
			19.9344
			32.80612

Part 10.1 Comparison of pupil variance

Dark	Stim	Stim + Atropine
0.1584	25.024	0.4929
0.7623	16.719	0.0825
0.1878	10.154	0.206

Part10.2 Spectral analysis of pupil response calculated as % of 1Hz band (0.99-1.01Hz) to total power from 0Hz to 5Hz

Dark	Stim	Stim+Atropine

0.125953443	4.782128809	0.200842583
0.149911416	1.47676723	0.179964554
0.150363185	5.385512441	0.149605904
	4.658998555	
	10.88579099	
	2.137049301	

Part10.3 Cumulative pupil change

Dark (mm)	Stim (mm)	Stim+Atropine (mm)
35.21616162	76.37820513	17.98355634
26.85858586	83.94230769	37.85050505
19.01010101	83.68589744	22.08080808
	139.2842713	
	142.3030303	
	74.0040404	

Part 11.1 hAβ signal in the optic nerve of old DBA and its controls

distance from eye (μm)	DBA/2J 3mo (A.U.)			DBA/2J 6mo (A.U.)			DBA/2J 11mo (A.U.)			D2 Ctrl. 11mo (A.U.)		
	mean	SEM	n	mean	SEM	n	mean	SEM	n	mean	SEM	n
0	4.40559	1.122	11	20.3889	3.77737	6	33.4907	13.8699	9	2.68281	0.91119	11
100	34.459	6.62914	11	28.7333	6.40516	6	83.4537	24.1085	9	15.6953	2.89114	11
200	36.8602	6.32285	11	31.1667	8.6992	6	95.3796	21.6733	9	16.5845	3.05478	11
300	34.4059	6.04056	11	22.5167	4.88338	6	97.0259	24.0982	9	14.2077	3.04871	11
400	31.707	5.34111	11	19.7833	6.35937	6	92.3426	23.0634	9	12.5931	2.89367	11
500	28.7463	4.63421	11	17	5.20683	6	89.0926	23.6161	9	11.6603	2.74188	11
600	25.7359	3.93005	11	14.1833	5.10612	6	87.6204	24.2579	9	10.3459	2.39668	11
700	22.8736	3.44498	11	13.1	4.22858	6	85.2037	24.7466	9	9.32155	2.15464	11
800	20.388	2.97648	11	12.1167	2.8974	6	79.4537	25.2984	9	8.7774	2.13137	11
900	18.4065	2.7419	11	10.2667	3.04818	6	75.787	24.6522	9	8.0106	1.99327	11
1000	16.3739	2.52023	11	9.6	2.34945	6	74.2593	26.0852	9	7.5199	1.89152	11
1100	15.323	2.41713	11	9.56667	1.95688	6	64.2037	23.079	9	6.90517	1.96967	11
1200	14.0559	2.24968	11	9.35	2.08333	6	59.6852	21.9864	9	6.56132	1.92588	11

1300	12.8373	2.13803	11	7.58333	2.0874	6	59.3611	21.992	9	6.37642	1.74332	11
1400	11.9593	2.03827	11	6.33333	1.70748	6	54.9722	20.9075	9	5.93148	1.63409	11
1500	10.9278	1.90492	11	5.88333	1.67189	6	53.0944	21.0228	9	5.37918	1.53549	11
1600	10.2706	1.81303	11	5.38333	1.49609	6	52.0074	21.489	9	4.89837	1.59465	11
1700	9.88859	1.64819	11	5.91667	1.26444	6	48.3148	20.277	9	4.48109	1.55694	11
1800	9.20256	1.48759	11	6.3	1.44974	6	46.2445	19.8315	9	4.37208	1.60737	11
1900	8.58009	1.2889	11	6.68333	1.57948	6	45.6111	19.4358	9	4.61931	1.71779	11
2000	8.24782	1.18197	11	7.03333	1.63733	6	41.8796	20.0888	9	4.81807	1.79933	11
2100	8.06587	1.13755	11	6.63333	1.24302	6	38.963	19.2889	9	4.02955	1.5404	11
2200	8.01998	1.29518	11	6.31667	1.38589	6	36.3611	18.5298	9	3.64231	1.39397	11
2300	7.67944	1.29735	11	4.83333	1.71373	6	36.2815	18.1015	9	3.50252	1.34968	11
2400	7.65922	1.52831	11	4.11667	2.14386	6	35.3574	16.5974	9	3.50551	1.19937	11
2500	7.5352	1.85636	11	5.18333	2.73374	6	33.6315	14.5979	9	3.54776	1.19329	11
2600	7.52677	2.03268	11	4.65	2.4182	6	28.0333	12.5994	9	3.7226	1.1934	11
2700	7.32578	1.77335	11	5.13333	2.9114	6	24.9185	10.7403	9	3.77696	1.19447	11
2800	7.15035	1.45828	11	5.48333	3.3047	6	23.3778	10.7766	9	3.93709	1.174	11
2900	6.85035	1.62432	11	4.58333	2.4942	6	21.8148	9.87041	9	3.51358	1.04877	11
3000	6.99386	1.88534	11	4.36667	2.37458	6	20.9593	9.80644	9	3.26152	1.16507	11
3100	7.02051	1.91177	11	3.76667	2.18959	6	17.087	8.12203	9	2.86225	1.10015	11
3200	8.50492	3.03615	11	4.38333	2.87924	6	22.237	9.67609	9	2.31162	0.95866	11
3300	10.4384	4.09651	11	5.71667	3.22077	6	21.9389	9.27274	9	2.00284	0.76985	11
3400	10.5329	3.76376	11	5.96	2.90441	6	21.1093	7.94448	9	1.78759	0.60433	11
3500	10.3935	3.3552	11	4.80667	2.64392	6	22.4407	8.161	9	1.59336	0.55083	11
3600	9.35251	2.53495	11	5.86667	3.84814	6	18.8389	6.97362	9	1.80461	0.72125	11
3700	8.96517	2.41235	11	8.29	5.81206	6	20.3056	7.69492	9	2.03561	0.92679	11
3800	8.56097	2.48816	11	8.63333	6.20251	6	18.0463	6.77723	9	2.06958	0.92343	11
3900	8.65815	2.58993	11	6.96667	4.80671	6	17.1111	6.22972	9	1.73234	0.98261	11
4000	8.29072	2.5568	11	5.25	3.32274	6	15.6556	5.6698	9	1.93827	1.14933	11
4100	8.03411	2.49605	11	3.58	1.89546	6	12.7537	4.98287	9	2.38097	1.42468	11
4200	7.60034	2.33169	11	2.23	1.39705	6	11.4222	4.99564	9	2.5019	1.48264	11
4300	7.27703	2.0955	11	2.2	1.2969	6	14.7926	7.15418	9	3.12017	1.76952	11
4400	7.59442	2.06182	11	2.6	1.28444	6	17.4722	8.14384	9	3.64033	2.0248	11
4500	9.01815	2.30476	11	3.31	1.29536	6	15.487	7.11096	9	4.73202	2.06295	11
4600	10.3983	2.83074	11	4.04	1.47415	6	17.8148	6.10593	9	5.24366	2.21026	11
4700	10.8739	2.79602	11	6.00333	2.11979	6	16.6732	5.15974	9	6.67686	2.19008	11
4800	11.0577	3.2601	11	3.40667	1.92143	6	20.9648	5.15719	9	7.05661	1.98924	11
4900	12.4172	3.92292	11	3.3	1.86277	6	23.6741	6.41736	9	7.14431	1.75548	11

Part 11.2 Distance of hAβ transport in the optic nerve of old DBA and its controls

DBA/2J 3mo (μm)	DBA/2J 6mo (μm)	DBA/2J 11mo (μm)	D2 Ctrl. 11mo (μm)
2519.278	9522.527	9428.789	988.1008

14638.19	9872	22867.57	4192.056
16574.93	28385.17	47367.03	5324.646
19966.39	11086.69	171856.8	1555.774
15890.79	10373.79	22165.38	9266.689
28218.72	1809.901	26244.25	17169.49
19903.31		20683.72	7849.399
23030.07		167617.8	16820.44
23986.59		96802.59	10952.07
18083.13			4151.822
			12062.71

Part 11.3 hAβ signal in the optic nerve of CLS mice and its control

	CD-1 Ctrl (A.U.)			CD-1 CLS (A.U.)		
distance from eyeball (μm)	**mean**	**SEM**	**n**	**mean**	**SEM**	**n**
0	17.655	10.671	7	20.673	10.406	7
100	42.877	7.5833	7	45.124	7.0984	7
200	43.646	7.3529	7	55.589	4.8783	7
300	36.981	7.9493	7	57.079	5.6733	7
400	31.646	8.0406	7	53.373	6.7881	7
500	25.741	7.908	7	48.644	8.1209	7
600	19.599	6.1416	7	43.59	8.624	7
700	14.339	4.7325	7	38.827	9.0969	7
800	10.682	3.6571	7	34.601	9.3115	7
900	8.1892	2.9004	7	30.635	8.8781	7
1000	6.2764	2.2965	7	27.115	8.5249	7
1100	4.9911	1.9487	7	23.62	8.1808	7
1200	4.4343	1.7607	7	21.107	7.4962	7
1300	3.8252	1.5868	7	18.021	6.684	7
1400	3.31	1.3698	7	15.59	5.714	7
1500	2.897	1.2705	7	13.44	4.8709	7
1600	2.6541	1.1676	7	11.734	4.136	7
1700	2.4288	1.1233	7	10.405	3.6469	7
1800	2.167	0.9775	7	8.6353	3.1819	7
1900	2.1335	0.96801	7	6.6955	2.9013	7
2000	2.0146	0.92367	7	6.0989	2.5623	7
2100	1.5179	0.57541	7	5.816	2.2607	7
2200	1.1505	0.44516	7	5.6886	2.1555	7
2300	1.181	0.46505	7	5.4202	2.0914	7
2400	1.2	0.48542	7	5.1665	1.9531	7
2500	1.1652	0.49328	7	4.8367	1.5745	7

2600	1.0388	0.47631	7	4.3681	1.3899	7
2700	1.0195	0.43034	7	4.574	1.4768	7
2800	1.0275	0.44225	7	4.4119	1.2488	7
2900	0.99862	0.43031	7	4.2416	1.172	7
3000	1.0882	0.46404	7	3.9268	0.99297	7
3100	1.0968	0.51181	7	3.8271	0.92957	7
3200	1.1436	0.56211	7	3.8637	0.9661	7
3300	1.1543	0.55025	7	3.9642	1.0353	7
3400	1.1655	0.55991	7	4.2395	1.1603	7
3500	1.2561	0.61198	7	4.0638	1.2395	7
3600	1.3605	0.70895	7	4.262	1.3392	7
3700	1.6534	0.96113	7	4.8699	1.7486	7
3800	1.8665	1.1854	7	5.3718	2.1663	7
3900	1.9588	1.2517	7	5.5715	2.2398	7
4000	2.0613	1.3134	7	5.4736	2.012	7
4100	1.9107	1.1347	7	5.627	1.96	7
4200	1.6257	0.83898	7	5.8001	2.1383	7
4300	1.5684	0.80048	7	5.278	2.2721	7
4400	1.5616	0.70033	7	7.1333	4.4499	7
4500	1.7581	0.79759	7	9.6326	6.8326	7
4600	1.6566	0.68241	7	7.3873	4.6527	7
4700	1.9918	1.0674	7	2.327	1.2795	7
4800	3.294	2.3512	7	2.3941	1.4492	7
4900	3.8234	2.8506	7	2.3934	1.6166	7

Part 11.4 Total hAβ signal in the optic nerve of CLS mice and its control

CD-1 Ctrl (A.U.)	**CD-1 CLS (A.U.)**
6048.279	36061.44
22232.34	27861.33
8093.597	27184.53
13418.36	59071.4
14177.32	16784.59
6748.669	43955.42
32890.63	26976.63

Part 11.5 500kDa Dextran signal in the optic nerve of old DBA and its age matched control

distance from eye (μm)	D2 Ctrl. 11mo (A.U.)			DBA/2J 11mo (A.U.)		
	mean	**SEM**	**n**	**mean**	**SEM**	**n**
0	5.794633	1.71194	9	22.5964	11.9304	6
100	16.45677	4.43643	9	80.2635	30.0653	6
200	14.47449	3.947	9	106.791	33.8262	6
300	11.83754	3.59948	9	118.829	34.2525	6
400	10.70568	3.12503	9	125.431	31.6945	6
500	10.73339	2.95333	9	124.049	28.6515	6
600	10.91138	2.92728	9	116.81	26.6348	6
700	10.69047	2.93033	9	109.236	23.9325	6
800	10.26898	2.88347	9	99.0607	21.8234	6
900	10.02573	2.97885	9	88.543	19.3725	6
1000	9.324422	2.86093	9	82.7714	19.0638	6
1100	9.701027	2.89149	9	77.8231	19.0194	6
1200	10.07966	3.04173	9	73.3011	19.1496	6
1300	10.1952	3.24655	9	66.6046	18.9714	6
1400	10.24246	3.53663	9	62.4111	16.5668	6
1500	10.44739	3.80147	9	53.6943	10.5227	6
1600	10.49373	3.98067	9	48.3527	8.02039	6
1700	10.26608	4.00602	9	44.3066	6.10677	6
1800	9.875813	3.94275	9	42.328	5.19324	6
1900	9.458702	3.74669	9	41.5266	5.31485	6
2000	8.972755	3.58213	9	41.7926	6.42966	6
2100	8.395367	3.38418	9	43.5317	9.09532	6
2200	7.865248	3.08545	9	42.8326	8.99539	6
2300	7.333102	2.82464	9	39.1041	8.60574	6
2400	6.932678	2.52484	9	36.6879	9.34891	6
2500	6.236809	2.37009	9	33.851	9.98599	6
2600	4.846825	2.08143	9	30.435	8.77724	6
2700	4.208311	1.84603	9	28.1736	7.63042	6
2800	3.777844	1.66641	9	27.4214	7.71469	6
2900	3.258463	1.51574	9	27.0784	8.03476	6
3000	3.019343	1.45329	9	27.424	9.52747	6
3100	2.853884	1.37518	9	29.3398	11.0845	6
3200	3.008384	1.50079	9	28.7989	12.5789	6
3300	3.031611	1.5485	9	30.6378	13.1357	6

3400	3.195379	1.55524	9	39.9836	17.4116	6
3500	3.122912	1.5755	9	39.118	15.5982	6
3600	3.201378	1.63785	9	34.1233	10.854	6
3700	3.679333	1.84065	9	31.1444	10.7337	6
3800	3.699778	1.85949	9	33.259	11.0777	6
3900	3.408811	1.70937	9	34.8767	10.6433	6
4000	2.913667	1.46374	9	34.4099	13.3523	6
4100	2.232489	1.14704	9	35.0087	14.7782	6
4200	1.709867	1.00425	9	36.1436	16.079	6
4300	1.419728	0.81013	9	35.9923	17.4052	6
4400	1.752177	0.80055	9	36.1324	14.5635	6
4500	3.144889	0.85563	9	29.7101	11.2919	6
4600	5.676911	1.9407	9	26.353	9.73958	6
4700	5.233622	1.57694	9	20.4399	6.58967	6
4800	7.1779	2.02271	9	18.6726	5.84151	6
4900	9.887478	2.71888	9	17.0506	5.37636	6

Part 11.6 500kDa Dextran signal in the optic nerve of CLS mice and its control

distance from eye (μm)	CD-1 Ctrl			CD-1 CLS		
	mean	SEM	n	mean	SEM	n
0	1.5936	0.7325	6	5.2838	1.8436	7
100	1.4092	0.5274	6	14.707	6.8677	7
200	0.7191	0.4549	6	17.748	8.2902	7
300	0.7553	0.4869	6	18.568	10.085	7
400	0.2865	0.2778	6	12.499	5.151	7
500	0.3332	0.3332	6	11.337	4.8815	7
600	0.2381	0.2381	6	8.7235	3.7985	7
700	0.1876	0.1876	6	6.8487	2.9645	7
800	0.1708	0.1708	6	5.6904	2.6158	7
900	0.0934	0.0934	6	4.7829	2.2011	7
1000	0.085	0.085	6	4.1432	1.9335	7
1100	0.0748	0.0748	6	3.8076	1.7683	7
1200	0.0612	0.0612	6	3.5212	1.6127	7
1300	0.1462	0.1462	6	3.3366	1.5189	7
1400	0.0511	0.0511	6	3.1397	1.4524	7
1500	0	0	6	3.1379	1.4087	7
1600	0	0	6	3.2764	1.4724	7

1700	0	0	6	3.0803	1.4757	7
1800	0	0	6	3.1012	1.5374	7
1900	0	0	6	3.3699	1.7948	7
2000	0	0	6	3.2268	1.7044	7
2100	0	0	6	3.2498	1.672	7
2200	0	0	6	3.3729	1.7033	7
2300	0	0	6	3.4154	1.6808	7
2400	0	0	6	3.3103	1.6641	7
2500	0	0	6	3.2526	1.6619	7
2600	0	0	6	3.2154	1.6284	7
2700	0	0	6	3.1975	1.5287	7
2800	0	0	6	3.0678	1.4102	7
2900	0	0	6	2.9232	1.3403	7
3000	0	0	6	2.8752	1.2831	7
3100	0	0	6	2.8976	1.3262	7
3200	0	0	6	3.0469	1.4258	7
3300	0	0	6	3.2629	1.5172	7
3400	0	0	6	3.745	1.6651	7
3500	0	0	6	3.7257	1.7577	7
3600	0	0	6	3.7013	1.7035	7
3700	0	0	6	3.6805	1.6031	7
3800	0	0	6	3.5666	1.4548	7
3900	0	0	6	3.5612	1.468	7
4000	0	0	6	3.6045	1.5673	7
4100	0	0	6	3.4469	1.6818	7
4200	0	0	6	3.4094	1.6784	7
4300	0	0	6	3.848	1.7412	7
4400	0.0741	0.0741	6	3.7409	1.8075	7
4500	0.1759	0.1759	6	3.5607	1.6704	7
4600	0	0	6	3.5153	1.6199	7
4700	0.0888	0.0564	6	3.2414	1.4421	7
4800	0.4347	0.3176	6	3.1997	1.3853	7
4900	1.256	0.8348	6	3.0746	1.0489	7

Part 11.7 Total signal of different dextran in the optic nerves of two mice glaucoma models and their controls

dextran size	500kDa (A.U.)	500kDa (A.U.)	10kDa (A.U.)	3kDa (A.U.)

glaucoma model	CD-1 Ctrl.	CD-1 CLS	D2 Ctrl. 11mo	DBA/2J 11mo	DBA/2J 3mo	DBA/2J 11mo	D2 Ctrl. 11mo	DBA/2J 11mo
	297.8509	1286.385	1750.731	39558.14	12218.17	34111.7	12233.09	47024.23
	597.8905	1470.588	1301.425	96625.98	8861.764	74216.92	15898.82	56956.74
	110.2935	2301.449	4779.372	35768.63	23284.87	26383.66	4031.583	13037.52
	575.2042	32150.28	2159.71	99617.18	3205.451	31211.09	8480.338	27666.13
	822.9588	776.6968	6134.054	45061		125108	8645.772	22091.63
	79.38021	18583.75	20935.95	145667.9		188591.3	2714.166	76232.88
		22796.74	24730.83			57907.11	2805.363	
			23279.85			173773	13359.23	
			9902.153				8272.484	
							12243.13	

Part 12.1 Total hAβ signal in the optic nerve negatively correlate with RGC number

RGC count (cells/mm^2)	total hAβ fluorescence (A.U.)
2189.775	164523.7
2272.611	56194.5
2602.895	98800.54
3093.75	41760.86
2801.106	57428.18
3183.803	9428.789
3093.75	47367.03
2688.289	22867.57

Part 12.2 Total Dextran signal in the optic nerve dose not negatively correlate with RGC number

RGC count (cells/mm^2)	total AF-dextran fluorescence (A.U.)
3793.945	76236.65
205.8919	131686.5
342.6106	96625.98
59.40755	99617.18
2603.353	145667.9
1970.216	73910.83

Part 13.1 Extracellular space volume fraction in old DBA and control

DBA/2J 11mo

D2 Ctrl. 3mo	
0.1277808	0.05218048
0.04427668	0.0967153
0.08472373	0.1299573
0.09790101	0.100421
0.09346873	0.1555812
0.134136	0.0868948
0.09331937	
0.06992523	
0.05239931	
0.1274201	
0.08516324	
0.1974788	
0.2091909	
0.1230862	
0.08681854	
0.04811665	
0.05762661	
0.1380949	
0.03466598	
0.03530263	

Part 13.2 Extracellular space tortuosity in old DBA and control

D2 Ctrl. 3mo	DBA/2J 11mo
1.139146	1.017529
1.588974	1.353967
1.784764	1.266446
1.818752	1.352141
1.953889	1.524034
1.364635	1.371302
1.833814	
2.127087	
1.581585	
1.797664	
1.533157	
0.9313498	
1.301732	
1.293376	
1.288681	

1.39006
1.417184
1.233522
1.169676
1.421748

Part 14 Quantification of $^{86}Rb^{+}/^{3}H$-mannitol radioactivity in the ipsilateral eye and optic nerve following ICA

Eye ($^{86}Rb/^{3}H$-Mann)	Proximal Optic nerve ($^{86}Rb/^{3}H$-Mann)	Distal Optic nerve ($^{86}Rb/^{3}H$-Mann)
2.333826277	1.837519681	1.470324718
1.95865103	2.203229469	1.092333428
1.922997455	1.435595597	2.220438475
3.501852075	2.992476924	1.655030282
3.487262624	1.488751972	1.442568198
1.987088793	1.372843381	1.350402481
3.290637337	1.958136408	1.842999044

Part 15 Line scans of longitudinal optic nerve images including dura. Data shown are mean fluorescence intensity (AU) for 5 line scans per animal, measuring 25 x 150 μm and collected perpendicular to the optic nerve surface between 300 to 900 μm behind the lamina.

Distance (μm)	C57BL6_1	C57BL6_2	C57BL6_3	C57BL6_4
0.0	105.0284	13.95118	90.0232	81.6736
0.4	109.0716	13.62844	92.1914	84.4294
0.8	106.355	13.65502	88.3448	80.4238
1.1	106.6404	14.13054	87.8928	78.7676
1.5	111.4382	14.62734	88.5332	79.3176
1.9	113.8926	15.1405	84.5132	76.0854
2.3	113.6192	15.61498	86.9014	74.347
2.7	110.8834	15.56708	88.51	75.294
3.0	107.3834	16.05934	86.7452	76.8852
3.4	108.912	16.38906	85.2522	77.1852
3.8	109.2644	16.46062	87.5654	77.5794
4.2	109.8714	16.79242	88.429	77.0884
4.5	108.8216	17.10094	88.2582	76.1824
4.9	106.5282	17.09082	90.2696	76.5058
5.3	105.0668	17.32426	93.5682	75.7206
5.7	108.2832	17.41784	91.516	74.3236

6.1	104.0548	17.38822	91.3654	71.8884
6.4	111.9168	17.166	89.6086	69.5412
6.8	107.538	17.11394	90.6028	64.65
7.2	107.5762	17.40942	90.2494	63.0116
7.6	107.8264	17.55194	90.5304	62.0206
8.0	108.619	18.5586	89.3592	61.2824
8.3	105.7286	19.57584	89.5972	60.691
8.7	107.769	20.78256	89.4928	59.45
9.1	105.5332	20.46104	90.2404	58.5324
9.5	107.8596	19.22914	91.4086	63.903
9.8	104.262	18.81886	88.832	68.103
10.2	102.5642	18.82776	88.8728	67.897
10.6	101.4048	18.08528	91.9564	67.7794
11.0	101.0452	18.78408	87.1854	72.7472
11.4	93.9952	20.03796	89.8956	69.2854
11.7	94.7286	20.97582	93.1536	64.456
12.1	93.7312	20.81364	88.8842	61.8116
12.5	91.938	21.09998	88.7972	60.6088
12.9	89.7024	23.0168	90.423	62.5942
13.3	91.043	21.67416	91.3624	61.8146
13.6	89.2214	20.4313	87.6058	60.347
14.0	90.4644	19.39588	91.2582	59.5824
14.4	90.8928	17.94218	92.0754	59.1912
14.8	87.8286	18.51068	93.9654	55.9294
15.2	89.4574	17.3076	92.003	54.4646
15.5	92.512	16.3227	93.2552	54.1414
15.9	96.7238	16.16608	91.2172	53.094
16.3	100.9644	15.95892	89.2376	52.5588
16.7	100.7978	16.17146	88.7824	52.206
17.0	102.2192	16.4117	88.881	53.1736
17.4	103.3406	16.02224	91.287	55.3384
17.8	102.988	16.41666	89.4608	54.5118
18.2	103.8404	17.1394	85.5998	54.2734
18.6	107.1428	16.43292	86.2116	53.7558
18.9	106.0808	16.59898	87.3562	54.3646
19.3	110.9642	16.45742	90.2376	55.4176
19.7	118.4668	16.05826	89.255	55.1294
20.1	116.0142	15.98956	89.081	55.8294
20.5	112.9952	16.267	86.6522	56.3382
20.8	108.8546	16.2681	84.568	55.8794
21.2	110.0094	16.06972	85.8146	56.559

21.6	108.0568	15.66154	85.0058	56.5708
22.0	105.4096	15.12266	87.1912	55.4912
22.3	108.838	14.9272	86.8694	53.0146
22.7	114.0024	15.99032	85.89	53.6
23.1	110.5382	15.42086	82.971	51.6118
23.5	113.3022	15.25732	83.1392	51.7972
23.9	114.8096	16.56852	86.632	50.7206
24.2	112.9858	16.81542	83.9042	48.194
24.6	115.8356	16.88612	81.8842	48.6236
25.0	110.938	17.20774	80.9912	50.2734
25.4	110.9594	18.33848	80.6058	46.9176
25.8	111.6572	19.5703	78.9944	47.638
26.1	111.4334	21.28376	80.7654	45.6648
26.5	110.0116	22.29308	80.9624	44.3824
26.9	106.1214	24.00782	79.7972	43.9412
27.3	101.4478	23.40554	76.9972	44.953
27.7	99.762	21.94798	78.7012	45.5824
28.0	98.4688	20.07426	76.4202	45.9176
28.4	99.7334	19.9123	76.9942	46.1618
28.8	97.5356	19.20622	77.258	46.8736
29.2	100.538	19.84926	76.6086	45.603
29.5	100.6858	19.38804	76.148	47.4234
29.9	98.3452	17.859	72.9218	47.1558
30.3	97.9192	17.55952	73.7562	48.6646
30.7	98.2762	17.73256	74.9506	48.1648
31.1	99.1308	17.1961	76.3884	48.4588
31.4	96.5192	17.52298	76.1014	49.8676
31.8	96.5524	17.5575	80.287	50.9676
32.2	98.8404	17.7782	81.5652	51.8676
32.6	96.6596	18.17374	80.9972	52.3912
33.0	94.9402	17.81088	78.3102	53.8414
33.3	95.5476	18.25716	77.9856	54.103
33.7	98.3594	18.9735	76.9596	53.8352
34.1	99.6858	20.34598	74.7216	56.1884
34.5	98.493	21.53712	78.2262	56.2882
34.8	101.6474	21.93864	79.1448	55.45
35.2	100.8332	23.22946	78.5798	54.3382
35.6	102.2524	23.20758	76.2376	56.6414
36.0	99.4452	22.7041	74.858	59.653
36.4	97.5952	22.10092	76.226	57.5704
36.7	99.7144	21.59302	77.6318	57.9266

37.1	101.7902	21.16812	75.6146	57.0146
37.5	97.7	20.95696	77.371	57.3882
37.9	99.9618	19.50598	76.1534	58.244
38.3	98.3954	18.97952	77.4262	59.4942
38.6	102.2714	18.70262	78.3854	64.1236
39.0	105.7762	18.48072	77.4318	64.5648
39.4	103.5192	17.97408	77.345	61.4616
39.8	104.1856	17.10284	81.487	60.7502
40.2	101.15	16.57252	85.2838	61.5826
40.5	96.8334	17.0892	87.2322	62.4442
40.9	94.6808	16.97728	85.232	61.35
41.3	93.9572	17.04922	85.6868	61.444
41.7	92.5786	17.3208	83.3218	60.1794
42.0	91.4046	17.33256	84.3968	61.4942
42.4	96.062	16.51018	85.2058	64.5028
42.8	100.8188	16.65532	84.597	67.1794
43.2	104.5212	16.09514	85.9768	66.7824
43.6	104.2716	15.95554	84.994	70.2118
43.9	103.3048	15.15388	84.7186	69.35
44.3	100.6214	15.64578	83.058	70.2852
44.7	97.6882	15.61794	81.7622	69.2118
45.1	98.4312	15.62954	81.455	72.0088
45.5	93.1522	15.40162	81.658	73.5854
45.8	93.7902	15.5899	82.0552	74.8266
46.2	97.8716	15.4191	83.171	74.4382
46.6	99.2668	15.9302	85.061	72.3146
47.0	100.3474	15.91988	84.6524	72.1058
47.4	97.8334	15.8616	85.339	68.3852
47.7	100.9998	15.70454	88.9188	68.447
48.1	102.188	15.40774	87.9158	68.35
48.5	97.95	15.20384	85.6722	69.7442
48.9	96.6832	15.33476	88.1708	72.3704
49.2	94.4738	15.43206	93.1536	72.897
49.6	94.1096	15.193	95.9884	74.4766
50.0	91.9144	15.19428	91.6986	72.147
50.4	90.8214	15.4553	86.8636	71.8444
50.8	88.8786	15.2633	80.255	75.391
51.1	90.905	14.76852	79.6608	78.259
51.5	93.2118	15.06726	80.9448	76
51.9	91.6094	15.28748	80.6434	76.8144
52.3	88.9834	15.22198	81.658	77.5

52.7	88.5738	14.96692	81.2926	80.5292
53.0	86.3166	14.99208	84.6174	81.1794
53.4	83.0546	14.65666	87.6694	80.5588
53.8	82.5428	14.20698	93.287	79
54.2	83.1784	14.42216	96.5828	81.8528
54.5	82.431	13.9888	96.4116	81.056
54.9	86.9784	14.20764	92.1478	78.303
55.3	83.9286	13.85024	90.971	79.5324
55.7	84.2548	13.91438	94.3678	79.4032
56.1	83.2644	13.97174	93.7798	82.3088
56.4	86.269	14.12296	90.235	80.7148
56.8	87.9024	14.0611	84.1594	78.3766
57.2	87.181	14.24286	84.3828	76.7324
57.6	87.9622	14.64672	85.1536	77.3618
58.0	90.9334	13.86404	85.348	76.603
58.3	90.9762	13.59494	83.2348	77.753
58.7	94.0764	13.07376	82.5362	73.503
59.1	93.2572	12.5952	80.977	68.5
59.5	86.874	12.51968	82.7912	70.4
59.9	88.1524	12.82062	81.5566	71.2352
60.2	92.4738	12.78534	79.1478	69.5678
60.6	90.6928	12.65682	74.9856	70.7676
61.0	87.657	12.59016	75.1246	71.244
61.4	89.8904	12.85538	74.5594	72.4352
61.7	88.0262	13.32802	75.9596	73.7678
62.1	83.638	13.31718	74.6724	76.4618
62.5	82.1952	13.3633	76.4984	77.8294
62.9	79.2572	13.04816	77.093	75.8472
63.3	78.5476	13.2707	76.7796	77.2678
63.6	84.943	13.28998	77.4492	79.6294
64.0	85.8736	13.54756	74.5188	80.9498
64.4	85.474	13.58604	79.1826	80.7472
64.8	85.9356	13.86676	78.8172	79.2914
65.2	85.7216	14.33584	77.5886	79.7088
65.5	83.8478	14.6161	77.9766	79.9088
65.9	80.3024	14.96902	77.0492	77.0442
66.3	75.1716	15.49554	78.6086	75.4764
66.7	73.343	16.04602	78.6608	77.0942
67.0	71.0074	15.41448	77.1854	76.8676
67.4	67.0238	16.29392	78.4582	74.45
67.8	67.6716	16.85548	78.974	72.9442

68.2	69.3952	17.59202	79.058	71.2792
68.6	70.9904	18.25872	80.4636	70.0264
68.9	71.7166	19.04646	77.8898	71.2796
69.3	70.4524	19.31986	75.081	70.4352
69.7	71.9548	18.9889	75.6492	68.7118
70.1	73.4144	17.77872	73.997	71.4058
70.5	71.4926	17.7823	75.5218	70.006
70.8	77.643	18.00866	75.7678	67.5618
71.2	80.9286	17.99636	74.2464	70.6676
71.6	79.5212	18.69714	74.0928	68.3234
72.0	79.35	19.11162	75.3362	66.7852
72.4	78.7262	19.30814	77.2434	65.8942
72.7	80.2786	20.46084	77.855	67.697
73.1	81.819	22.34816	76.9684	68.0732
73.5	84.2808	25.25564	79.1624	64.8706
73.9	85.1404	27.04344	77.3506	65.6734
74.2	85.9406	28.57468	77.5566	66.188
74.6	89.0144	26.41052	78.1824	67.294
75.0	84.0144	25.90468	81.1074	67.6674
75.4	84.9096	26.63646	79.8522	66.6382
75.8	88.2548	28.68062	78.2694	65.3588
76.1	84.843	28.50092	78.0928	62.4762
76.5	82.7952	26.16732	78.6	58.9352
76.9	82.5452	25.30362	76.7014	56.85
77.3	81.2	27.84098	76.2406	57.5528
77.7	76.8646	26.7505	77.719	52.944
78.0	72.4858	26.19158	75.9768	54.212
78.4	69.507	26.81564	78.2812	52.4678
78.8	70.3642	29.74394	80.058	54.453
79.2	69.2286	33.4294	76.919	55.8766
79.5	75.4716	37.15632	78.8348	55.4264
79.9	83.031	36.52434	77.2986	52.809
80.3	80.6	37.74216	76.255	51.4616
80.7	80.6714	37.06684	75.4636	50.9826
81.1	77.0358	39.7777	75.629	50.997
81.4	76.6262	42.24906	74.7506	52.1646
81.8	78.7644	44.5463	75.5768	53.7706
82.2	76.4096	45.93738	74.1478	53.2824
82.6	73.5618	47.34242	74.8374	54.706
83.0	75.1882	48.05774	74.1796	53.7708
83.3	71.4286	48.27878	74.2958	54.3852

83.7	69.7836	48.92726	73.3884	54.8852
84.1	74.6046	45.24714	75.0088	53.5058
84.5	72.0714	42.4414	74.1798	52.8266
84.9	69.3336	38.50674	74.7594	54.1086
85.2	68.181	34.34318	73.0406	53.494
85.6	64.6454	32.31834	74.8378	52.6264
86.0	63.4762	32.52472	74.4346	52.5442
86.4	61.743	30.64194	72.1594	53.0238
86.7	62.8834	29.47846	72.3508	51.847
87.1	61.7096	30.12146	72.7738	52.1528
87.5	62.3214	28.54976	73.2868	49.5088
87.9	59.1714	27.93326	74.3244	49.5884
88.3	56.369	29.38062	75.6752	47.6528
88.6	53.8954	33.14528	75.974	45.9234
89.0	54.0452	36.76232	76.7276	46.6852
89.4	53.0548	40.22316	76.2638	44.9472
89.8	54.2548	44.83494	74.0812	44.1618
90.2	55.076	47.6618	74.0782	43.9148
90.5	57.4596	47.90104	73.464	42.2176
90.9	56.4976	47.10312	71.484	38.8764
91.3	56.381	46.38298	72.7596	38.6734
91.7	56.3716	45.15724	73.7592	38.9588
92.0	55.2428	45.28544	72.0694	38.2382
92.4	57.6548	45.8425	72.029	36.497
92.8	59.1548	43.25514	73.0058	34.9144
93.2	61.2122	42.17652	72.8666	35.15
93.6	63.1596	41.60588	72.7534	35.3824
93.9	63.0906	43.25986	75.3972	34.4206
94.3	68.3406	44.80336	74.5132	34.2794
94.7	71.5144	44.79342	72.916	33.9526
95.1	71.7524	43.08442	71.2174	33.5736
95.5	72.2952	42.29966	68.8666	32.6736
95.8	68.0192	42.21464	68.0956	31.594
96.2	64.445	41.82146	67.6116	32.112
96.6	63.0308	41.5655	67.2058	32.7294
97.0	62.324	41.15582	65.8376	33.7412
97.4	58.6976	41.03678	63.0608	32.1412
97.7	53.6262	37.71212	64.6	31.803
98.1	49.0452	30.37626	62.113	32.0558
98.5	45.1692	20.19394	64.3044	31.441
98.9	42.95	16.31178	63.3508	32.1352

99.2	45.769	13.2229	66.6234	31.691
99.6	43.7262	12.07408	67.1914	31.9588
100.0	41.862	11.52508	65.942	31.4088
100.4	42.0908	11.27306	68.0436	31.0174
100.8	42.4954	11.06212	67.8232	31.1382
101.1	39.4524	10.35244	68.4058	31.3178
101.5	41.433	10.90946	67.0812	30.3824
101.9	41.062	10.61808	65.3912	31.3324
102.3	37.843	9.50614	63.6898	29.6766
102.7	35.3998	9.38258	64.1276	29.9324
103.0	33.6806	9.8351	65.0406	29.1204
103.4	34.9476	9.80184	64.6378	28.912
103.8	37	8.82434	63.2088	28.0058
104.2	38.9406	8.35874	63.0174	28.6354
104.5	39.1714	8.2006	62.2204	29.9588
104.9	38.7192	9.42274	62.096	30.038
105.3	37.4644	10.82944	62.6026	29.5912
105.7	37.3334	10.88728	61.5102	30.056
106.1	38.4236	13.074	61.058	30.141
106.4	37.9642	17.04022	63.3796	31.153
106.8	38.5618	20.86112	63.6638	31.9556
107.2	39.2596	22.8254	63.9564	31.3384
107.6	41.2952	26.91456	64.835	31.9532
108.0	43.4334	25.4953	64.4174	34.1826
108.3	43.6834	22.06306	65.7276	36.1796
108.7	44.3332	23.3637	65.2576	33.644
109.1	45.4978	23.19452	65.1972	33.0502
109.5	43.9644	23.05496	65.7856	34.5766
109.9	45.5498	20.80236	65.487	34.2118
110.2	44.0476	21.09014	67.035	32.1352
110.6	44.1832	20.93934	66.4754	31.903
111.0	49.6026	20.32198	67.1132	29.9706
111.4	51.3692	21.5701	71.0668	29.953
111.7	50.557	22.7766	71.5594	31.25
112.1	47.3978	22.70512	76.6348	33.5502
112.5	47.9144	24.6872	81.7216	30.4762
112.9	44.231	24.79806	84.5538	29.8822
113.3	39.7784	25.18946	85.484	28.244
113.6	40.3168	27.38496	84.339	28.4118
114.0	38.793	28.6626	85.539	29.5032
114.4	41.3738	30.65284	88.545	28.5912

114.8	40.6142	30.59846	92.2812	27.9146
115.2	38.5024	31.11424	94.2378	26.5794
115.5	42.269	28.9382	94.1246	25.7324
115.9	44.2738	30.33872	97.9276	25.9794
116.3	43.7168	34.00144	97.5592	25.4264
116.7	42.5714	36.46238	98.2262	25.6588
117.0	43.9406	34.91114	98.8638	24.5176
117.4	45.4476	34.23196	98.7594	24.2118
117.8	45.2214	35.28998	96.3712	24.3914
118.2	44.8666	39.68848	97.7508	24.956
118.6	46.4452	42.0208	100.1188	25.8438
118.9	48.8096	44.878	99.8144	26.3768
119.3	50.6332	46.47028	96.991	27.697
119.7	54.7476	44.18914	99.1798	31.4972
120.1	54.8192	43.34664	99.6784	32.7942
120.5	55.4642	45.6011	101.5216	33.9648
120.8	58.5452	48.24478	104.09	33.3676
121.2	60.6908	50.0319	104.9508	35.1
121.6	67.6454	50.5485	107.693	41.1178
122.0	72.4332	51.71516	106.4666	44.6794
122.4	71.3214	52.0314	107.2262	49.6794
122.7	72.8952	52.2208	108.6058	55.156
123.1	70.7666	53.36534	109.7856	63.5794
123.5	71.2262	52.0261	111.1998	67.2618
123.9	73.1238	51.16514	112.8724	70.744
124.2	74.3762	50.34486	115.2956	68.5292
124.6	82.1476	49.62056	119.1272	75.3588
125.0	87.6378	48.46002	121.4578	81.7706
125.4	98.1094	47.3155	122.1564	94.3322
125.8	98.8096	46.60002	123.4	100.1882
126.1	105.3286	44.3069	124.4316	112.55
126.5	110.1428	41.29234	125.1884	119.556
126.9	113.1378	39.58562	128.229	123.8884
127.3	121.8548	39.9064	133.3276	129.4528
127.7	132.9094	38.57298	136.0204	136.5502
128.0	141.033	36.23368	140.194	137.244
128.4	152.0454	33.18974	142.0406	141.4646
128.8	168.0928	31.63806	146.9478	156.95
129.2	182.731	30.0575	141.6782	159.4
129.5	186.9666	30.15244	145.9248	164.4972
129.9	188.1524	28.4946	149.7364	159.2676

130.3	189.3714	27.8095	147.0174	160.3736
130.7	188.0238	27.4554	146.49	164.7588
131.1	186.95	28.5111	147.3044	172.5088
131.4	184.2714	25.66876	145.3624	177.356
131.8	181.631	23.55446	148.8462	183.4766
132.2	174.8218	21.24674	147.9302	191.2706
132.6	174.6474	21.01944	147.942	183.4
133.0	163.3094	20.76162	149.6638	173.1794
133.3	161.1404	21.93862	149.771	167.2498
133.7	154.2286	21.8488	146.4264	168.1352
134.1	144.05	21.21238	144.374	165.6764
134.5	134.3548	19.85136	144.9538	171.953
134.9	126.2692	19.75826	145.258	171.612
135.2	114.7476	18.4377	149.971	156.9204
135.6	99.1548	17.51668	150.0956	149.5822
136.0	82.9	16.48108	147.8668	151.5148
136.4	67.588	15.9884	146.6668	146.8234
136.7	56.1478	16.42188	146.168	147.659
137.1	48.4312	15.85538	145.5302	149.4618
137.5	40.9546	15.16542	146.6028	144.8088
137.9	34.295	15.86782	139.7188	136.9002
138.3	27.0834	13.70488	138.7334	129.559
138.6	22.2976	12.2047	133.7596	92.65182
139.0	16.5692	11.54436	125.8116	87.79602
139.4	14.5952	11.11464	118.9884	85.2506
139.8	12.524	10.1777	110.1536	74.279
140.2	12.7404	9.12644	95.1566	63.1446
140.5	12.6166	8.73804	76.0838	58.1657
140.9	12.1022	8.4548	67.0378	52.79816
141.3	12.1214	8.23248	58.3216	43.91786
141.7	12.3712	7.91	52.2782	40.6128
142.1	12.0382	7.6836	46.8406	36.94572
142.4	12.1168	7.32626	43.7422	30.34688
142.8	11.8284	7.44174	41.7594	21.14808
143.2	11.7788	7.18182	39.1536	19.01916
143.6	11.7146	7.2111	36.0608	18.0727
143.9	11.6286	7.36976	35.571	14.37674
144.3	11.7574	7.35574	33.6606	10.73142
144.7	11.2428	7.59452	31.0898	9.07582
145.1	11.9476	7.48618	31.2002	9.12946
145.5	11.5404	7.52188	30.4868	9.06338

145.8	12.5072	7.58738	29.11	9.07032
146.2	11.5046	7.49908	28.3594	10.50158
146.6	11.4904	7.65716	28.8058	11.17768
147.0	12.0454	7.48038	29.548	11.167
147.4	11.6286	7.10396	29.5132	10.6558
147.7	12.4262	7.04462	30.09	10.2506
148.1	11.6688	7.06632	31.5914	7.9604
148.5	11.738	6.86566	32.3336	7.7222
148.9	11.426	7.0926	32.774	8.015
149.2	11.9382	6.99338	29.887	8.1766
149.6	12.2738	7.92246	29.855	8.1034
150.0	11.5476	8.46438	27.9824	5.9722

Part 16.1 GFAP signal in the hAβ tracer administered eye and the vehicle administered eye

vehicle (% of retina area)	hAβ (% of retina area)
0.029200603	0.027736545
0.092910995	0.054939994
0.049066218	0.03657289
0.045503533	0.028333721
0.037599918	0.029142266
0.053320964	0.083719404
0.031855022	0.06142869
0.037608486	0.031592457
0.022088042	0.035283
	0.041679956
	0.036097131

Part 16.2 Evan's blue signal in the hAβ tracer administered eye and the vehicle administered eyes (normalized to vehicle)

30min after infusion		120min after infusion	
vehicle	hAβ	vehicle	hAβ
1.37238	1.06161	1.112603	0.910407
0.926898	0.921323	0.79275	1.010161
0.700722	0.923077	1.126363	0.639452
		0.968283	0.608666

Part 17.1 Cell uptake of hAβ in the retina

% RBPMS+ cells that uptake hAβ tracer	% AP2α+ cells that uptake hAβ tracer

25.8658	6.973702
33.7168	34.33214
47.6522	44.89005
24.6013	17.0649
57.6307	33.86445
58.2292	38.69092
37.4314	13.0415

Part 17.2 Glial uptake of hAβ in the optic nerve (observation was treated as biological replicate)

% Olig2+ glia that uptake hAβ tracer	% Glt1+ glia that uptake hAβ tracer
7.142857	22.22222
12.5	14.28571
3.703704	37.5
69.23077	17.85714
50	
33.33333	
64.70588	
58.82353	
53.33333	
30	
30	
53.33333	

Part 18 IOP following intravitreal hAβ administration in rat

time (min)	rat 1 (mmHg)	rat 2 (mmHg)	rat 3(mmHg)
0	10	10.66667	10.66667
5	8.25	10.66667	12
7	9	8.666667	9
9	8.666667	10	8.666667
11	8.666667	8	7
12	8	8.666667	9
37	8	9	8.333333

Part 19.1 hAβ signal in the optic nerve of rat with and without light stimulation

distance from the eye (mm)	dark unstim (A.U.)			1Hz stim (A.U.)		
	mean	**SEM**	**n**	**mean**	**SEM**	**n**
0	1.26027	0.60592	5	2.56271	0.81244	7
207.414	4.22402	1.29111	5	14.6156	2.66013	7
414.828	3.23298	1.13895	5	15.3052	2.66085	7
622.242	2.58078	1.1001	5	12.9148	2.13649	7
829.657	2.32017	1.05452	5	11.2075	1.95131	7
1037.07	2.44704	1.05146	5	9.90833	1.60655	7
1244.49	2.41914	1.05461	5	7.89347	1.0786	7
1451.9	2.29956	1.03521	5	6.95113	1.03451	7
1659.31	2.0702	0.98364	5	6.26637	1.01953	7
1866.73	2.50864	1.12907	5	6.50141	1.07086	7
2074.14	2.329	1.05869	5	6.49794	1.07652	7
2281.56	1.96584	1.03167	5	5.98419	1.10027	7
2488.97	2.42866	1.16601	5	6.02171	1.1757	7
2696.38	2.26754	1.15892	5	5.87861	1.12671	7
2903.8	1.98352	0.98309	5	5.56136	1.12245	7
3111.21	2.3424	1.02704	5	5.71583	1.15415	7
3318.63	2.42266	1.00365	5	5.79499	0.99625	7
3526.04	2.3686	1.02939	5	5.45141	0.99195	7
3733.45	2.60436	1.11758	5	5.08997	0.86684	7
3940.87	2.59082	1.09222	5	4.98196	0.96135	7
4148.28	1.93902	0.83811	5	4.36652	0.87929	7
4355.7	1.70598	0.73995	5	3.88835	0.82681	7
4563.11	1.47586	0.62209	5	4.06977	0.9838	7
4770.53	1.28584	0.54122	5	3.99333	1.02571	7
4977.94	1.81146	0.75992	5	4.37358	1.04755	7
5185.35	1.60058	0.7071	5	3.64102	1.00442	7
5392.77	1.1989	0.57541	5	3.2226	1.05594	7
5600.18	0.89942	0.36776	5	2.87479	1.02108	7
5807.6	1.37516	0.58972	5	3.06467	0.93532	7
6015.01	1.51257	0.80014	5	2.93158	0.95416	7
6222.42	1.55214	0.75272	5	3.49062	1.07409	7
6429.84	1.66412	0.74061	5	3.42909	1.13613	7
6637.25	1.41612	0.59419	5	3.25519	1.06268	7
6844.67	1.31602	0.57538	5	2.95994	1.09558	7
7052.08	1.4206	0.59423	5	3.26471	1.19878	7
7259.49	1.2404	0.50736	5	3.25424	1.08398	7
7466.91	1.38866	0.74817	5	3.21063	0.81306	7

7674.32	1.74572	0.76319	5	2.68181	0.71914	7
7881.74	0.94407	0.69825	5	2.24824	0.811	7
8089.15	0.41474	0.41474	5	1.93549	0.70301	7
8296.57	0.56266	0.56266	5	2.22613	0.79188	7
8503.98	1.03207	0.51273	5	2.81718	0.82167	7
8711.39	1.0386	0.49639	5	3.68766	1.40553	7
8918.81	1.03723	0.64935	5	3.7887	1.61159	7
9126.22	1.07652	0.62457	5	3.74413	1.694	7
9333.64	1.58617	0.95277	5	4.57981	2.34382	7
9541.05	2.80558	1.5656	5	4.33162	2.13545	7
9748.46	5.6651	2.93251	5	3.50764	1.61028	7
9955.88	6.51488	2.9049	5	3.76832	1.64718	7
10163.3	5.90432	2.50277	5	3.96303	1.91804	7

Part 19.2 Distance of hAβ signal transportation in the optic nerve of rat with and without light stimulation

dark unstim (μm)	1Hz stim (μm)
695.8783	2783.513
601.2929	1236.366
1466.074	5087.343
648.5856	6965.539
3026.733	6965.539
	3337.513
	3763.148

Part 19.3 Total hAβ signal in the optic nerve of rat with and without light stimulation

dark unstim (A.U.)	1Hz stim (A.U.)
13.441	8312.735
4092.786	2250.463
5647.269	7818.696
252.9344	11524.03
6044.834	9313.169
	5018.664
	9447.185

Part 19.4 Peak hAβ signal in the optic nerve of rat with and without light stimulation

dark unstim (A.U.)	1Hz stim (A.U.)
0.002624	17.60641
6.274052	11.24781
8.895044	32.19388
4.78863	15.53936
6.702624	17.98834
	20.95481
	10.3863

Part 20.1 The impact of infusion rate on hAβ transportation

0.2ul/min (A.U.)	0.035ul/min (A.U.)
0.579009	1.039977
2.160404	1.089935
1.482565	1.950244
1.880863	1.438731
0.497498	1.020291
3.432623	0.361221
0.056173	
0.164478	
0.145756	
0.578946	
0.021684	

Part 20.2 The impact of infusion volume on hAb transportation

1.0 μl (A.U.)	0.3 μl (A.U.)
0.181931	1.039977
0.532709	1.089935
0.472072	1.950244
1.875077	1.438731
0.07023	1.020291

3.489411 0.361221
0.37857

Part 21.1 hAβ signal in the optic nerve of mice exposed to darkness during 15min, 30min, 60min or 120min experiment time

distance from eye (μm)	15min dark unstim (A.U.)			30min dark unstim (A.U.)			60min dark unstim (A.U.)			120min dark unstim (A.U.)		
	mean	SEM	n	mean	SEM	n	mean	SEM	n	mean	SEM	n
0	17.146	4.4992	4	11.333	2.5894	6	14.972	3.3475	6	10.033	3.9118	6
100	18.188	3.3903	4	30.583	5.7798	6	31.917	5.2234	6	48.95	9.0687	6
200	14.813	2.7994	4	24.264	5.3545	6	37.361	5.5563	6	56.683	11.534	6
300	12.729	2.908	4	23.569	4.3372	6	38.139	4.7974	6	58.933	10.986	6
400	12.021	3.5707	4	20.486	4.6926	6	35.694	5.157	6	55.617	10.98	6
500	10.313	3.5998	4	18.278	4.0759	6	32	4.9974	6	46.1	7.1178	6
600	7.6042	3.5782	4	15.722	3.3764	6	25.436	4.2142	6	43.667	6.68	6
700	7.3958	6.2536	4	12.583	2.6105	6	22.744	3.8995	6	42.917	6.6343	6
800	6.3958	6.3069	4	11.403	1.7975	6	19.833	2.9884	6	40.967	5.9021	6
900	6.9375	6.1294	4	10.514	1.4532	6	18.353	2.5463	6	35.75	5.2388	6
1000	6.4792	7.7055	4	8.8472	1.4784	6	16.667	2.6062	6	33.607	4.727	6
1100	6.625	9.5959	4	8.3194	1.1594	6	14.603	1.8687	6	30.71	3.9462	6
1200	6.1875	11.52	4	7.325	1.1564	6	13.511	2.3075	6	26.827	3.4563	6
1300	6.4375	12.209	4	7.1	1.1526	6	11.994	2.3721	6	23.917	3.4078	6
1400	4.9792	9.0147	4	6.6361	0.9249	6	11.164	2.6731	6	22.983	2.5752	6
1500	4.0625	8.3452	4	6.1306	1.1203	6	10.608	2.7297	6	20.767	1.8521	6
1600	3.3542	8.6831	4	5.1333	1.0098	6	9.3972	2.5311	6	15.833	2.0721	6
1700	3.0833	8.0036	4	4.9306	0.7374	6	9.2722	2.5799	6	15.633	2.0712	6
1800	3.0208	7.7056	4	4.7528	0.9571	6	8.8333	2.5747	6	13.3	1.5009	6
1900	2.8125	7.24	4	4.4083	1.0662	6	8.8056	2.6517	6	14.683	2.3524	6
2000	2.3542	6.1469	4	4.2917	1.0048	6	8.525	2.3533	6	13.883	2.243	6
2100	2.6458	5.6112	4	4.5472	1.2918	6	8.7861	1.958	6	12.15	1.0853	6
2200	2.2292	4.5959	4	3.3556	1.2921	6	6.7333	1.7928	6	11.817	1.4024	6
2300	2.9792	3.8077	4	4	1.1609	6	6.2417	1.5962	6	11.533	1.5625	6
2400	3.6042	3.0754	4	4.4306	1.1659	6	5.9	1.8573	6	12.017	1.823	6

2500	2.0208	2.0469	4	4.5611	1.0781	6	5.1111	1.9301	6	12.417	2.0097	6
2600	2	1.578	4	4.7194	0.9828	6	5.3944	2.1396	6	9.8167	1.7476	6
2700	1.9792	1.3381	4	4.1194	1.1617	6	6.6194	2.6647	6	9.75	1.6894	6
2800	1.6167	0.6274	4	4.2361	1.1849	6	6.2417	2.7097	6	10.1	2.4969	6
2900	2.2083	1.2306	4	4.6667	1.1967	6	6.175	2.7812	6	11.117	2.9461	6
3000	2.5089	1.3356	4	4.2361	1.1879	6	6.15	2.1567	6	11.217	3.9577	6
3100	2.9653	2.0564	4	4.6139	1.245	6	6.5417	2.0289	6	10.417	4.1463	6
3200	5.0417	3.382	4	4.4167	1.5249	6	6.175	1.9982	6	9.75	4.6954	6
3300	6.5972	3.7977	4	4.7333	1.5022	6	5.2694	1.8551	6	9.35	4.2356	6
3400	7.9722	4.5875	4	5.9861	1.5531	6	3.7194	1.3663	6	9.65	4.7695	6
3500	9.5417	5.1107	4	6.4222	1.4933	6	3.7944	1.3994	6	7.3	4.0501	6
3600	8.4653	4.525	4	7.4722	2.2783	6	3.4722	1.0547	6	9.0667	4.7992	6
3700	7.5625	3.9878	4	7.375	2.2117	6	2.6306	1.0798	6	6.8833	3.7033	6
3800	8.625	4.901	4	7.1806	2.4948	6	1.3667	0.9086	6	5.5	3.4065	6
3900	8.8125	5.4678	4	7.1694	2.3371	6	1.4167	0.857	6	5.45	3.4719	6
4000	6.9722	3.896	4	7.8028	2.4719	6	1.6083	0.9427	6	4.7167	3.0634	6
4100	4.1458	2.0405	4	7.6778	2.7301	6	1.8417	1.1206	6	5	3.5853	6
4200	1.7444	0.7213	4	7.1639	2.9676	6	1.8	1.1212	6	4.55	3.4372	6
4300	1.5042	1.0112	4	6.35	2.8368	6	2.0083	1.0633	6	4	2.6624	6
4400	1.5	1.3416	4	5.9	3.1345	6	1.95	0.9374	6	6.2514	3.6937	6
4500	1	0.8944	4	6.7778	3.3971	6	2	0.7391	6	7.8605	4.6094	6
4600	1.4167	1.2671	4	5.675	2.7093	6	1.7694	0.6944	6	8.23	4.3531	6
4700	1.25	1.118	4	4.4583	2.3185	6	1.9833	0.8381	6	10.361	4.4802	6
4800	1.1667	1.0435	4	3.6806	1.729	6	1.6667	0.9105	6	9.861	3.2855	6
4900	1.6667	1.4907	4	3.752	1.5794	6	1.5333	0.7245	6	10.35	3.2824	6
5000	0.6042	0.5404	4	3.7877	1.2673	6	1.2167	0.5536	6	15.698	4.6301	6

Part 21.2 hAβ signal in the optic nerve of mice exposed to 1Hz light stimulation during 15min, 30min, 60min or 120min experiment time

distance from eye (µm)	**15min 1 Hz stim (A.U.)**			**30min 1Hz stim (A.U.)**			**60min 1Hz stim (A.U.)**			**120min 1Hz stim (A.U.)**		
	mean	**SEM**	**n**	**mean**	**SEM**	**n**	**mean**	**SEM**	**n**	**mean**	**SEM**	**n**
0	12.611	3.3481	3	17.542	5.7742	6	14.94	4.2609	8	22.607	16.696	7
100	22.722	8.5695	3	53.153	7.7127	6	54.905	11.219	8	41.881	33.285	7
200	17.056	5.5617	3	63.861	8.4135	6	53.94	10.598	8	41.893	30.315	7
300	15.722	4.9616	3	66.069	7.4279	6	46.455	8.4517	8	38.571	28.79	7
400	14.778	4.7947	3	66.097	9.6042	6	44.602	8.347	8	38.131	31.489	7

500	13.444	4.3957	3	58.931	9.4495	6	40.679	7.4789	8	36.774	31.234	7
600	11.972	4.0791	3	55.694	10.18	6	35.738	7.0597	8	31.512	22.777	7
700	11.278	3.9425	3	49.558	9.9811	6	31.198	6.159	8	30.06	22.288	7
800	11.556	3.6474	3	40.969	9.1822	6	27.381	5.4651	8	27.238	19.514	7
900	11.278	3.1464	3	32.086	7.1441	6	22.512	4.6102	8	24.167	17.474	7
1000	11.194	3.3388	3	26.95	6.1608	6	19.836	3.9844	8	20.907	15.013	7
1100	10.111	2.8904	3	23.092	5.1383	6	17.94	3.9377	8	23.014	19.243	7
1200	10.667	2.7195	3	19.325	3.7597	6	17.043	3.8966	8	21.795	18.773	7
1300	10.222	2.5545	3	17.236	3.0052	6	15.943	3.6144	8	18.214	15.514	7
1400	9.0278	2.4002	3	15.028	2.6668	6	14.921	3.4419	8	16.905	14.574	7
1500	8.3333	2.2278	3	13.403	2.4598	6	13.49	3.0698	8	14.786	12.481	7
1600	8.75	2.4441	3	10.944	2.8918	6	12.979	3.3741	8	14.44	11.148	7
1700	6.2667	2.0379	3	10.222	3.0866	6	12.405	3.4874	8	13.479	10.926	7
1800	5.7278	2.3099	3	8.8472	2.7917	6	12.731	3.2933	8	13.924	10.776	7
1900	3.9556	2.0147	3	7.8472	2.4762	6	12.19	3.2412	8	15.655	18.032	7
2000	3.5778	2.5431	3	8.0278	2.3293	6	12.145	3.2948	8	15.702	20.939	7
2100	4.4722	2.6554	3	7.8333	2.5475	6	11.2	3.312	8	15.393	21.018	7
2200	4.5278	2.6985	3	7.1389	2.3126	6	10.181	3.2715	8	13.964	16.533	7
2300	5.5	2.323	3	8.1528	2.5968	6	9.131	3.1746	8	10.381	9.7885	7
2400	5.6667	1.9031	3	8.0972	3.5789	6	8.6	3.0452	8	8.5238	7.278	7
2500	4	1.5264	3	8.6111	3.2343	6	8.2571	2.4995	8	9.369	7.194	7
2600	3.6389	1.0966	3	7.7083	3.0903	6	8.4786	2.7129	8	9.4762	7.2543	7
2700	3.4722	1.1544	3	6.9722	2.6166	6	7.9429	2.3388	8	10.679	8.3028	7
2800	3.2778	0.8959	3	6.5	2.2639	6	7.7238	2.4952	8	9.2143	6.7539	7
2900	3.4722	1.0225	3	6.9444	2.5708	6	8.6929	2.8332	8	11.31	8.8523	7
3000	3.0556	1.1077	3	7.6944	2.8595	6	9.8548	2.9326	8	8.6905	8.4055	7
3100	3.3333	0.8898	3	8.7167	3.4693	6	10.143	3.8943	8	9.5238	8.793	7
3200	3.9444	1.1609	3	9.1806	2.7784	6	9.6976	4.0772	8	9.1786	9.7251	7
3300	3.6667	1.0035	3	8.0972	1.6251	6	10.293	4.1049	8	8.2976	8.343	7
3400	4.5556	1.0889	3	5.9167	1.8835	6	9.2762	3.6707	8	8.0714	8.3188	7
3500	4.6389	1.4753	3	6.5972	2.6608	6	8.4238	2.8973	8	6.6333	5.6464	7
3600	5.0278	3.0141	3	6.1806	1.8784	6	8.6429	3.2615	8	6.25	6.0538	7
3700	5.3611	2.3105	3	6.5833	2.035	6	7.4429	2.7434	8	7.2891	5.8754	7
3800	5.6944	2.0377	3	6.0389	1.5636	6	5.6595	2.0721	8	6.7798	5.1922	7
3900	5.7222	2.2393	3	4.9306	1.7417	6	5.6833	1.7867	8	6.4071	4.9238	7
4000	5.5722	2.1346	3	5.2083	1.8271	6	4.8643	1.7989	8	7.6095	5.9545	7
4100	6.0111	2.6575	3	5.5306	2.4126	6	4.0905	1.7936	8	6.6115	4.8005	7
4200	5.2944	2.1427	3	6.7956	2.0888	6	4.0143	1.4036	8	7.04	4.4115	7
4300	2.7833	2.0875	3	6.1898	1.8929	6	4.7357	1.3739	8	5.2262	4.8804	7
4400	1.3333	1	3	4.6065	2.0213	6	4.4762	1.3683	8	4.6758	4.8381	7

4500	3.7667	1.6864	3	4.0537	1.9307	6	5.0262	1.5988	8	4.4198	6.6406	7
4600	5.1167	2.372	3	3.8861	1.7835	6	5.0667	1.7676	8	3.88	6.3409	7
4700	5.1333	2.6875	3	4.8194	2.4384	6	3.4422	1.6599	8	3.2452	4.2917	7
4800	7.4222	3.9128	3	3.5833	2.0782	6	4.8435	1.9084	8	3.6571	6.0817	7
4900	8.5556	3.8512	3	4.5246	2.6223	6	3.6744	2.1984	8	3.701	7.1355	7
5000	10.778	4.0009	3	3.9744	2.6163	6	5.5167	3.1314	8	3.2627	4.9824	7

Part 21.3 Distance of hAβ signal transport in the optic nerve of mice exposed to darkness or 1Hz light stimulation during 15min, 30min, 60min or 120min experiment time, or postmortem at 120min

15min dark unstim (μm)	15min 1Hz light stim (μm)	30min dark unstim (μm)	30min 1Hz light stim (μm)	60min dark unstim (μm)	60min 1Hz light stim (μm)	120min dark unstim (μm)	120min 1Hz light stim (μm)	120min post mortem (μm)
1370.37	157.4074	191.358	3975.309	1638.889	3956.79	2962.963	438.2716	253.0864
716.0494	1787.037	1756.173	1981.481	2123.457	3972.222	3271.605	2070.988	586.4197
2151.235	558.642	1361.111	2104.938	4413.58	2719.136	3404.321	2472.222	604.9383
61.72839		2243.827	3206.79	3432.099	4586.42	3188.271	4166.667	
		839.5062	2299.383	3271.605	1703.704	953.7037	777.7778	
		1632.716	4567.901	2259.259	1700.617		4447.531	
				1780.864	2182.099		4265.432	
					1814.815			

Part 21.4 Total hAβ signal in the optic nerve of mice exposed to darkness or 1Hz light stimulation during 15min, 30min, 60min or 120min experiment time, or postmortem at 120min

15min dark unstim (A.U.)	15min 1Hz light stim (A.U.)	30min dark unstim (A.U.)	30min 1Hz light stim (A.U.)	60min dark unstim (A.U.)	60min 1Hz light stim (A.U.)	120min dark unstim (A.U.)	120min 1Hz light stim (A.U.)	120min post mortem (A.U.)
18788.57	7967.075	2841.144	40343.54	10521.45	37301.63	19401.54	7432.04	2033.294
4392.827	15575.83	13867.49	33003.37	13918.13	101294	20274.12	13352.75	9244.315
9891.681	11552.36	9367.861	14767.07	15633.34	11073.33	33132.85	33566.59	8215.813
4636.162		11913.5	20571.5	33790.33	41521.48	26650.14	28331.93	
		3197.173	31318.49	20507.41	14491.83	10202.56	3370.983	
		21509.13	28347.37	8730.973	12993.17	54388.73	50845.58	
				23322.8	28588.91		43074.52	
					18889.35			

Part 21.5 Peak hAβ signal in the optic nerve of mice exposed to darkness or 1Hz light stimulation during 15min, 30min, 60min or 120min experiment time, or postmortem at 120min

15min dark unstim (A.U.)	15min 1Hz light stim (A.U.)	30min dark unstim (A.U.)	30min 1Hz light stim (A.U.)	60min dark unstim (A.U.)	60min 1Hz light stim (A.U.)	120min dark unstim (A.U.)	120min 1Hz light stim (A.U.)	120min post morten (A.U.)
22.5656	13.12245	17.60641	103.0321	39.24198	89.94169	41.12974	10.793	6.153061
25.49563	22.12099	43.75364	105.8309	39.47522	233.6006	33.62245	28.99417	11.9898
32.60204	45.11662	16.50437	46.72012	33.11224	20.22595	94.02332	85.67056	11.96501
24.08892		36.67638	60.10204	69.69388	118.7755	61.12245	59.56268	
		27.76968	100.2332	49.19825	37.72595	35.97668	22.70408	
		42.3105	53.79009	28.73178	42.3105	97.2449	71.89504	
				79.65015	79.41691		94.60641	
					58.33819			

Part 21.6 hAβ temperal kinetics

time (min)	dark unstim (μm)			1Hz light stim (μm)			postmortem (μm)		
	mean	SEM	n	mean	SEM	n	mean	SEM	n
15	1074.8	447.32	4	834.36	400.26	3			
30	1337.4	296.99	6	3022.6	438.89	6			
60	2702.8	387.19	7	2829.5	415.46	8			
120	2745.9	372.71	6	2662.7	634.4	7	481.48	114.32	3

Part 21.7 Peak location of hAβ signal in the optic nerve of mice exposed to darkness or 1Hz light stimulation during 15min, 30min, 60min or 120min experiment time (ANOVA P =0.9259, mean = 274, SEM = 20.4)

15min dark unstim (μm)	15min 1Hz light stim (μm)	30min dark unstim (μm)	30min 1Hz light stim (μm)	60min dark unstim (μm)	60min 1Hz light stim (μm)	120min dark unstim (μm)	120min 1Hz light stim (μm)
709.87654	166.667	219.136	345.679	388.889	175.926	262.346	345.67901
101.85185	506.173	305.556	345.679	314.815	570.988	540.123	345.67901
89.506173	145.062	175.926	283.951	422.84	132.716	345.679	388.88889
37.037037		388.889	358.025	293.21	101.852	101.852	314.81481
		132.716	345.679	271.605	154.321	262.346	166.66667
		336.42	324.074	228.395	185.185	185.185	101.85185
				175.926	358.025		154.32099
					262.346		

Part 22.1 Rebound tonometry detected ΔIOP in response to light stimulation (normalized to dark unstim group)

Dark unstim	1Hz light stim	1Hz light stim+1% atropine
0.9491525	1.220339	1.142857
0.6447368	0.7640449	0.875
0.8514493	0.6761905	1.413462
1.342105	0.8607595	0.9518
1.017857	0.8607595	1.21875
1.149123	0.482192	1.028571
0.819444	0.668605	1.041667
1.096774	0.942222	0.854545
1.457143	0.892857	0.816327
1.040541	0.8	0.9955
1.057143	0.709302	0.823529
1	0.779874	0.740741
0.537313	0.584615	
1.6	1.017544	1.115385
1.222222	0.787879	0.875

Part 22.2 Intracameral tonometry detected ΔIOP in response to light stimulation (baseline IOP subtracted)

dark unstim	1Hz light stim
-0.124	-1.4674
2.027	8.9771
4.482	-3.1173
4.2521	-0.7611
-0.399	0.924
3.3031	

Part 22.3 Spectral analysis

dark unstim	1Hz light stim
0.241232	0.024099
0.081962	0.085418
0.262511	0.111277
0.089991	0.194813
0.080867	0.075817
	0.116514

Part 23.1 hAb signal in the optic nerve of mice exposed to darkness or 1Hz light stimulation while ICP was elevated

distance from eye (μm)	high ICP dark unstim (A.U.)			high ICP 1Hz stim (A.U.)		
	mean	**SEM**	**n**	**mean**	**SEM**	**n**
0	1.062	0.56788	6	4.812883	2.315463	6
100	3.4592	1.6326	6	12.1405	3.600801	6
200	3.4628	0.87164	6	10.24495	3.348834	6
300	3.6518	0.9026	6	8.92647	2.963547	6
400	2.3792	0.69824	6	7.963067	2.645191	6
500	2.1545	0.74845	6	7.268883	2.456883	6
600	1.6449	0.56926	6	6.653283	2.222167	6
700	1.6749	0.81297	6	6.068867	2.143779	6
800	2.3198	1.0539	6	5.920133	2.353049	6
900	3.4022	1.2751	6	5.845183	2.561005	6
1000	4.0524	1.4431	6	5.697933	2.604872	6
1100	4.7987	1.6061	6	5.449333	2.733257	6
1200	4.3424	1.5509	6	5.270865	2.566534	6
1300	3.831	1.8563	6	5.803483	2.254385	6
1400	5.511	1.8211	6	7.492533	3.130926	6
1500	4.6011	2.0583	6	10.72393	6.120454	6
1600	4.629	1.973	6	4.013817	2.036648	6
1700	4.2067	1.8299	6	3.991683	2.107868	6
1800	3.9099	1.7872	6	3.416033	1.85423	6
1900	3.0955	1.6262	6	3.016467	1.789961	6
2000	3.057	1.6177	6	2.456833	1.416977	6
2100	2.7477	1.5939	6	2.148917	1.0847	6
2200	2.1216	1.4091	6	1.87556	0.8045245	6
2300	2.1299	1.464	6	2.4371	0.9624452	6
2400	2.4065	1.6945	6	3.08285	1.159217	6
2500	2.662	1.8867	6	2.8315	1.212967	6
2600	2.7246	1.9284	6	2.619412	1.45982	6
2700	2.9064	2.0401	6	2.56575	1.363392	6
2800	3.1471	1.852	6	2.726017	1.451039	6
2900	3.6125	2.1	6	2.80915	1.525867	6
3000	4.2864	2.297	6	3.224117	1.796341	6
3100	4.0471	2.1076	6	3.381417	1.837222	6
3200	2.9051	1.6267	6	3.484833	1.897819	6
3300	2.349	1.1459	6	3.744383	1.933866	6

3400	1.665	0.83079	6	3.13555	1.553927	6
3500	1.0959	0.58482	6	3.386033	1.613361	6
3600	1.204	0.8014	6	3.90725	1.831953	6
3700	0.94873	0.60623	6	3.815783	1.730061	6
3800	0.72488	0.48686	6	3.735667	1.680375	6
3900	0.9647	0.61094	6	3.8004	1.747221	6
4000	1.5588	1.0137	6	4.066617	1.877995	6
4100	1.5177	0.96636	6	3.848533	1.788912	6
4200	1.2642	0.79978	6	3.740467	1.81183	6
4300	0.72384	0.56804	6	3.92265	2.354552	6
4400	1.3316	1.0365	6	4.43025	2.868221	6
4500	0.99925	0.68805	6	4.885517	3.054883	6
4600	1.4422	1.4422	6	4.33455	2.73047	6
4700	1.9537	1.9537	6	4.970422	3.066435	6
4800	1.5555	1.5555	6	4.645167	2.986013	6
4900	3.292	2.4924	6	4.978833	3.199281	6

Part 23.2 hAβ signal in the optic nerve of mice exposed to darkness or 1Hz light stimulation while ICP was reduced

distance from eye (μm)	**low ICP unstim (A.U.)**			**low ICP 1Hz stim (A.U.)**		
	mean	**SEM**	**n**	**mean**	**SEM**	**n**
0	9.147	2.504	6	4.8201	1.5149	5
100	69.762	14.822	6	60.55	22.64	5
200	77.498	15.347	6	69.466	16.278	5
300	71.57	14.811	6	67.764	15.972	5
400	64.813	14.066	6	63.829	15.576	5
500	58.871	14.521	6	57.383	13.554	5
600	49.257	13.304	6	48.789	12.308	5
700	40.599	11.205	6	41.874	11.828	5
800	33.292	9.0681	6	34.576	10.911	5
900	28.412	7.8266	6	28.3	10.028	5
1000	24.484	6.9827	6	23.982	8.8804	5
1100	20.926	6.1191	6	21.283	7.297	5
1200	19.175	5.2868	6	18.864	6.4192	5
1300	16.01	4.3397	6	16.829	5.6087	5
1400	13.674	3.7239	6	14.789	4.8167	5

1500	12.027	3.3742	6	13.514	4.2312	5
1600	10.385	2.8089	6	12.283	3.6281	5
1700	8.3769	2.4103	6	10.836	3.1106	5
1800	7.0507	1.7855	6	9.2066	2.5705	5
1900	5.7745	1.5012	6	7.3052	2.408	5
2000	4.3319	1.2844	6	5.965	2.3175	5
2100	3.8054	0.9068	6	5.2718	2.1815	5
2200	3.4088	0.8864	6	5.0976	2.5798	5
2300	3.1948	0.9844	6	5.0908	2.9781	5
2400	3.0732	0.9795	6	6.0038	3.9302	5
2500	3.7658	1.1525	6	7.2832	5.0837	5
2600	4.2983	1.4826	6	8.1994	5.6759	5
2700	5.0579	1.62	6	7.3938	5.2028	5
2800	4.8126	1.5555	6	6.6219	4.9487	5
2900	4.9089	1.4529	6	4.0962	2.4117	5
3000	4.9462	1.4953	6	3.5545	1.82	5
3100	4.4381	1.0514	6	4.3288	1.9782	5
3200	4.3759	0.7943	6	4.6625	1.9517	5
3300	4.5403	0.9761	6	4.493	1.7831	5
3400	5.6398	1.1998	6	4.1973	1.6853	5
3500	7.3903	1.8566	6	4.5157	2.0782	5
3600	10.424	2.6597	6	5.6747	2.9451	5
3700	12.31	3.1485	6	5.2424	3.2153	5
3800	10.765	2.5231	6	4.5061	2.1923	5
3900	10.191	3.3111	6	3.6611	1.7491	5
4000	10.431	3.4362	6	3.0721	1.8829	5
4100	9.7988	3.3559	6	2.331	1.4278	5
4200	9.3365	3.4164	6	1.7191	0.7547	5
4300	8.6002	3.5829	6	1.0967	0.6615	5
4400	8.6902	3.7237	6	1.4482	1.4482	5
4500	10.971	5.5724	6	1.0426	0.7789	5
4600	14.743	7.7248	6	0.7866	0.7866	5
4700	17.778	9.8659	6	0.8024	0.5054	5
4800	17.138	9.6544	6	1.7241	1.0684	5
4900	15.042	8.8947	6	5.2686	3.2282	5

Part 23.3 Distance of hAβ transport in the optic nerve of mice exposed to darkness or 1Hz light stimulation while ICP was elevated

high ICP dark unstim (μm) **high ICP 1Hz stim (μm)**

265.4321	972.2222
287.037	709.8765
40.12346	1969.136
95.67902	52.46914
339.5062	1922.84
40.12346	138.8889

Part 23.4 Distance of hAβ transport in the optic nerve of mice exposed to darkness or 1Hz light stimulation while ICP was decreased

low ICP dark unstim(μm)	low ICP 1Hz stim (μm)
1768.519	2182.099
1543.21	1657.407
858.0247	1756.173
2222.222	1172.84
1598.765	1879.63
1552.469	

Part 23.5 Total hAβ signal in the optic nerve of mice exposed to darkness or 1Hz light stimulation while ICP was elevated

high ICP dark unstim (A.U.)	high ICP 1Hz stim (A.U.)
3766.539	3260.211
10373.04	8346.439
418.8765	17774.54
3259.896	1736.556
732.8639	10989.58
6642.699	99.9707

Part 23.6Total hAβ signal in the optic nerve of mice exposed to darkness or 1Hz light stimulation while ICP was decreased

low ICP dark unstim (A.U.)	low ICP 1Hz stim (A.U.)
35304.02	45706.05
31528.34	19317.12
23395.59	11929.1

38139.27	12510.54
17938.15	23951.42
11936.13	

Part 23.7 Peak hAβ signal in the optic nerve of mice exposed to darkness or 1Hz light stimulation while ICP was elevated

high ICP dark unstim (A.U.)	high ICP 1Hz stim (A.U.)
6.074344	20.37172
4.874636	23.43294
3.900875	14.68222
28.64432	5.772595
6.214286	22.99563
8.994169	4.584548

Part 23.8 Peak hAβ signal in the optic nerve of mice exposed to darkness or 1Hz light stimulation while ICP was elevated

low ICP dark unstim (A.U.)	low ICP 1Hz stim (A.U.)
151.3703	150.9038
94.60641	63.77551
54.79592	40.34257
117.0262	63.57143
40.21137	55.71429
68.87755	

Part 24.1 Distance of 10kD dextran transport in the optic nerve of mice exposed to normal or decreased ICP

10kD Dextran norm ICP (μm)	10kD Dextran low ICP (μm)
52.46914	466.0494
1432.099	589.5062
1222.222	126.5432
623.4568	1805.556
348.7654	135.8025

780.8642	339.5062
	228.3951
	1509.259

Part 24.2 Total 10kD dextran signal in the optic nerve of mice exposed to normal or decreased ICP

10kD Dextran norm ICP (A.U.)	10kD Dextran low ICP (A.U.)
14.60704	762.0862
3034.931	1134.455
4045.385	0
7489.069	13255.45
504.4148	637.8689
3086.948	284.8863
	875.7382
	4060.149

Part 24.3 Peak 10kD dextran signal in the optic nerve of mice exposed to normal or decreased ICP

10kD Dextran norm ICP (A.U.)	10kD Dextran low ICP (A.U.)
0.474927	7.172012
11.21283	11.10787
9.635569	2.816327
3.629738	2.759475
10.75802	7.591837
18.62974	

Part 25.1 Colocalization of hAb tracer with TUJ1 staining in aged DBA or young control

	11month DBA	3month DBA
Pearson's correlation coefficient	0.15	0.65
	0.02	0.67
	0.01	0.7
	-0.01	0.73
	0.19	0.49

0	0.53
-0.02	0.65
0.28	0.27
0	0.3
-0.01	0.25
0.11	0.12
-0.04	
0.18	
-0.09	
-0.19	
0.11	
-0.01	
-0.01	
-0.01	
0.11	

Part 25.2 RGC count in young and aged DBA

DBA/2J 3 mo	DBA/2J 11 mo
371.7133	326.0214
341.561	351.2052
576.3469	275.2808
617.5328	224.2329
672.6819	232.7153
720.124	266.5364
456.0625	306.6361
640.1964	269.2917
605.3478	317.2083
895.3783	

Part 25.3 Quantification of lamina defects. Mean pixel intensity and standard deviation (SD) for EM images is shown (255 = white, 0 = black). Lamina defects were estimated as the proportion (%) of pixels >2 SD above mean pixel intensity, manually excluding blood-vessels.

	Mean	SD	Defects
Ctrl_1	142.25	48.38	5.59%
Ctrl_2	136.50	41.19	2.49%
Ctrl_3	154.16	42.32	7.30%
Ctrl_4	143.20	39.54	4.91%
Ctrl_5	125.97	28.54	1.02%
Ctrl_6	143.53	31.54	2.85%
Ctrl_7	149.93	32.05	3.50%

DBA_1	150.43	44.92	11.34%
DBA_2	148.82	48.75	12.13%
DBA_3	173.23	41.84	15.85%
DBA_4	185.94	48.97	31.91%
DBA_5	169.71	53.73	24.06%
DBA_6	132.62	53.31	10.51%
DBA_7	153.86	53.60	19.80%
DBA_8	170.32	45.96	16.76%
DBA_9	162.84	52.58	18.62%
DBA_10	194.20	47.98	39.56%

Part 26.1 IOP of different glaucoma model normalize to control level at the time of experiment

D2 Ctrl. 11mo (mmHg)	DBA/2J 11mo (mmHg)	CD-1 sham (mmHg)	CD-1 CLS (mmHg)
9	13.33333	10	8.333333
13.66667	9.666667	16	14
11	10.66667	11.4	16
14.66667	8.666667	12.66667	10.66667
9.666667	9	13.33333	13.33333
10	10	13	15
14.33333	7.666667	13.66667	16.66667
10.33333	15		

Part 26.2 CD-1 mice IOP significantly elevated acutely following surgery

CD-1 control IOP (mmHg)	CD-1 CLS IOP (mmHg)
16.33333	26.66667
15.33333	33
13.66667	28.66667
15. 33333	33.33333
15.66667	27
14.66667	20.66667
14	27

Part 27.1 Distance of hAβ transport in the optic nerve of old DBA mice and its control

DBA/2J 3mo (μm)	DBA/2J 6mo (μm)	DBA/2J 11mo (μm)	D2 Ctrl. 11mo (μm)
283.9506	1361.111	453.7037	200.6173

1635.802	817.9012	1385.802	293.2099
1817.901	1379.63	1839.506	496.9136
1685.185	1046.296	700	206.7901
1753.086	1524.691	4630	537.037
2240.741	379.6296	1824.074	1820.988
2145.062		2138.889	583.3333
1466.049		429.0123	2141.975
1160.494		4630	283.9506
1024.691		3219.136	604.9383
			404.321
			1277.778

Part 27.2 Peak of hAβ signal in the optic nerve of old DBA mice and its control

DBA/2J 3mo (A.U.)	DBA/2J 6mo (A.U.)	DBA/2J 11mo (A.U.)	D2 Ctrl. 11mo (A.U.)
12.71866	32.39796	19.32945	9.94898
28.29446	73.81924	86.98251	16.65452
32.90816	54.83965	86.19534	33.0102
81.99708	13.55102	222.6676	4.976676
23.36006	27.68222	60.91837	11.9898
55.71429	14.05977	55.1895	34.7449
48.46939		88.03207	11.73469
38.30904		222.6676	27.50729
18.60058		138.9796	13.40379
56.23907			14.27843
			31.9898

Part 27.3 Distance of hAβ transport in the optic nerve of CLS mice and its control

CD-1 Ctrl (μm)	CD-1 CLS (μm)
2636.848	4998.935
2547.391	4673.056
1035.144	4998.935

1759.318	4843.45
1652.822	2509.052
1265.176	4856.23
2564.43	4709.265

Part 27.4 Peak of hAβ signal in the optic nerve of CLS mice and its control

CD-1 Ctrl (A.U.)	CD-1 CLS (A.U.)
15.32362	71.25364
56.76385	57.95918
39.00875	36.32653
52.91545	71.48688
56.41399	55.88921
42.0481	71.02041
72.8863	68.67347

Part 27.5 Distance of 500kD dextran transport in the optic nerve of CLS mice and its control

CD-1 Ctrl (μm)	CD-1 CLS (μm)
70.28754	359.9574
70.28754	319.4888
80.93717	745.4739
112.886	4998.935
289.6699	110.7561
80.93717	4998.935
	4866.88

Part 27.6 Peak of 500kD dextran signal in the optic nerve of CLS mice and its control

CD-1 Ctrl (A.U.)	CD-1 CLS (A.U.)
0.0153	7.055394
1.6224	3
1.5124	7.661808
9.0525	53.76093
2.7507	5.71137
1.5137	19.32362
	79.11079

Part 27.7 Distance of 500kD dextran transport in the optic nerve of old DBA mice and its control

D2 Ctrl. 11mo (μm)	DBA/2J 11mo (μm)
104.9382716	1904.321
126.5432099	3429.012
114.1975309	2496.914
126.5432099	2435.185
104.9382716	2959.876
250	2533.951
148.1481481	
259.2592593	
231.4814815	

Part 27.8 Total of 500kD dextran in the optic nerve of old DBA mice and its control

D2 Ctrl. 11mo (A.U.)	DBA/2J 11mo (A.U.)
1750.731	39558.14
1301.425	96625.98
4779.372	35768.63
2159.71	99617.18
6134.054	45061
20935.95	145667.9
24730.83	
23279.85	
9902.153	

Part 27.9 Peak of 500kD dextran in the optic nerve of old DBA mice and its control

D2 Ctrl. 11mo (A.U.)	DBA/2J 11mo (A.U.)
4.510204	57.65306
6.975219	210.277
6.676385	41.52332
9.693877	204.4461

10.09329	65.61224
37.95918	192.1283
15.45918	
35.27697	
26.98251	

Part 27.10 Distance of 10kD dextran transport in the optic nerve of old DBA mice and its control

DBA/2J 3mo (μm)	DBA/2J 11mo (μm)
114.1975309	339.5062
92.59259259	3694.444
18.51851852	904.321
148.1481481	2185.185
	4219.136
	4148.148
	4518.519
	4524.691

Part 27.11 Total of 10kD dextran signal in the optic nerve of old DBA mice and its control

DBA/2J 3mo (A.U.)	DBA/2J 11mo (A.U.)
12218.17	34111.7
8861.764	74216.92
23284.87	26383.66
3205.451	31211.09
	125108
	188591.3
	57907.11
	173773

Part 27.12 Peak of 10kD dextran signal in the optic nerve of old DBA mice and its control

DBA/2J 3mo (A.U.)	DBA/2J 11mo (A.U.)
13.35277	10.40816
12.10204	164.519

11.48688	53.2653
15.05102	56.06414
	237.2449
	212.4636
	118.4257
	201.5306

Part 27.13 Distance of 3kD dextran transport in the optic nerve of old DBA mice and its control

D2 Ctrl. 11mo (μm)	DBA/2J 11mo (μm)
820.9877	61.72839506
805.5556	209.8765432
679.0123	308.6419753
1858.025	40.12345679
962.963	83.33333333
398.1481	
327.1605	
632.716	
1845.679	
1959.877	

Part 27.14 Total of 3kD dextran signal in the optic nerve of old DBA mice and its control

D2 Ctrl. 11mo (A.U.)	DBA/2J 11mo (A.U.)
12233.09	47024.23
15898.82	56956.74
4031.583	13037.52
8480.338	27666.13
8645.772	22091.63
2714.166	76232.88
2805.363	
13359.23	
8272.484	
12243.13	

Part 27.15 Peak of 3kD dextran signal in the optic nerve of old DBA mice and its control

D2 Ctrl. 11mo (A.U.)	DBA/2J 11mo (A.U.)
67.2449	220.481
93.36735	77.52187
16.81924	20.51312
30.56122	50.46647
83.04665	47.44898
20.15306	154.6356
12.14286	
34.43878	
29.94898	
42.3105	

Part 28 Retinal cytokine assay

cytokine tested (pg/mL)

	Vehicle						hAβ					
Sample	**1**	**2**	**3**	**4**	**5**	**6**	**1**	**2**	**3**	**4**	**5**	**6**
Eotaxin	3.09	1.07	0.8	3.78	1.95	0.99	3.3	1.72	1.63	2.71	3.22	1.11
G-CSF		0.33	0.29	0.74	0.29	0.37	0.38	0.39	0.36	0.56	0.54	0.36
GM-CSF		2.84	2.56	3	2.71	2.56	2.68	2.64	2.64	2.64	2.56	2.45
IFNy		0.24	0.23	0.31	0.31	0.28	0.21	0.29	0.24	0.28	0.27	0.31
IL-1a	40.78	19.29	30.23	23.12	21.99	21.86	58.93	26.03	28.58	20.53	28.76	25.71
IL-1B		4.62	3.79	4.75	5.17	4.89	6.86	4.49	3.29	4.01	6.67	4.01
IL-2	17.01	12.41	16.51	16.02	13.36	16.86	20.46	10.72	14.19	14.38	20.78	7.57
IL-3		0.35	0.32	0.38	0.34	0.35	0.34	0.32	0.36	0.35	0.39	0.32
IL-4	0.51	0.47	0.46	0.46	0.48	0.47	0.5	0.47	0.48	0.47	0.47	0.47
IL-5		0.38	0.37	0.4	0.4	0.4	0.4	0.4	0.39	0.4	0.38	0.39
IL-6	1.76	1.29	0.73	1.69	1.57	0.8	0.47	0.83	1.76	1.05	0.68	0.74
IL-7		0.84	0.43	1.18	0.35	0.39	1	0.26	0.25	0.46	0.41	0.31
IL-9	25.09	18.44	17.91	19.65	16.8	13.88		18.53	19.65	16.88	23.66	15.63
IL-10		3.29	3.07	2.59	2.7	2.48	2.28	3.53	4.62	2.1	3.29	2.19

IL-12 (p40)		0.08	0.04	0.08	0.02	0.04	0.09	0.08	0.06	0.04	0.18	0.08
IL-12 (p70)		2.18	1.8	2.44	2.18	2.01	1.96	1.66	2.57	1.76	2.31	1.91
IL-13	1.75	1.41	1.68	1.52	1.45	1.6		1.5	1.51	1.58	1.68	1.43
IL-15		2.99	3.09	3.2	5.12	3.42	3.2	2.71	4.47	3.66	3.2	3.09
IL-17	0.6	0.49	0.47	0.48	0.45	0.49	0.63	0.48	0.48	0.51	0.46	0.47
IP-10	2.08	1.15	0.95	2.23	1.26	1.27	2.82	3.67	3.22	2.08	1.55	1.15
KC	7.33	6.03	5.74	7.36	6.98	5.69		5.53	7.76	6.38	8.22	4.83
LIF		0.36	0.31	0.34	0.36	0.36	0.43	0.34	0.43	0.36	0.37	0.39
LIX		0.13	0.12	0.13	0.09	0.12	0.13	0.12	0.11	0.12	0.1	0.12
MCP-1		2.43	5.07	3.85	6.09	3.67	7.32	3.06	2.66	7.32	6.09	3.67
M-CSF		0.52	0.62	0.52	0.69	0.42	0.66	0.36	0.61	0.52	0.81	0.49
MIG	6.72	6.06	7.02	8.91	8.04	16.71	16.14	5.55	12.97	12.48	10.22	11.43
MIP-1a	11.21	4.32	6.28	2.97	4.16	4.01	17.13	5.61	5.01	3.72	2.97	1.14
MIP-1B		1.46	0.98	1.81	2.98	0.92	1.36	0.62	1.31	1.31	0.85	0.66
MIP-2		26.16	11.19	16.73	9.36	19.13	17.5	11.19	17.5	8.56	13.38	19.13
RANTES	0.88	0.64	0.51	0.55	0.53	0.57	0.66	0.55	0.7	0.59	0.69	0.51
TNFa		0.26	0.26	0.26	0.33	0.33	0.36	0.26	0.31	0.34	0.34	0.29
VEGF	0.77	0.61	0.67	0.74	0.56	0.51		0.6	0.97	0.56	0.6	0.45

Table S2. Retinal cytokine assay.

Cytokine	Vehicle	Amyloid-β	*p*-value
Eotaxin	1.95 ± 0.51	2.28 ± 0.38	0.8147
G-CSF	0.40 ± 0.09	0.43 ± 0.04	0.9222
GM-CSF	2.73 ± 0.09	2.60 ± 0.03	0.2682
IFN-γ	0.27 ± 0.02	0.27 ± 0.02	0.9430
IL-1α	26.21 ± 3.28	31.42 ± 5.63	0.7324
IL-1β	4.64 ± 0.23	4.89 ± 0.61	0.9412
IL-2	15.36 ± 0.81	14.68 ± 2.14	0.9655
IL-3	0.35 ± 0.01	0.35 ± 0.01	0.9949
IL-4	0.48 ± 0.01	0.48 ± 0.01	0.9785
IL-5	0.39 ± 0.01	0.39 ± 0.003	0.9101
IL-6	1.31 ± 0.18	0.92 ± 0.19	0.2646
IL-7	0.64 ± 0.16	0.45 ± 0.12	0.6271
IL-9	18.63 ± 1.52	18.87 ± 1.38	0.5997
IL-10	2.83 ± 0.15	3.00 ± 0.41	0.9498
IL-12 (p40)	0.05 ± 0.01	0.09 ± 0.02	0.4405
IL-12 (p70)	2.12 ± 0.11	2.03 ± 0.14	0.8350
IL-13	1.57 ± 0.05	1.54 ± 0.04	0.9821
IL-15	3.56 ± 0.40	3.39 ± 0.25	0.9343
IL-17	0.50 ± 0.02	0.51 ± 0.03	0.9576
IP-10 (CXCL10)	1.49 ± 0.22	2.42 ± 0.40	0.2877
KC (CXCL1)	6.52 ± 0.32	6.54 ± 0.64	0.9999
LIF	0.35 ± 0.01	0.39 ± 0.02	0.0957
LIX (CXCL5)	0.12 ± 0.01	0.12 ± 0.004	0.9960
MCP-1 (CCL2)	4.22 ± 0.63	5.02 ± 0.88	0.6815
M-CSF	0.55 ± 0.05	0.58 ± 0.06	0.9645
MIG (CXCL9)	8.91 ± 1.61	11.47 ± 1.43	0.4758
MIP-1α (CCL3)	5.49 ± 1.23	5.93 ± 2.33	0.9819
MIP-1β (CCL4)	1.63 ± 0.38	1.02 ± 0.14	0.1897
MIP-2 (CXCL2)	16.51 ± 3.00	14.5 ± 1.70	0.8264
RANTES (CCL5)	0.61 ± 0.06	0.62 ± 0.03	0.9980
TNFα	0.29 ± 0.02	0.32 ± 0.02	0.4132
VEGF	0.64 ± 0.04	0.64 ± 0.09	0.9953

Table S3. Comparing the controls for the DBA/2J strain

Measurements	Values (mean ± SD)		*p*-value
	C57BL/6J	*Gpnmb*$^{+}$/SjJ (D2-control)	
young unstim total signal	5463 ± 4843.8 (A.U.)	11753 ± 6001.2 (A.U.)	0.14
young stim total signal	22889 ± 9173.3 (A.U.)	23621 ± 14946.6 (A.U.)	0.97
young unstim distance	890 ± 354.0 (μm)	1208 ± 327.5 (μm)	0.15
young stim distance	2020 ± 775.4 (μm)	1205 ± 402.7 (μm)	0.09
young unstim peak	28 ± 11.7 (A.U.)	47 ± 23.1(A.U.)	0.24
young stim peak	76 ± 27.4 (A.U.)	95 ± 59.2 (A.U.)	0.74
young IOP	13.0 ± 3.57 (mmHg)	11 ± 3.1 (mmHg)	0.16
old unstim total signal	9670 ± 4911.8 (A.U.)	6830 ± 5069.6 (A.U.)	0.36
old unstim distance	472 ± 114.3 (μm)	402 ± 396.4 (μm)	0.70
old unstim peak	18 ± 7.0 (A.U.)	21 ± 11.1 (A.U.)	0.50
old IOP	13.3 ± 3.58 (mmHg)	12 ± 1.8 (mmHg)	0.11

Table S4. Tracers used in this study and their routes of administration

Tracer	Route
^{3}H-mannitol	Intra-arterial
$^{86}Rb^{+}$	Intra-arterial
Cadaverine, FITC-conjugated	Intra-arterial
Cadaverine, FITC-conjugated	Intravitreal
Cadaverine, FITC-conjugated	Supra-choroidal
Ovalbumin, FITC-conjugated	Supra-choroidal
hAβ, HiLyte Fluor 488-conjugated	Intravitreal
3 kD dextran, Alexa Fluor 488-conjugated	Intravitreal
3 kD dextran, Alexa Fluor 555-conjugated	Intracisternal
3 kD dextran, Alexa Fluor 555-conjugated	Intravitreal
3 kD dextran, Alexa Fluor 647-conjugated	Intravitreal
10 kD dextran, Alexa Fluor 488-conjugated	Intravitreal
10 kD dextran, Alexa Fluor 555-conjugated	Intravitreal
10 kD dextran, Alexa Fluor 647-conjugated	Intravitreal
500 kD dextran, Alexa Fluor 488-conjugated	Intravitreal
500 kD dextran, Alexa Fluor 555-conjugated	Intravitreal
500 kD dextran, Alexa Fluor 647-conjugated	Intravitreal

Movie S1. Animation of the proposed mechanism for ocular glymphatic clearance in the healthy optic nerve and glaucoma. Top-left panel shows intraocular fluid (IOF, blue) propelling the translaminar transport of intra-axonal solutes (orange) along the ocular-cranial pressure gradient, which then is cleared by a perivenous and lymphatic route. Top-right panel demonstrates how the lamina barrier (dark grey) might guide IOF into unmyelinated retinal ganglion cell (RGC) axons at the level of the optic nerve head. Bottom-left panel shows how in glaucoma, defects in the lamina barrier could allow IOF (blue) to bypass the intra-axonal compartment and diffuse directly into the extracellular space of the retro-laminar optic nerve. The reduction in intra-axonal solute flow would be expected to cause an accumulation of neurotoxic compounds such as Aβ (dark orange). Bottom-right panel illustrates how lamina defects cause a redirection of IOF, so it is no longer driving directional intra-axonal flow, causing intra-axonal solute accumulation.